LA-9131-PR
Progress Report
UC-28
Issued: January 1982

LA--9131-PR

DE82 008958

Accelerator Technology Program

July—December 1980

Compiled by

E. A. Knapp
R. A. Jameson

Los Alamos National Laboratory
Los Alamos, New Mexico 87545

CONTENTS

ACCELERATOR TECHNOLOGY PROGRAM

July—December 1980

Compiled by
E. A. Knapp and R. A. Jameson

ABSTRACT

The activities of Los Alamos National Laboratory's Accelerator Technology Division are discussed. This report covers the last six months of calendar 1980 and is organized around the Division's major projects. These projects reflect a wide variety of applications and sponsors. The major technological innovations promoted by the Pion Generator for Medical Irradiation (PIGMI) program have been developed; accelerator technologies relevant to the design of a medically practical PIGMI have been identified. A new group in AT Division deals with microwave and magnet studies; we describe the status of some of their projects. We discuss the prototype gyrocon, which has been completed, and the development of the radio-frequency quadrupole linear accelerator, which continues to stimulate interest for many possible applications. One section of this report briefly describes the results of a design study for an electron beam ion source that is ideally suited as an injector for a heavy ion linac; another section reports on a turbine engine test facility that will expose operating turbine engines to simulated maneuver forces. In other sections we discuss various activities: the Fusion Materials Irradiation Test program, the free-electron laser program, the racetrack microtron project, the Proton Storage Ring, and H^- ion sources and injectors.

SUMMARY

The Accelerator Technology (AT) Division of the Los Alamos National Laboratory is extending the science and art of subatomic particle accelerators to a wide spectrum of contemporary needs. This series of reports began in 1978 and includes LA-8218-PR, LA-8350-PR, LA-8592-PR, and LA-8736-PR.

During this period, we consolidated the innovations and studies made under the National Cancer Institute's program for development of a hospital-based machine for cancer therapy using pions. We call this the PIGMI (Pion Generator

for Medical Irradiations) technology, because it can serve a variety of needs by altering the configuration of the component parts. Pions, neutrons, or light-to-heavy ions could be provided for radiotherapy. Radioisotopes also could be produced in copious quantities. The PIGMI system is described in this report.

We consolidated our efforts on radio-frequency (rf) systems, accelerator-structure tuning and development and magnetic systems; a number of these systems are under construction. The prototype gyrocon assembly was completed and testing started.

We continued to place heavy emphasis on the development of a major new type of accelerator, the radio-frequency quadrupole (RFQ), that has attracted attention around the world. We summarize the design procedures at their present stage of development and show a number of preliminary designs for comparison and to illustrate the wide application that this device will have. These designs include RFQs for accelerator research in AT Division, a new European Organization for Nuclear Research (CERN) injector, neutral beam heating, PIGMI, the Fusion Materials Irradiation Test (FMIT) linac, the Chalk River ZEBRA project, the Lawrence Berkeley Laboratory (LBL) Medical Heavy Ion Synchrotron injector, and the Brookhaven National Laboratory (BNL) polarized proton injector. The combination of an Electron-Beam Ion Source (EBIS) with an RFQ for a heavy ion linac is suggested as an ideal machine for medical and scientific research.

Preliminary work has begun on an unusual electron-linac radiographic machine that could obtain x rays of turbine engines operating under simulated flight-maneuver conditions on a centrifuge.

Work on the FMIT accelerator facility and the FMIT prototype accelerator (FPA) at Los Alamos proceeded on schedule. Preliminary design reviews for the entire system were completed in August, and all components are now in final design. Contracts were awarded for the FPA linac tank, and major effort was directed toward the prototype facilities. Details of the design and development activities of the major systems are presented.

To illustrate the progress on our free-electron-laser (FEL) program, we outline the design and construction of the tapered wiggler for our amplifier/oscillator experiment. This device promises a much better energy-extraction efficiency than a uniform one and uses a sophisticated permanent-magnet design.

The collaborative Los Alamos/National Bureau of Standards (NBS) microtron design matured during this period, and long-lead procurements were initiated. The injection system design was altered to give improved performance. The end magnet and control system concepts also are outlined.

The Proton Storage Ring (PSR) construction was authorized, and the design parameters consolidated into final configuration. The Ring's operating characteristics are reviewed in this report, followed by a status report on its various systems. Particular attention was given to the extraction system during this period.

The final section outlines progress on H^- source and accelerator development activities.

I. INTRODUCTION

Accelerator technologies relevant to the design of a medically practical PIGMI have been identified and developed under the PIGMI program at Los Alamos.[1-4] The major technological innovations promoted by the PIGMI program are listed in Fig. 1. A "base-case" design for PIGMI is presented in this section. Figure 2 shows a typical layout for this basic configuration near a major medical center. We expect the accelerator portion of the facility to cost ~$10 million,[5] the treatment facility to cost ~$10 million, and site preparation to cost ~$5 million, giving a total cost of ~$25 million for a PIGMI facility.

II. ACCELERATOR SYSTEMS - GENERAL DESCRIPTION

A. Summary

As shown in Fig. 3, the accelerator portion of the PIGMI facility consists of an injector, an RFQ linac structure, a drift-tube linac (DTL) structure, a coupled-cavity linac (CCL) structure, a 440-MHz rf system, six 1320-MHz rf systems, and a control and instrumentation system. All of these components have been under development in the PIGMI program at Los Alamos. The 134-m-long accelerator can be installed in an underground tunnel of modest cross section.

The 440-MHz RFQ linac dramatically simplifies the front end of the accelerator.[6] It can accept a proton beam with an energy of only 30 keV and can bunch and accelerate it to an energy of 2.5 MeV in ~1.8 m, here the beam is ideally suited for injection into the DTL. The RFQ does this essential task better than any other known structure. Its average accelerating gradient is ~1.4 MeV/m.

The DTL is a 440-MHz, single-cavity, post-coupled linac structure, ~30 m long, that accelerates the beam from 2.5 MeV to 125 MeV. It contains 150 drift tubes, each containing a small, permanent-magnet quadrupole lens to focus the beam. The DTL is driven by a single klystron that is coupled to the structure through an iris near the center of the DTL. The average axial electric field gradient is 6 MV/m.

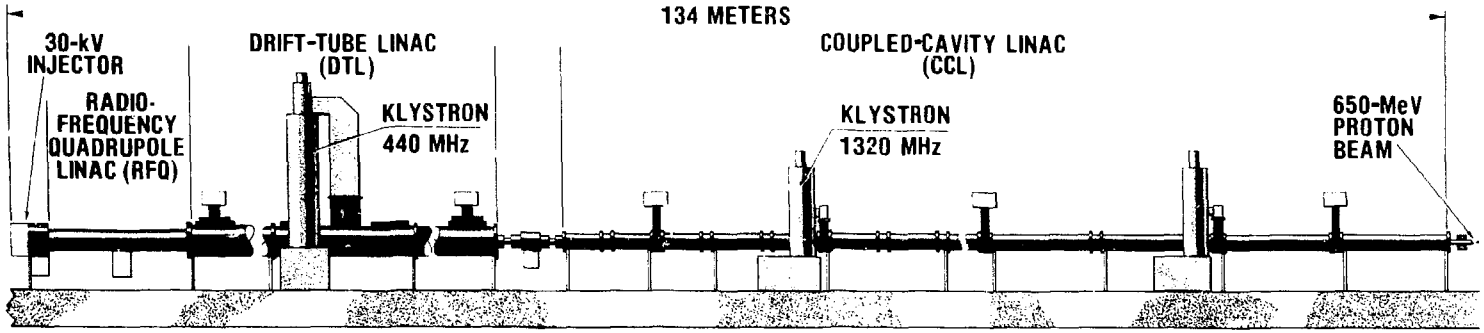

MAJOR TECHNICAL INNOVATIONS

- HIGHER FREQUENCIES
- HIGHER GRADIENTS
- LOWER INJECTION ENERGY
- RFQ LINAC STRUCTURE
- POST-COUPLED DTL STRUCTURE
- PERMANENT-MAGNET QUADRUPOLE LENSES
- DISK-AND-WASHER CCL STRUCTURE
- COAXIAL BRIDGE COUPLERS
- DISTRIBUTED MICROPROCESSOR CONTROL

PROTON BEAM PARAMETERS

INJECTION ENERGY	30 keV
RFQ/DTL TRANSITION ENERGY	2.5 MeV
DTL/CCL TRANSITION ENERGY	125 MeV
FINAL ENERGY	650 MeV
PEAK BEAM CURRENT	28 mA
PULSE LENGTH	60 μs
REPETITION RATE	60 Hz
AVERAGE BEAM CURRENT	100 μA

PROTON-LINAC PARAMETERS

	FREQUENCY	KLYSTRONS	GRADIENT
RFQ & DTL SECTION	440 MHz	1	6 MV/m
CCL SECTION	1320 MHz	6	8 MV/m

Fig. 1.
Pion generator for medical irradiations.

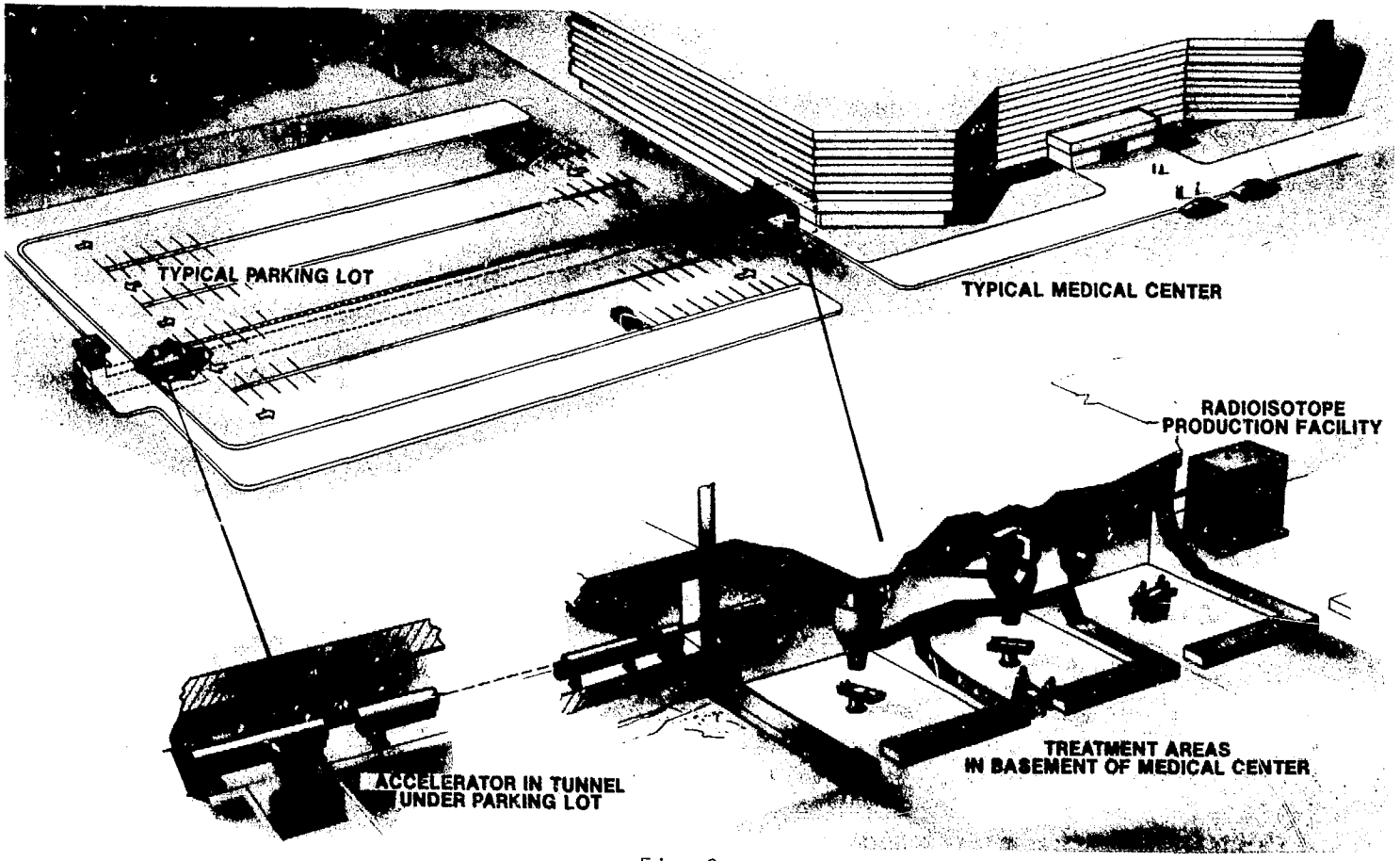

Fig. 2.
Typical PIGMI-facility layout.

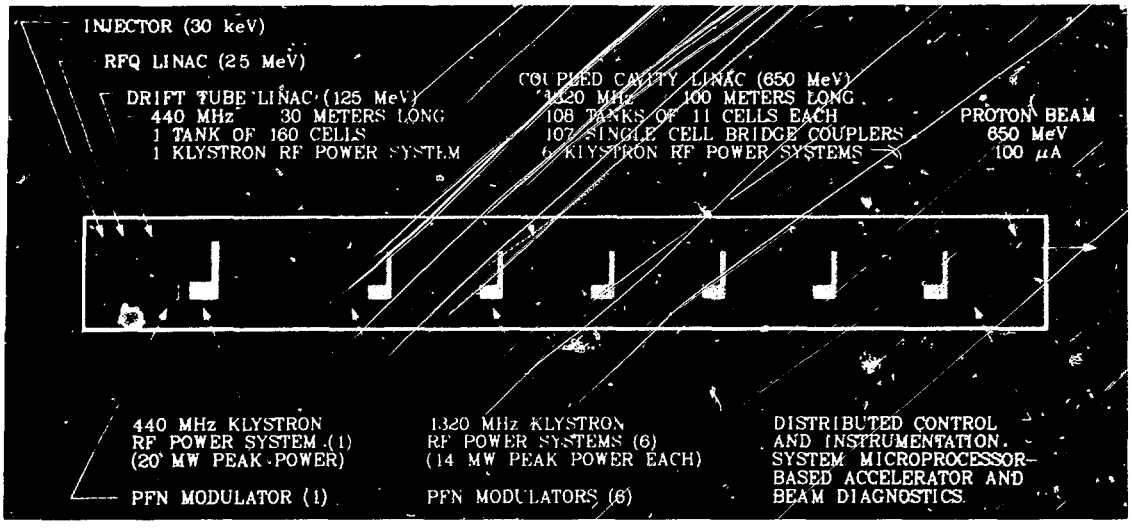

Fig. 3.
Principal components of PIGMI.

The CCL is a 1320-MHz structure of the "disk-and-washer" (DAW) type[7] that accelerates the beam from 125 MeV to 650 MeV in ~100 m. The structure consists of 108 tanks of 11 cells each, with the cell geometry of each tank optimized for the energy range it spans. The entire structure is coupled by 107 single-cell coaxial bridge couplers into a single resonant unit. Each bridge coupler contains a permanent-magnet quadrupole singlet to focus the beam. The entire CCL is driven by six klystrons that are coupled to the CCL through six bridge couplers symmetrically located along the structure. The average axial electric field gradient is 8 MV/m.

A very attractive feature of the PIGMI accelerator is its stark simplicity. There are only two resonant units: one at 440 MHz, and one at 1320 MHz. This implies that there are only three principal set points in the control of the rf fields: namely, the amplitude of each and their relative phase. All magnetic quadrupoles (except those in the transition region between the DTL and CCL) are of the permanent-magnet type that requires no power supplies or associated instrumentation. The injection voltage is furnished by a rack-mounted 30-kV power supply. The low-energy beam-transport system consists of a single einzel lens for control of the focusing, and minimal steering for correction of any misalignments. In all, there are very few power supplies and very few active control parameters.

Copper plating is an important feature of the PIGMI technology. Because copper-plated steel structures are lighter weight and stronger than corresponding copper structures, we can handle completed subassemblies of PIGMI as mechanical entities already tuned and aligned. A bright-leveling copper-plating process[8] (standard in our automotive industry since 1960 for achieving smooth surfaces on chrome-plated parts), used to fabricate PIGMI prototype parts, gives the parts excellent electrical, mechanical, and vacuum properties.

A modest, distributed, MULTIBUS-based control system--of the type being developed for other projects at FERMILAB and Los Alamos[9]--can handle the control and diagnostic requirements of this facility. It is entirely practical to realize a three-state control: namely, OFF, STANDBY, and ON.

B. Injector System

The injector system traditionally has been an expensive and complicated component of a proton linac. The conventional injection energy of ~750 keV was reduced to 250 keV by the alternating-phase-focused (APF) structure in the PIGMI prototype,[10] further reduced to 100 keV in the RFQ proof-of-principle (POP) experiment, and finally reduced to 30 keV for PIGMI.[11] Injector operation at 30 kV dramatically simplifies the design, allowing the ion source and associated electronics to be enclosed in a small vacuum housing and a single equipment cabinet (Fig. 4).

The 30-keV injection energy satisfies the RFQ requirement for efficient bunching in a minimum distance and for reliable operation of the single-gap high-brightness extraction system. Because of this low energy, electrostatic focusing of the ion beam is more effective than the magnetic focusing used in the PIGMI prototype. A three-element unipotential einzel lens was designed to provide this electrostatic focusing; Fig. 5 shows the calculated beam profile for a 32-mA proton beam, extracted from the ion source and transported through this system.

The einzel lens was selected because of simplicity of fabrication, minimal space requirement, and because no power and cooling are needed by magnetic focusing. The excitation of this lens can be derived from a high-voltage divider system on the injector power supply. Calculations for this lens and extraction system have shown that ion currents ranging from 20-35 mA can be focused into the RFQ when the lens voltage ranges from 20-30 kV. Below 20 mA of extracted beam current, the beam divergence is too large for all of the beam

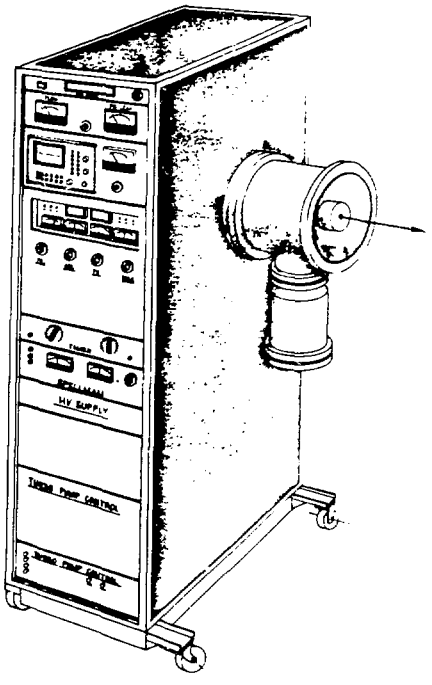

Fig. 4.
Ion source and associated equipment.

to enter the einzel lens aperture, although most of the beam entering the einzel lens is focused into the RFQ.

C. Radio-Frequency Quadrupole Linac

The RFQ represents a revolutionary new focusing, bunching, and accelerating structure that promises to be an important part of many future proton, light ion and heavy ion facilities.[12-15] The first RFQ structure in the Western Hemisphere was tested in the PIGMI laboratory in February 1980.[16] A series of highly successful tests confirmed the general properties of the RFQ structure and gave excellent agreement between the measured beam properties and the predicted performance. The tests established that the RFQ operates in a stable manner that is remarkably insensitive to injection energy errors, rf excitation errors, and structural fabrication errors.

The RFQ is considered by many to be the "missing link" in linac technology. It represents a superb answer to one of the most difficult remaining

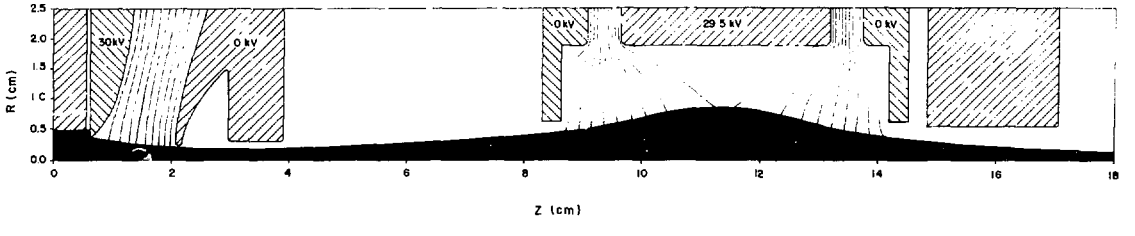

Fig. 5.
Beam profile for the PIGMI injection system.

questions of how to build simple, reliable, and inexpensive proton or ion linacs. The RFQ offers the lowest injection energy of any known linac structure. It is the best buncher that has ever been conceived, bunching and accelerating the beam with less emittance growth than any other known system.[17] It represents the best transformation that has been seen between the continuous beams that come from ion sources and the bunched and accelerated beams required by conventional linacs. The RFQ eliminates the need for large and costly Cockcroft-Walton power supplies, complex multicavity buncher systems, low-energy beam-transport systems, and their associated control instrumentation.

As shown in Fig. 6, the RFQ is essentially a vane-loaded cylinder excited in a modified TE_{210} cavity mode that produces a strong electric quadrupole field near the axis. The transverse components of this field, which are uniform in space and alternating in time, give rise to strong, alternating-gradient, focusing effects that can focus beams of particles traveling along the structure's axis. Scalloping the vane-tip geometry, as shown in Fig. 6, introduces a longitudinal component into the rf electric field near the axis; this component bunches and accelerates the beams. Thus, the RFQ structure is capable of focusing, bunching, and accelerating beams of charged particles.

The structure is so simple that, for the first time, it is possible to configure the linac for adiabatic capture of continuous beams at low energy. This is done by introducing the scallops gradually so that the structure acts primarily as a buncher at the beginning, transforming gradually to an accelerator at the end. A computer-generated picture of such a vane tip is shown in Fig. 7. A cutaway view of the RFQ structure is shown in Fig. 8.

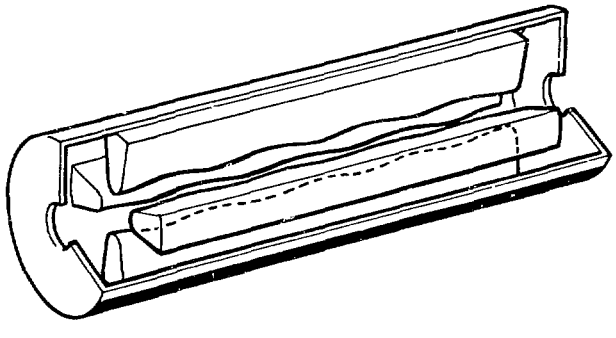

Fig. 6.
General configuration of the RFQ.

The RFQ is composed of four regions: the radial matching section, the shaper, the gentle buncher, and the accelerating section.[18] In the radial matching region, the vane aperture is tapered to adjust the focusing strength from almost zero to its full value, in a very short distance; this allows the dc injected beam to be matched

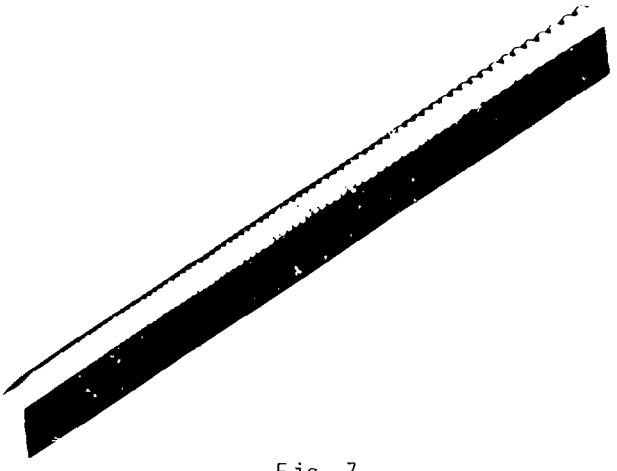

Fig. 7.
Computer-generated view of the RFQ vane tip.

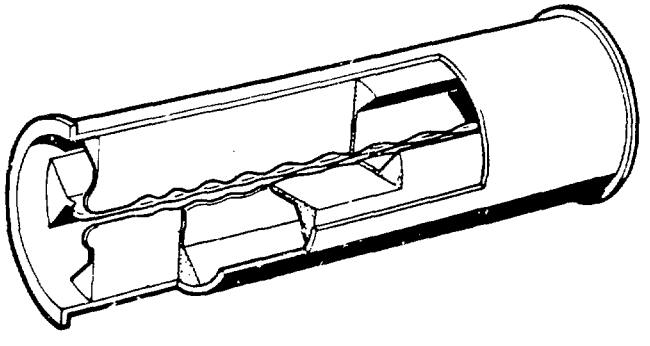

Fig. 8.
Cutaway view of the RFQ structure.

into the time-dependent focusing. In the next two regions, the shaper and the gentle buncher, the beam is adiabatically bunched as it is accelerated. At the end of the gentle buncher, the synchronous phase angle of the beam reaches its final value and the bunched beam is then accelerated in the final region. In this region, the vane radius, vane modulation, and phase angle are held constant to obtain the maximum possible acceleration gradient.

The PIGMI RFQ (designed and analyzed with the aid of the RFQ linac design-and-simulation code PARMTEQ) operates at a 440-MHz frequency and will accept a 30-keV proton beam from the ion source. It will focus, bunch, and accelerate the beam to a 2.5-MeV energy in 1.8 m. Each vane tip has a total of 200 scallops, varying in length from 0.27 cm at the beginning to 2.47 cm at the end. The structure's minimum radial aperture is 1.9 mm.

The RFQ's performance also was analyzed in detail with the PARMTEQ code, which showed that it captures 92% of a 30-mA beam to yield the PIGMI design current of 28 mA. The size, phase, and energy profiles are shown in Fig. 9. The normalized emittance [(area/π)$\cdot\beta\gamma$] of the input beam was taken to be 0.048 cm$\cdot$mrad. Figure 10 shows the beam's input and output phase spaces. The transverse emittance growth (for the 90% contour) is a factor of ~1.4, which is better than can be achieved by any other buncher/linac combination.

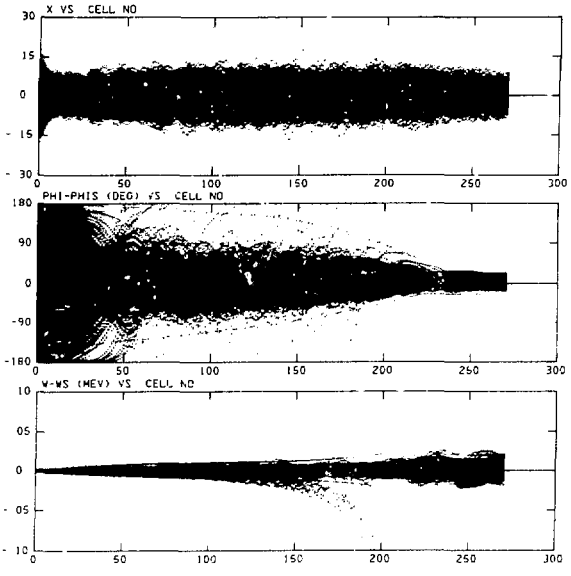

Fig. 9.
Beam profiles for the PIGMI RFQ.

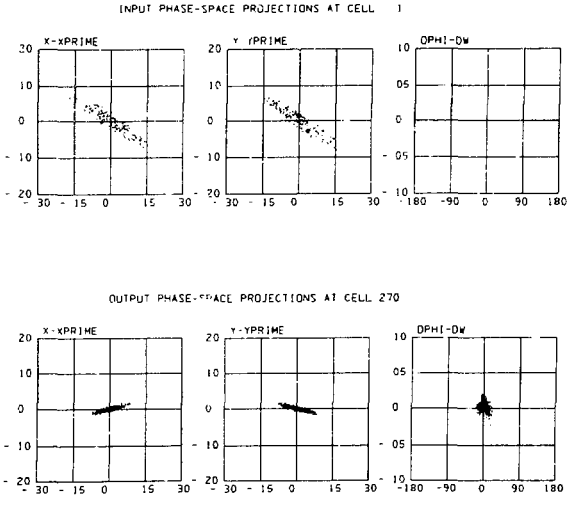

Fig. 10.
Beam phase spaces for the PIGMI RFQ.

A coaxial manifold has been developed that provides a symmetrical, multislot driving arrangement for the RFQ cavity.[19] A coaxial cavity, surrounding the RFQ cavity, is excited in a coaxial transverse electromagnetic (TEM) mode. The magnetic fields in the TEM mode are orthogonal to the magnetic fields in the RFQ mode. These fields can be coupled by diagonal slots, where the slot angles are determined by the magnitude and direction of the magnetic fields near the slots. Techniques are under investigation for resonating these slots to provide resonant coupling between the RFQ manifold and the RFQ cavity.

A technique has been proposed for coupling the RFQ manifold to the DTL so that the RFQ can derive its rf power from the DTL, thus eliminating the necessity for a separate rf power source and drive line for the RFQ.[20] This technique is being developed and will be tested in the PIGMI laboratory in 1981.

D. Drift-Tube Linac

Most proton linacs are of the DTL type. Most linacs designed in the last 10 years use post couplers[21] (developed at Los Alamos by the

principal investigators of the PIGMI program) to stabilize the distribution of the electromagnetic fields within the structure. The properties and performance of these structures are well known.

The PIGMI DTL differs from conventional DTLs primarily in scale; it has more than twice the frequency and hence less than half the cross-sectional diameter of conventional linacs. PIGMI's high frequency and low duty factor make its optimum accelerating rate higher than normal for conventional linacs, thus making possible a significantly shorter facility.

The small size of the PIGMI DTL does not require normal fabrication and assembly techniques that call for entry of personnel into the interior of the structure for assembly and alignment.[8,22] The PIGMI scheme is based on the preassembly of short (2.5-m) linac-tank sections into which the drift tubes can be introduced (from the ends or through slots in the top) into precision-bored holes along the bottom of the tank sections.

The PIGMI drift tubes also are considerably smaller than those in conventional DTLs, precluding the use of electromagnetic quadrupole lenses for focusing the beam. The PIGMI solution is to use permanent-magnet quadrupole lenses, made of modern materials in optional geometrical configuration (Fig. 11), which results in very compact, but sufficiently strong, magnetic lenses.[23,24] The design is further simplified by specifying that all quadrupoles have the same length and strength throughout the structure.

The PIGMI DTL is a single-tank, post-coupled DTL, ~30 m long and 0.4 m in diameter. It operates at 440 MHz, as does the RFQ linac, and accelerates the proton beam from 2.5 MeV to 125 MeV, with an average axial electric field of 6 MV/m. Peak power dissipation in the structure is 14.2 MW and peak beam power is 3.4 MW, for a total peak power requirement of 17.6 MW. The average power dissipated in the structure is only 51 kW or 1.7 kW/m.

The DTL structure has 150 drift tubes and 74 post couplers. All drift tubes have a 6-cm o.d., a 1-cm-diam bore hole, and are supported on a single stem from the bottom of the tank. Figure 12 shows a cutaway view of a portion of the DTL structure.

Each drift tube contains a permanent-magnet quadrupole lens to focus the beam. All 150 quadrupole magnets are identical in size and strength. They

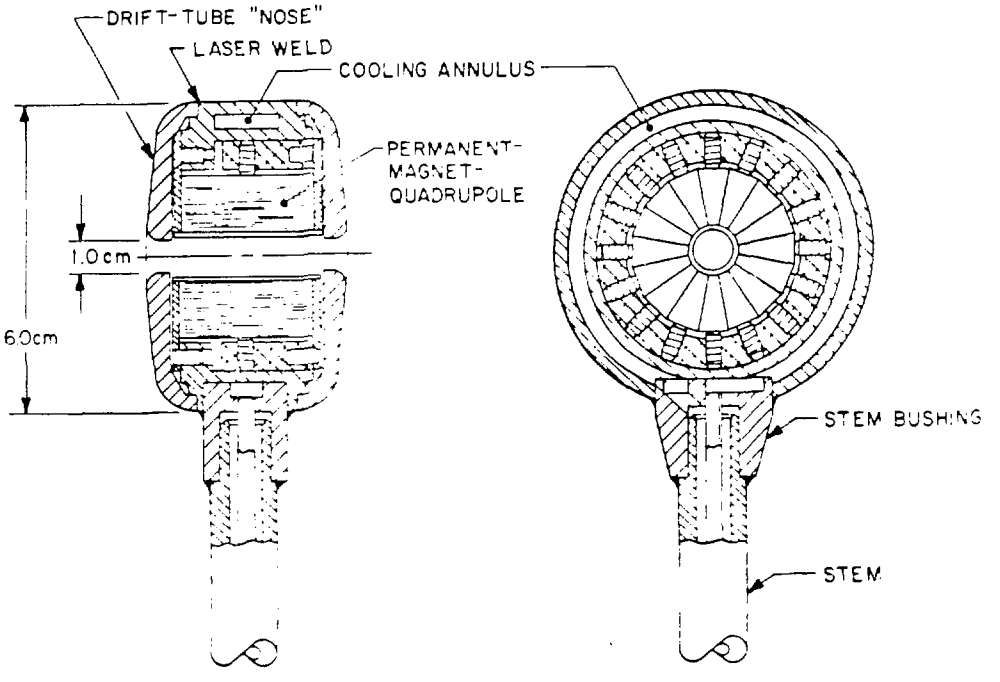

Fig. 11.
Drift-tube and quadrupole configuration in DTL.

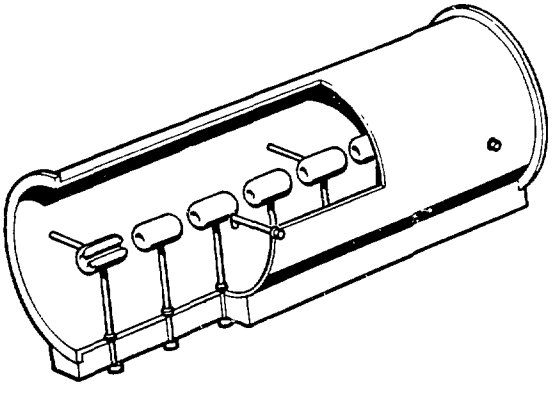

Fig. 12.
Cutaway view of the DTL structure.

are made of samarium cobalt and are magnetized to produce a quadrupole gradient of 20 kG/cm over the 1-cm-diam bore.

The DTL structure is designed and analyzed with the aid of the linac design and simulation code, PARMILA. The structure accepts essentially 100% of the accelerated beam from the RFQ and accelerates it to 125 MeV. Figure 13 shows the size, phase, and energy profiles of the beam; Fig. 14 shows the input and output phase spaces. The beam suffers essentially no emittance growth in the DTL.

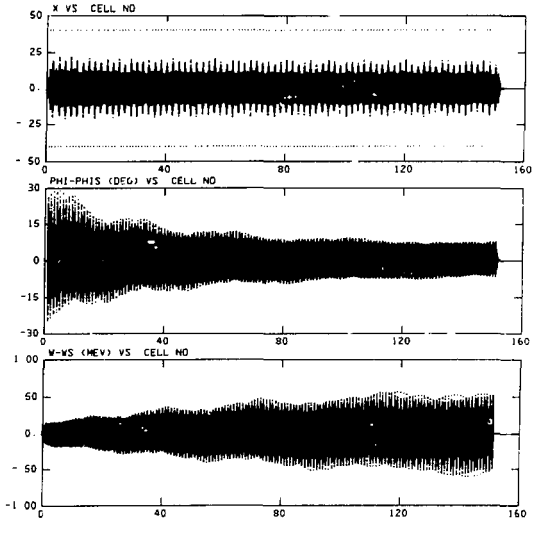

Fig. 13.
Beam profiles for the PIGMI DTL.

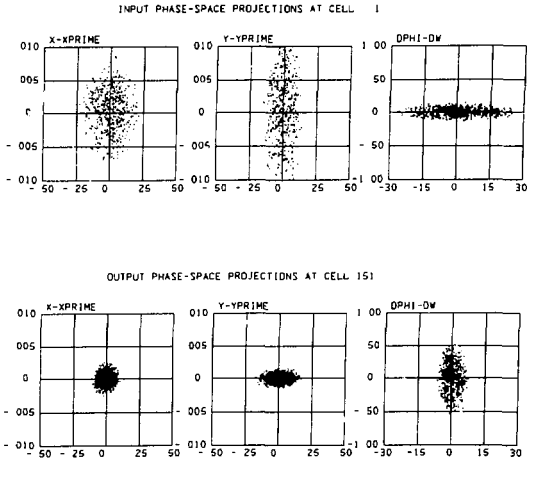

Fig. 14.
Beam phase spaces for the PIGMI DTL.

The 30-m linac structure is fabricated as 12 tank sections, each ~2.5 m long. The ends of the tank sections are located at points corresponding to the midplane of a drift-tube gap. The length, number of drift tubes, and maximum energy associated with each of the tank sections are given in Table I. The general mechanical features of the first and last tank sections are shown in Fig. 15.

TABLE I
PIGMI DTL TANK SECTIONS

Section	Length (m)	Number of DTs	Energy (MeV)
1	2.502	30	13.4
2	2.570	19	25.0
3	2.375	14	35.7
4	2.556	13	47.2
5	2.411	11	57.5
6	2.624	11	68.5
7	2.557	10	78.7
8	2.433	9	88.2
9	2.550	9	97.8
10	2.360	8	106.5
11	2.443	8	115.2
12	2.680	8	125.0
Total	30.061	150	125.0

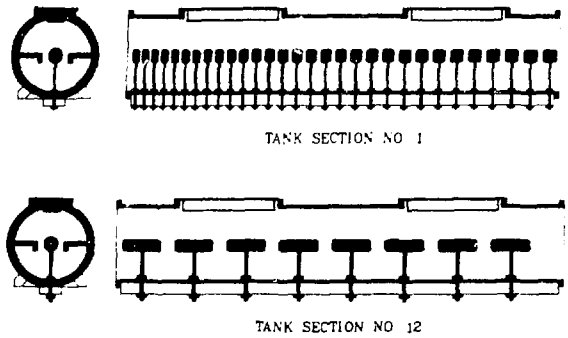

Fig. 15.
First and last DTL tank sections.

The tank sections are stiffened along the bottom by a structural member that supports the drift tubes. The drift-tube mounting holes are precision bored through this structural member and the tank wall. Post-coupler mounting holes are bored along the side of the tank at locations corresponding to the midplane of every other drift tube and alternating from side to side of the structure. Each tank section has two half-meter-long slots in the top surface for access to the interior and for mounting vacuum pumps, fixed tuners, variable tuners, etc.

Before assembly of the entire structure, each tank section is fully assembled, complete with drift tubes, post couplers, tuners, monitor loops, etc. The drift tubes are aligned with the centers of the end flanges. The tank sections can be terminated by a conducting plane at each end; then the fine tuning on the resonant frequency and the adjustment of the post couplers can be done.

For final assembly, the tank sections are joined together and supported by their end flanges, which are aligned. The end flanges are supported directly from the floor by support structures that have good transverse rigidity and poor longitudinal rigidity. The center of the DTL structure is anchored to a rigid longitudinal support.

E. Coupled-Cavity Linac

Significant discoveries made at Los Alamos during the development of LAMPF in the 1960s led to the development of practical CCL structures for acceleration of protons at energies in excess of 200 MeV. The major advance made at that time was the recognition of the importance of using biperiodic standing-wave structures excited in the $\pi/2$ cavity mode.[25] The structure developed at that time is called the side-coupled structure[26] and, when properly tuned, offers high efficiency in the conversion of rf power to beam power, with exceptional stability in the distribution of the accelerating fields--a feature that is essential for reliable operation.

The Russians, interested in building a LAMPF-type machine, considered the LAMPF side-coupled structure and two other structures: namely, the ring-coupled structure and a DAW structure. They selected the latter because of its large intercavity coupling constant and its potential for simple fabrication.

When the PIGMI program began, we assumed that the "high-beta" portion of PIGMI would use a scaled-down version of the LAMPF side-coupled structure, and we sought only to increase the intercavity coupling and to simplify the fabrication. The result of our search was the development of the DAW structure, which satisfies both of these goals.[27] A cutaway view of the DAW structure is shown in Fig. 16.

SUPERFISH,[28] a powerful rf-cavity calculational program was developed at Los Alamos, partly in response to the needs of the PIGMI program. This program was used to analyze the DAW structure in detail. Exhaustive computer studies with this program, coupled with test-cavity experiments, led to a thorough understanding of the performance of this structure and to an optimized set of parameters for the PIGMI application.[29]

In long linac structures, such as PIGMI, it is necessary to break the structure into shorter sections to allow introduction of auxiliary apparatus such as beam-focusing quadrupoles, beam-diagnostic equipment, vacuum isolation

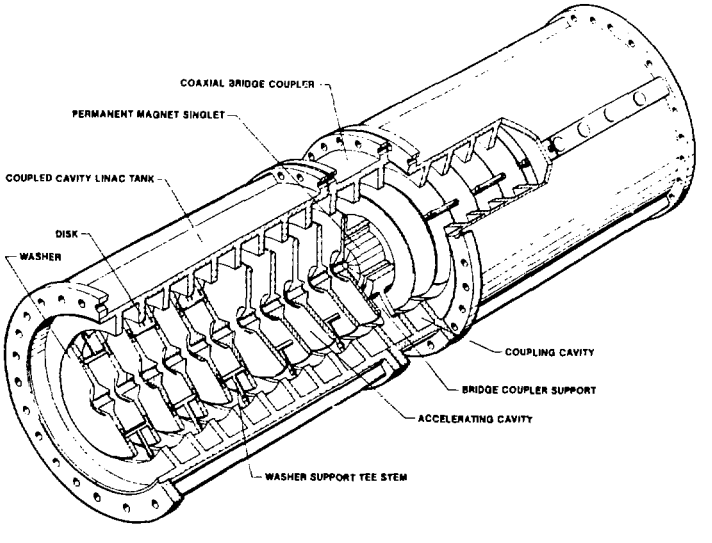

Fig. 16.
Cutaway view of the DAW structure.

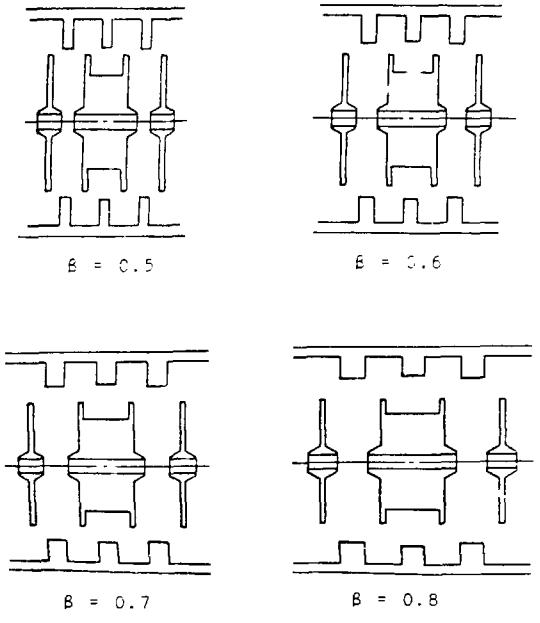

Fig. 17.
Single-cell bridge-coupler geometries.

valves, etc. In many cases, it also is desirable to couple these sections into longer resonant units to reduce the required number of rf-power drive points and to lock the relative phase and amplitude of the fields in adjacent sections. To take optimum advantage of the superior properties of this structure, any required rf couplers should also be of the resonantly coupled type, with large coupling constants; for practical reasons of structure tuning, the rf coupling of the linac structures should represent a minimum distortion of the field patterns in either element. Such couplers at LAMPF have been called bridge couplers because they bridge the resonant properties of the linac structure around the auxiliary apparatus.

To adequately house the required apparatus within the linac structure,[30] single-cell bridge couplers have been developed for the PIGMI application. Figure 17 shows the general geometry of these bridge couplers for the values of β equal to 0.5, 0.6, 0.7, and 0.8. There is a region of high magnetic field and zero electric field in the center of each bridge coupler. Conducting radial supports in this plane have a negligible effect on the accelerating mode and a tolerable effect on the coupling mode. Hollow conducting radial supports provide suitable channels for the services required by the auxiliary apparatus housed within the bridge couplers, such as cooling water for the bridge-coupler parts, signal leads for beam-diagnostic devices, and control rods for mechanical devices. Practical designs for bridge couplers have been made that incorporate a variety of these features.

The PIGMI CCL is ~100 m long and 0.34 m in diameter, operating at 1320 MHz--three times the frequency of the DTL. It accelerates the proton beam from 125 MeV to 650 MeV, with an average axial electric field of 8 MV/m. The

peak-power dissipation in the structure is 69 MW and the peak beam power is 14.6 MW; the total peak power requirement is 81.4 MW. The average power dissipated in the structure is only 250 kW or ~2.5 kW/m.

The PIGMI CCL comprises 108 tanks of 11 cells each, whose lengths vary from 0.6 to 1.0 m. The cell geometries are uniform throughout each tank but differ from tank to tank. The tanks are resonantly coupled by 107 single-cell bridge couplers, each containing a permanent-magnet quadrupole singlet for focusing the beam. Figure 18 shows the geometry of the quadrupole singlet; all 107 quadrupole singlets are identical. They are made of a ceramic material magnetized to produce a quadrupole gradient of 5 kG/cm over the 2-cm-diam bore. The bore-hole diameter of the structure and of the bridge coupler is 2 cm.

The CCL structure is designed and analyzed with the aid of the linac design program, DAWDSN, and the linac simulation program, DAWLIN.[31] The structure accepts essentially 100% of the accelerated beam from the DTL and accelerates it to 650 MeV. The size, phase, and energy profiles for the beam are shown in Fig. 19; the input and output phase spaces of the beam are shown in Fig. 20. Essentially, the beam suffers no emittance growth in this portion of the PIGMI facility.

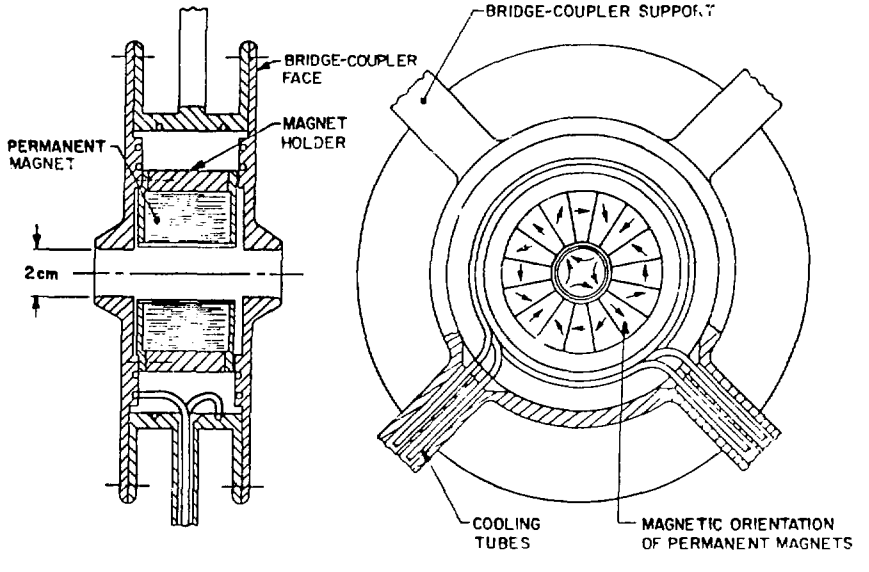

Fig. 18.
CCL bridge-coupler and quadrupole configuration.

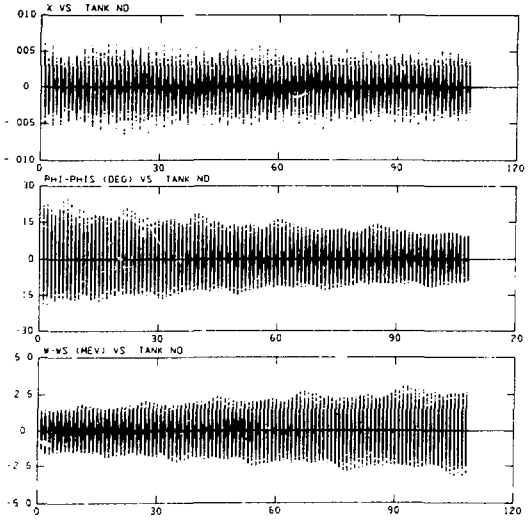

Fig. 19.
Beam profiles for the PIGMI CCL.

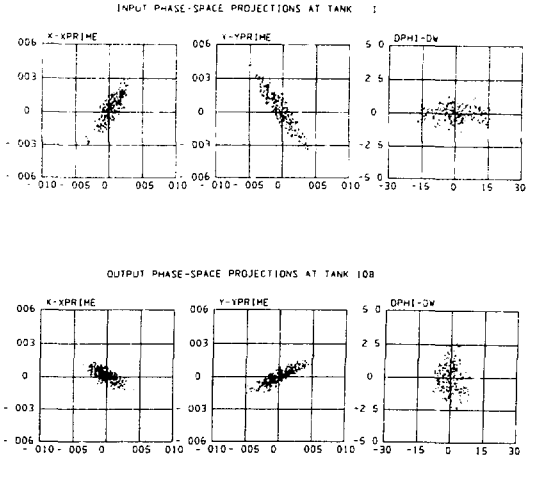

Fig. 20.
Beam phase spaces for the PIGMI CCL.

For the purpose of the facility's organization, the CCL is subdivided into 6 modules of 18 tanks each. A high degree of similarity is imposed on the organization of each module with regard to the distribution of the necessary auxiliary features such as rf drive points, beam and accelerator diagnostic instrumentation, and vacuum equipment. The center bridge coupler of each module accommodates one of the six 1320-MHz rf power systems. Each module's end bridge coupler is outfitted with a coaxial ceramic window and a compact beamline valve to provide vacuum isolation between modules for maintenance purposes. The remaining bridge couplers accommodate an array of vacuum pumps and diagnostic gear. Figure 21 shows a typical module, and Table II gives the length and maximum energy associated with each module.

Before fabrication of each tank, the parts are assembled in a temporary fashion to check the resonant frequency and the stop band between the accelerating mode and the coupling mode. If changes are necessary, they are made to the individual washers. When these constraints are satisfied, the fabrication of the tank is completed. The tanks are then joined in small groups to test the properties of the

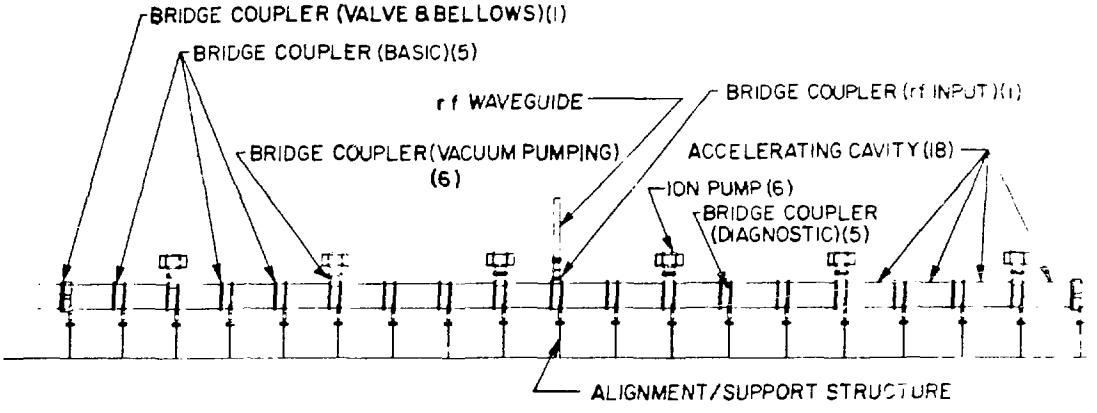

Fig. 21.
Typical module of the CCL.

TABLE II
PIGMI CCL MODULES

Modules	Length (m)	Number of Tanks	Energy (MeV)
1	12.60	18	193
2	14.61	18	271
3	16.22	18	357
4	17.52	18	450
5	18.56	18	548
6	19.42	18	650
Total	98.93	108	650

bridge couplers; if minor changes are required in the bridge couplers, they can be made at this time. When the entire structure is assembled at its final destination, only minor tuning should be needed to achieve the desired resonant frequency and field distribution.

F. The Radio-Frequency Power Systems

The PIGMI frequencies of 440 MHz and 1320 MHz were chosen partly on beam-dynamics considerations and partly on the availability of suitable klystrons. Many military radar klystrons have been designed to operate in the 400- to 450-MHz band and the next higher frequency band of 1250 to 1350 MHz. The PIGMI frequencies, which must be harmonically related, were chosen to fall in these ranges.

The costs of the rf systems were compared for three different beam-pulse patterns of similar duty factor: namely, 10-μs beam pulses at a 360-Hz repetition rate, 30-μs beam pulses at a 120-Hz repetition rate, and 60-μs

beam pulses at a 60-Hz repetition rate. The shorter beam pulse and higher repetition rate reduce the cost of the pulse-forming network (PFN) modulator but consume more average power because of the larger number of cavity fill times. The longer beam pulse and lower repetition rate result in a 100-kW power saving over the medium-pulse alternative and in a 240-kW power saving over the short-pulse alternative. The 60-μs, 60-Hz option has been adopted for PIGMI because the power savings resulting from the lower repetition rate will override the additional cost of the PFN modulators associated with the longer pulse length.

The cavity power dissipation for the 440-MHz portions of PIGMI (RFQ and DTL) are estimated to be 16.2 MW, and the beam loading for this same region corresponds to 3.5 MW. The rf pulse length must exceed the beam pulse length by the cavity fill time of ~15.6 μs. The rf duty factor is $60 \times 75.6 \times 10^{-6}$ or 0.004536. The total peak-power requirement at 440 MHz is 19.7 MW, and the average-power requirement is 89.4 kW. A single Varian VA-812E klystron can satisfy both the peak- and average-power requirements of the 440-MHz portions of PIGMI.

The cavity power dissipation for the 1320-MHz portion of PIGMI is estimated to be 66.8 MW, and the beam loading for this same region corresponds to 14.6 MW. The cavity fill time of the 1320-MHz structure is only 3.6 μs, and the rf duty factor is 0.003816. The total peak-power requirement at 1320 MHz is 81.4 MW, and the average-power requirement is 310.6 kW. Five Litton L-5081 klystrons are capable of satisfying both the peak- and average-power requirements of the 1320-MHz portion of PIGMI. The PIGMI design is based on six such klystrons operating at a reduced level, providing the possibility of continued operation if there is failure of a single klystron.

An appropriate PFN modulator has been designed and is being fabricated for the PIGMI component test program. Figure 22 shows the modulator and Fig. 23 shows the general physical properties of the 1320-MHz rf power system.

G. Computer Control and Instrumentation System

The PIGMI control and instrumentation system will provide the operator with a three-state control: namely, OFF, STANDBY, and ON. The STANDBY and ON states are identical in that all equipment is on and running within tolerance, with the exception that in the STANDBY state the beam is inhibited at the ion source and certain beam stops are inserted.

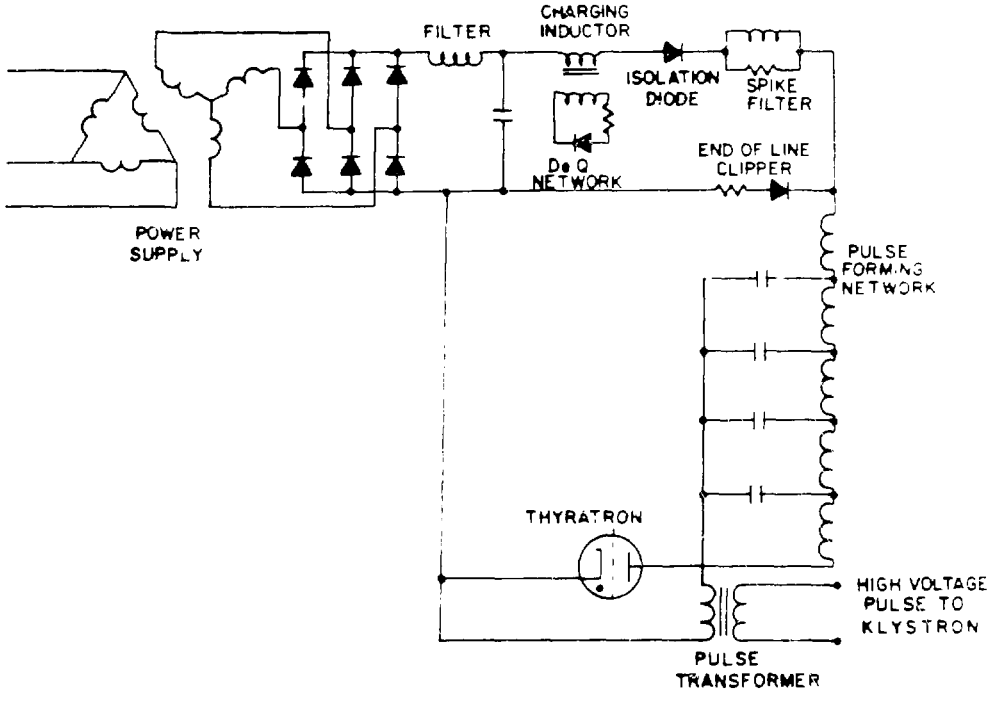

Fig. 22.
Diagram of PIGMI modulator.

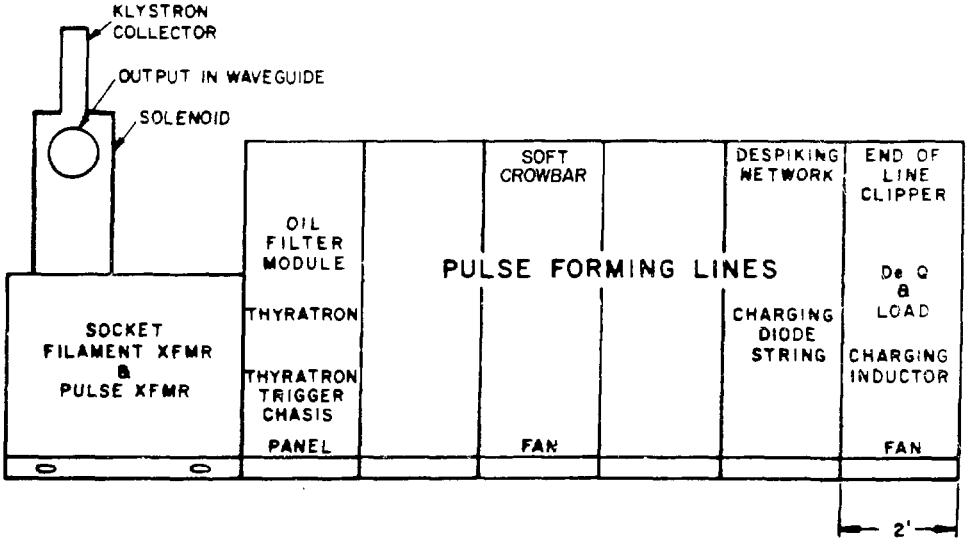

Fig. 23.
PIGMI rf power station.

In either of these states, the operator can monitor the detailed performance of every system in the facility. All set points designed to influence the performance of the machine are available to the operator through the control system; these set points can be set up, monitored, and/or recorded for future setup purposes by convenient parameter-management procedures.

In the ON state, the operator can monitor the beam properties, beam-loss evidence (if any), and beam-loading effects on the accelerator equipment systems. Certain tuning procedures will be available to the operator for fine tuning of the performance.

If there is equipment failure, the control and diagnostic system will identify the faulty equipment and will notify the operator. In some cases, further diagnostics may be available to pinpoint the unit that should be replaced; most repairs will be accomplished by unit replacement.

All critical parameters will be monitored periodically and will be compared to their current set-point values and tolerance limits. The operator will be notified of out-of-tolerance conditions, and in some cases corrective action will be automated. Selected data will be collected on a regular basis for general and specialized logs to support machine records and statistical studies of machine performance.

As shown in Fig. 24, the control system consists of a minicomputer, a control console, and a distributed array of small, modular, and intelligent control stations. The design is based on an advanced architecture developed and demonstrated at FERMILAB. The design benefits from state-of-the-art engineering and from years of experience in controlling an operating linac. This general configuration soon will control several new accelerator facilities, including the injector linac and the antiproton accumulator ring at FERMILAB. The PIGMI system will benefit from these related applications.

The equipment systems under the surveillance of the control system include injector parameters, cavity field parameters, temperature control, forward and reflected powers, PFN-modulator parameters, beam diagnostics, beam-spill radiation monitors, and some electromagnetic quadrupoles and steering magnets. Some protection systems, such as the personnel safety, the run-permit, and the fast-protect, are implemented independently of the control system and provide their status, but no control, to the computer control system.

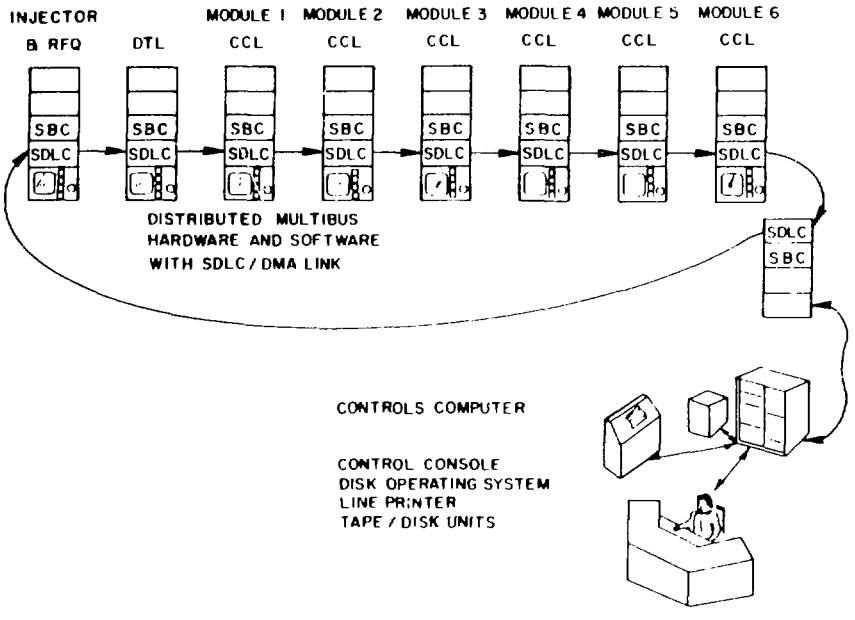

Fig. 24.
PIGMI control-system configuration.

The control system will experience its heaviest load during commissioning, routine accelerator-maintenance periods, and subsequent turn-on. These are also the periods in which the greatest demands will be made for good response from the system. The system will be expected to support accelerator maintenance with effective diagnostic testing and exercising of all subsystems. It will provide straightforward and, in some cases, automatic procedures for machine turn-on, tune-up, and fault recovery. Effective and responsive control will be provided at the operator's console, including visual displays and timely execution of operator instructions. During the initial commissioning period and subsequent machine-development periods, the control system will support a variety of beam-diagnostic measurements.

III. CONCLUSIONS

PIGMI can be built! All the technologies have been developed or identified. These technologies give rise to a new breed of proton linacs that will be reliable, modular, easy to maintain, and easy to operate. These new

linacs will find numerous applications in the arenas of both medical and nuclear science. Medical applications will include pion generation, neutron generation, radioisotope production, and proton beams for diagnosis and treatment. When combined with an EBIS, PIGMI yields a very attractive heavy ion acceleration scheme, which some of our medical friends have labeled with the acronym HIGMI. PIGMI offers to nuclear science economical sources of medium-energy protons at medium intensity and, if used with storage rings, also offers both long and very short pulses. There are many interesting applications of PIGMI technologies: for many of us in the medical and nuclear-science fields, there is a PIGMI in our future.

MICROWAVE AND MAGNET-SYSTEMS SECTION

I. INTRODUCTION

A new section was formed in AT Division in June 1980. Its purpose is to design, build, and test equipment in the following areas: high-power rf systems, rf structures, and magnet systems for beam transport. Below we discuss the status of different projects in these areas.

II. RADIO-FREQUENCY SYSTEMS

Parts have been ordered and assembly started on the PIGMI 1300-MHz rf system. The system has a variable pulse length (made possible by changing line sections) of from 5 to 100 μs; the output power is 7 MW peak and 30 kW average. The system is a straightforward line-type modulator design.

Continental Electronics of Dallas, Texas, is proceeding with the 80-MHz system for the FMIT Facility. A preliminary design review was held in August and only minor discrepancies were found. The low-power rf test system for Continental Electronics was completed and shipped to them in November. Work immediately began on the prototype low-power rf system. Two main tasks are being pursued to complete the design: finish breadboarding the phase-detector system and the frequency-control system. A contract was placed for the coaxial lines, as well as associated hardware for the entire project, with Dielectric Communications of Raymond, Maine.

Work has continued on the 440-MHz rf system for the Accelerator Test Stand (ATS) program; assembly is proceeding on schedule. This system is a long-pulse, modulating-anode system with a 100-μs pulse length and an output power of 1.25 MW peak and 60 kW average.

III. RADIO-FREQUENCY STRUCTURES

Three RFQs presently are being designed or rebuilt. AT Division has leased a three-axis milling machine. We are now able to machine our own RFQ vanes in the Division's branch shop. A decision was made to rebuild the PIGMI RFQ. After disassembly, examination revealed severe arcing on the vanes. It was not possible to determine the complete history of the vanes; however, it

was clear that they had been severely abused during initial aging, subsequent running, and the attempt to find the breakdown limit. The condition of the entire RFQ indicates that the required tolerances are not as tight as originally anticipated. New vanes are being fabricated for the PIGMI RFQ. RFQs for the ATS and FMIT programs also are being constructed. It appears that the best fabrication technique is to make the vanes out of mild steel and then plate them with copper. This gives a better surface finish on the vanes than electropolished copper and makes them stronger. Considerable work has been done to resonate the slots that couple the manifold to the RFQ. This is being done in an effort to interlock the fields in the two parts of the structure. The slots can be made resonant by using an adjustable, capacitive flap in the center of the slot; however, this scheme causes an increase in the coupling factor and creates a possibly troublesome potential for TE_{11N} modes in the manifold.

Buncher cavities are being designed for the PSR short-pulse mode. If these cavities are not tuned between each bunch extraction, then more than 350 kW of rf power will be required. If the cavities could be tuned during the bunch extraction time, the required power decreases to 25 kW. Preliminary tests on a cavity that is coupled to the buncher cavity, then tuned with an appropriately coated audio-speaker cone, look promising. We believe the cavity frequency can be varied at an appropriate rate when a ramp is driving the speaker.

Work is continuing on the DTL model for the FMIT Facility. The proton velocity varies rapidly from cell to cell, and so far, the extreme tilt sensitivity is causing considerable tuning difficulty. We will try to lower the Q to induce a measurable power-flow phase shift and thereby reduce the problem's magnitude.

Initial cold tests have been run on a DAW structure tuned to compensate for the T-shaped (TO) supports. The measured Q, with the supports brazed (but with the outer walls clamped), achieved 75% of the theoretical Q when the end-wall losses were removed from the measurement. Parts of the TE_{110} passband below 4.0 GHz have been identified. The measured R_{sh}, with an assumed Q of 15 000, was 8 MΩ/m at a 1.4-cm radius.

IV. MAGNETS

Preliminary designs of the injection magnets and the ring magnets for the PSR are being defined. Some time has been spent investigating the use of solid-core versus laminated-core magnets for the PSR ring magnets. It now appears that the laminated core will be used.

Permanent-magnet pieces for the drift-tube quadrupoles in PIGMI are on order. Assembly techniques now are being studied, as are measurement techniques for the small drift-tube bore. Experience has shown that the small magnet sections are extremely fragile.

V. THE GYROCON RADIO-FREQUENCY-GENERATOR PROJECT

The entire effort in this reporting period was devoted to completion of the prototype gyrocon. The gyrocon consists of several major units: the gun assembly, the deflection cavity, the output cavity, the bender cone, and the output couplers. Some interference was found between the valve on the gun section and the deflection cavity, and between the output and deflection cavities. These were rectified by modest remachining of these components. The most serious problem encountered was the mismatch of resonant frequencies in the deflection and output cavities. The resonant frequency of the output cavity had been measured before the cavity was copper plated; it was very close to that of the deflection cavity. After the output cavity was copper plated, the measurement was repeated and the mismatch problem was discovered. The output gap was remachined and four rings were added to lower the frequency. This process included several iterations of cutting the rings, measuring the new frequency, and then continuing the cutting. In late September 1980, the gyrocon was assembled, and all water and vacuum joints were found to be leak tight. A view of the assembled gyrocon is shown in Fig. 25, and a simplified cross section of the gyrocon is shown in Fig. 26.

The gyrocon is too large for the klystron oven, so it was baked with heater tapes to ~80°C. Initially, the vacuum pressure was too high to allow the beam and the rf drive to be on at the same time; but after ten days of pumping, both could be driven simultaneously. Severe multipactoring was noted at a low level of ~100-W drive, and further increases in drive power

Fig. 25.
The prototype gyrocon and its modulator after assembly.

produced no more fields in the deflection cavity. The beam current was varied from 0.5 to 8.0 A and the gyrocon was operated using 100-μs pulses at repetition rates from 0.2 to 1 Hz. Under most conditions of magnet and beam currents, 30 to 60 % of the cathode current was intercepted by the collector, and very small amounts of rf power (usually about 10 W) were produced at each rf output

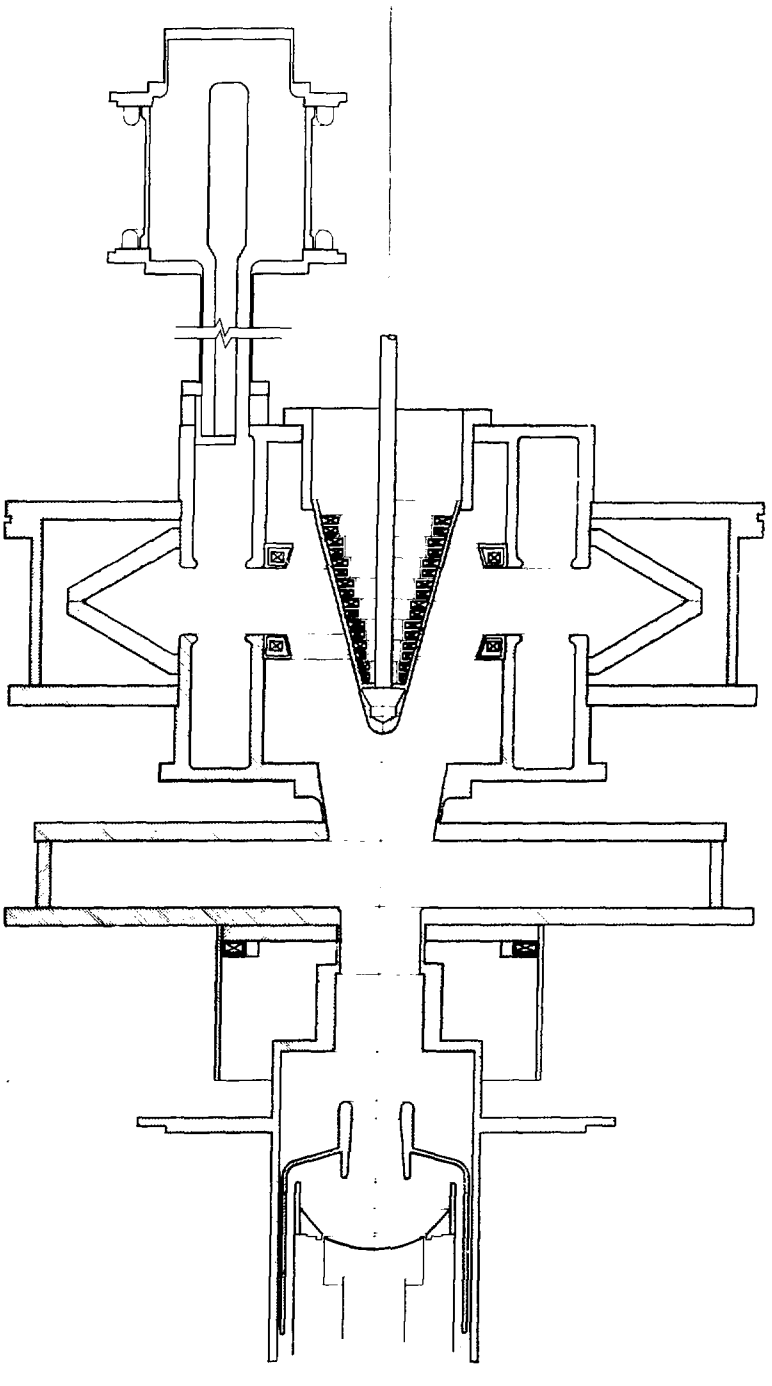

Fig. 26.
Cross section of the prototype gyrocon.

line. The collector is isolated from ground and a bias voltage of ±100 V can be applied to the collector. This experiment indicated that most of the electrons arriving at the collector were of low energy and were probably scattered by the bender cone. A quadrupole bender magnet, located between the electron gun and the vacuum valve, was designed and built. We obtained maximum transmission to the collector when the beam was misaligned and made to strike the side of the cone. By experiments with the quadrupole bender, we noted good agreement between the gyrocon's electrical and mechanical axes.

The electron gun had a leak that appeared as soon as the gun was assembled. This leak was temporarily repaired with Vac-Seal and the gun was baked in the klystron oven before the gyrocon was assembled. The gun has always been partially poisoned. It would produce full space-charge limited currents for only an hour, and then the cathode current would steadily diminish. By the end of the reporting period it was decided to take the bender cone out, coat the deflection cavity with titanium to reduce the multipactor problem, and build a phosphor-screen and aperture-plate system to view the electron beam after it reaches the deflection cavity. The electron gun will eventually have to be replaced, but this will be done only after the phosphor-screen experiments have been completed.

THE RADIO-FREQUENCY QUADRUPOLE LINEAR ACCELERATOR (RFQ)

I. RFQ GENERAL DEVELOPMENTS

A. RFQ Linacs with Lower Injection Energy and Higher Electric Fields

In the design of conventional linear ion accelerators there is usually a premium on having a dc injector with a voltage as high as possible. A high voltage reduces the length of the linac required to produce a given final beam energy. Also, a conventional linac normally is injected with a bunched beam, which causes a beam-current bottleneck at the input. Because the beam-current capacity increases with ion velocity, a higher injection energy also is desirable to increase the beam-current capability of the linac.

In a typical RFQ linac, this situation is radically changed. Because most of the RFQ is devoted to bunching the beam, the length required to produce a given final energy decreases with decreasing input energy.[32] An RFQ with a low input energy still has a high beam-current capacity because the current bottleneck occurs not at the input, but at the end of the gentle-buncher section where the energy is about 10 times the input value. Often this means that the RFQ input energy should be as low as possible, consistent with the ion source's ability to produce the specified ion beam current. In the final RFQ linac designs described later, these conflicting requirements have led to a 75-keV deuteron energy for the input to the FMIT prototype RFQ and a 30-keV proton energy for the input to the PIGMI RFQ linacs.

Another important aspect of RFQ linac design is the value chosen for the maximum-surface electric field.[33] The 425-MHz POP test used a value of about 30 MV/m, or 1.5 times the Kilpatrick limit. RFQ beam dynamics designs made at higher field values have shown greatly improved performance. It is unfortunate that there are very few definitive studies of how high a surface field can be used. A 425-MHz sparking test with a test resonator, performed before the POP RFQ was designed, suggested a practical limit of nearly 2.4 times the Kilpatrick limit. Based on these data and a general evaluation of the literature on rf breakdown, as well as the experience from linear accelerator laboratories, we have been led to the use of higher design fields. In Sec. II.A we discuss three 440-MHz RFQ linacs that were designed with surface electric fields of 40 to 41 MV/m (about twice the Kilpatrick limit). The final design for the 80-MHz FMIT prototype uses 17.6 MV/m (about 1.7 times the Kilpatrick

limit). The use of higher surface fields, together with the use of lower injection energy, has led to RFQ linac designs that have reduced overall length, improved beam-dynamics performance, and decreased rf power consumption.

B. Development of Computer Programs

1. The RFQ Design Program CURMAX. A computer program (CURMAX) has been written to choose the design frequency for those RFQ designs that require a maximum beam current. The program takes as input a maximum allowable zero-current transverse phase advance per focusing period, which is usually taken to be $\pi/2$; then, given the mass, charge, injection energy, and the product of initial particle wave number times aperture, the program finds the frequency that obtains the maximum phase advance. The program also produces an output in tabular form that allows an operating point to be determined at the end of the gentle buncher, which gives equal longitudinal and transverse current limits. CURMAX is useful for those high beam-current RFQ applications for which the frequency can be chosen to maximize output current. Heavy ion fusion and neutral beam heating are good examples.

2. The RFQ Design Program RFQUIK. A computer program (RFQUIK) has been written that permits fast and easy design for the RFQ. RFQUIK takes as input the charge, mass, frequency, input energy, final energy, and beam current--as well as five parameters that determine the RFQ current limit at the end of the gentle buncher. The current-limit systematics are evaluated from a different program (CURLI), which is based upon analytic formulas previously derived. RFQUIK has two modes of operation. In the first mode (fast-output mode), the user can input the remaining parameters that complete the RFQ's specification. One line of output allows the user to evaluate the expected length, power, and performance for that design. The user may continue in this mode, trying to optimize the parameters, until a satisfactory design is indicated by the line of output. Then the user can enter the desired optimized parameters in the second mode (complete-output mode), in which the program writes an input tape for a PARMTEQ beam-dynamics simulation. With the aid of RFQUIK, a complete RFQ design can be made and tested in less than 1 h. This procedure has been a valuable tool for the many RFQ preliminary designs that have been done.

3. The Beam-Dynamics Analysis Program PARMTEQ. After the parameters of a specific RFQ linac have been chosen by using CURMAX and RFQUIK, the detailed performance characteristics are determined from the multiparticle beam-dynamics simulation program PARMTEQ. This program, which was constructed within the general framework of the well-known PARMILA program, exists in three versions. The first version is referred to as PARMTEQ-A. The dynamics calculations used certain integrals that could be computed once and then stored for future use. By using these integrals, each cell could be divided into a few segments, typically four, and the coordinate transformations could be calculated for each segment. However, the transformations were valid only for particles having a kinetic energy near the synchronous energy.

In PARMTEQ-B, the second version, each cell is divided into more segments than in PARMTEQ-A, typically 8 or 10, and the changes in the coordinates are calculated at each segment by using a drift-impulse-drift technique. Compared to PARMTEQ-A, PARMTEQ-B requires more steps per cell, but each step is considerably simpler and no assumption is made about a particle's energy.

The third version, PARMTEQ-C, written by Bruce Chidley from Chalk River, differs from the other two versions by using time, rather than distance, as the independent variable. In this case, each rf period is divided into a number of segments and the changes in the particle coordinates are calculated at each time segment. The main advantages of using time as the independent variable are (1) the space-charge calculations are more straightforward and (2) the main focusing forces depend on time and not on distance. The disadvantage is that the programming logic is more complicated because, at the time the transformations are made, the particles are distributed in the z-coordinate.

All three versions have been standardized to accept the same input files and to produce similar output files, which are then usually processed by the program, OUTPROC. The output also is identified as to which version of PARMTEQ was used.

Normally, PARMTEQ-B is used as the standard version during the RFQ design process. After a satisfactory design has been achieved, the other two versions are then run as additional checks, because different techniques are used in the three versions.

C. Collaboration with CERN

(CERN) in Geneva, Switzerland, has asked the AT Division to cooperate in the design and construction of an RFQ linac. This linac would replace the SAMES dc injector, made by the SAMES Co. in France and used with the "old" 200-MHz injector linac for the CERN proton synchrotron. It will operate with a frequency of 200 MHz and will have a 100-mA peak proton current and a 515-keV output energy. We have generated a preliminary beam-dynamics design that is described later in this report. The plan is to carry out the mechanical design and construction of the RFQ vane assemblies at CERN, and then send them to Los Alamos for machining of the pole tips.

II. THE DESIGN OF SPECIFIC RFQ ACCELERATORS

A. Final Designs

Final beam-dynamics designs have been completed for three RFQ linacs. These are for the PIGMI prototype,[34] the PIGMI full accelerator,[35] and the FMIT prototype.[36] The main parameters are summarized in Table III The required rf power was estimated by using an approximate formula for structure power. The results from the formula were multiplied by 1.5 to correct for actual copper losses and for losses in the coaxial manifold surrounding the RFQ four-vane resonator.

Finally, the beam power was added to obtain the total peak power values in the table. The maximum value of the surface electric field is 40.6 MV/m for the two PIGMI designs and is 17.6 MV/m for the FMIT design.

It is interesting to compare the PIGMI prototype parameters with the parameters for the POP test. The POP RFQ beam-dynamics design, completed in August 1979, accelerated protons from 0.10 to 0.64 MeV in 1.1 m. Advances in RFQ design procedures have allowed us to design the PIGMI prototype RFQ to accelerate the same proton current from 0.03 to 1.50 MeV in the same 1.1-m distance.

The final beam-dynamics design for the FMIT RFQ has met all original specifications. The transmission efficiency is greater than 90%, the radial emittance growth is less than a factor of 3, and the overall length is less than 4 m. Figure 27 is a computer-generated plot of the FMIT prototype RFQ pole-tip shape in the x-z plane. Note that the transverse scale has been

TABLE III

RFQ LINAC FINAL DESIGN PARAMETERS

	PIGMI		FMIT
	Prototype	Full Accelerator	Prototype
Ion	H^+	H^+	D^+
Frequency (MHz)	440	440	80
Input energy (MeV)	0.03	0.03	0.075
Ouput energy (Mev)	1.50	2.52	2.00
Nominal current (mA)	30	30	100
Transmission efficiency (%)	93	91	94
Output emittance[a]	0.009	0.008	0.036
Length (m)	1.11	1.78	3.88
Peak rf power (kW)	193	400	491

[a] rms normalized area/π in cm•mrad units.

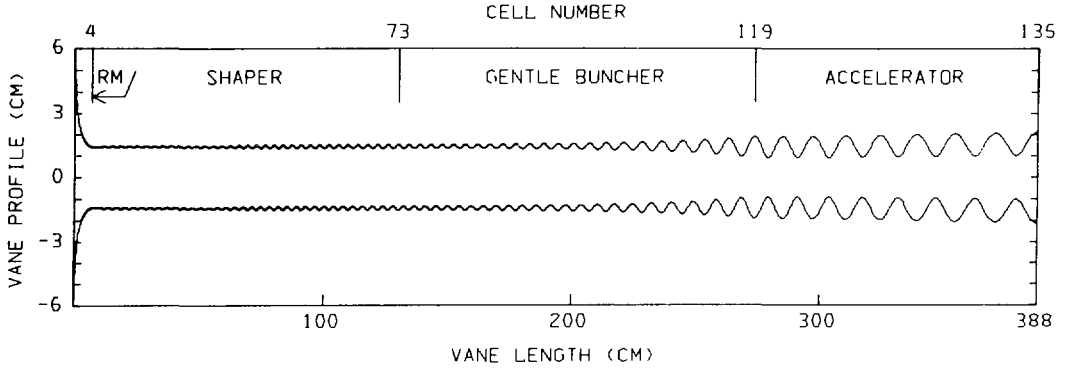

Fig. 27.
FMIT prototype RFQ pole-tip shape.

expanded relative to the longitudinal scale. The figure shows the lengths of the four functional sections: radial matching (RM), shaper, gentle buncher, and accelerator. The total length of the sections principally devoted to the bunching process (shaper and gentle buncher) constitutes a major portion of the RFQ overall length.

B. Preliminary RFQ Beam-Dynamics Designs

The design flexibility of the RFQ accelerator, together with the success of the POP test, has stimulated interest in a wide range of possible RFQ applications. Many Laboratories have requested information on how well an RFQ accelerator would perform in solving specific problems. Often, the best way to respond is by making a preliminary beam-dynamics design of an RFQ system. A great many such designs have been made, and usually they are sufficiently challenging that we benefit by working toward a solution. The following is a brief summary of six of these primary designs. A summary of the design parameters is presented in Table IV.

TABLE IV

RFQ PRELIMINARY DESIGN PARAMETERS

	AT Division	CERN	Neutral Beam	Chalk River	LBL	BNL
Ion	H^-	H^+	D^-	H^+	Q/A = 1/4	H^-
Frequency (MHz)	425	202.56	25	100	200	201.25
Input energy (MeV)[a]	0.1	0.05	0.2	0.1	0.0125	0.02
Output energy (MeV)[a]	2.0	0.515	1.0	2.0	1.0	0.75
Nominal current (mA)	100	100	1780	300	0.10	0.10
Transmission efficiency (%)	96	96	89	98	94	99
Output emittance[b]	0.018	0.04	2.1	0.10	0.016	0.01
Length (m)	2.89	1.33	3.44	4.10	4.20	1.23
Peak rf power (kW)	1150	280	3100	1640	215	66

[a]For the LBL design, the units are MeV/nucleon.
[b]rms normalized area/π in cm•mrad units.

1. RFQ for AT Division. A preliminary design was requested for an RFQ that could bunch and accelerate 100 mA of H^- from 100 keV to 2 MeV at 425 MHz, with a final normalized rms output emittance of 0.02π cm·mrad or less. The resulting design[37] was made, assuming a maximum surface field of 40 MV/m (2 times the Kilpatrick limit). The length was 2.89 m and the total peak-power requirement, including the manifold and the beam, was 1.15 MW. The beam-dynamics simulation with PARMTEQ predicted 96% transmission for an input beam of 105 mA with an input normalized rms emittance of 0.016π cm·mrad. The output beam of 101 mA had a normalized rms emittance of only 0.018π cm·mrad, which was within the design specifications.

2. RFQ for CERN. In anticipation of the proposed collaboration between CERN and Los Alamos, the linac group at CERN requested a preliminary design for a 100-mA RFQ injector into the old 50-MeV proton linac injector of the CERN protron synchrotron. The resulting design was made for a maximum surface field of 26.5-MV/m (1.8 times the Kilpatrick limit at 202.56 MHz). An input energy of 50 keV was chosen and the output energy was specified to be 515 keV. The length was 1.33 m and the peak-power requirement, including manifold and beam, was 280 kW. The PARMTEQ simulation predicts 96% transmission for an input proton beam current of 110 mA.

3. RFQ for Neutral Beam Heating. An RFQ preliminary design[38] was made for a presentation at the DOE Neutral Beam Workshop. The goal of our preliminary design was to obtain the maximum beam current of D^- at 1 MeV in a single channel. The resulting RFQ operated with a 25-MHz frequency and bunched and accelerated D^- from 200 keV to 1 MeV in 3.44 m. The maximum surface field was 20 MV/m. The PARMTEQ simulation predicted a 1.78-A output beam current for a 2.0-A input current. The peak power was estimated to be 1.8 MW.

4. RFQ for Chalk River ZEBRA Project. The accelerator group at Chalk River requested a preliminary evaluation of the RFQ as an injector for their electronuclear breeder accelerator. We designed an RFQ[12] that bunched and accelerated a nominal proton-beam current of 300 mA from 100 keV to 2 MeV in 4.1 m. At the 100-MHz frequency and a 22.7-MV/m peak surface field, the peak rf power was 1.64 MW.

5. RFQ Injector for LBL Medical Heavy Ion Synchrotron. In preparing a proposal[39] to the National Cancer Institute, LBL requested our help in designing an RFQ injector for a heavy ion synchrotron. The requirement was for a low-beam current of ions such as C^{+3} or Ar^{10} with a charge-to-mass ratio of 0.25. A 200-MHz frequency was chosen and the injection energy was 12.5 keV per nucleon; the peak surface field was 28.7 MV/m. It was efficient to use two separate RFQ tanks, each having different vane voltages and different apertures. The first tank bunched and accelerated the beam to 1 MeV/nucleon, and the second tank continued the acceleration to 4 MeV/nucleon. The performance of the first tank was simulated with PARMTEQ, and the results for this tank are summarized in Table IV.

6. RFQ for AGS Polarized Proton Injector. We were requested by an Argonne-Brookhaven joint collaboration to help in evaluating the RFQ as an injector into the 200-MeV linac at the Brookhaven Alternating Gradient Synchrotron (AGS). In this application, the RFQ would bunch and accelerate a low-beam current of H^- from a polarized ion source to a final energy of 750 keV. A design was generated with an input energy of 20 keV and a peak surface field of 22 MV/m (1.5 times Kilpatrick).

Information on the three other RFQ applications was presented in a paper[13] written for the Geneva Conference on High-Energy Accelerators. First, a preliminary FMIT design with a constant-bore aperture was described. Next, we discussed a 200-MHz RFQ linac for use as a DTL injector, and finally we described a low-frequency RFQ for use in a heavy ion fusion driver.

III. ACCELERATOR BEAM DYNAMICS

A. Space-Charge Limits in Linear Accelerators

Equations have been derived that allow an approximate evaluation of the limiting beam current for a large class of rf linear accelerators, using quadrupole strong focusing. Included are the Alvarez, the Wideroe, and the RFQ linacs. The limiting-current formulas[40] were obtained for both the longitudinal and transverse degrees of freedom by assuming that the average space-charge force in the beam bunch arises from a uniformly distributed charge

within an azimuthally symmetric, three-dimensional ellipsoid. For the transverse current limit, a smooth-approximation method was applied to the Mathieu equation. Close agreement has been obtained between the current limits from the formulas and the limiting current as obtained from computer studies using PARMTEQ. The resulting formulas have been an indispensable tool for RFQ design at high beam currents.

B. Improved Space-Charge Calculations for Beams Having Elliptical Cross Section

The standard space-charge subroutine used by the PARMILA family of programs, as well as by other dynamics programs, previously has made the assumption that the beam had a circular cross section. For purposes of computing the space-charge fields, each simulation particle was assumed to lie on a uniformly charged circular ring. This subroutine has been modified[41] so that beams having elliptical cross sections can be handled better.

In brief, the modification consists of determining the ellipticity of the beam from the rms properties of the x- and y-coordinates, transforming these coordinates from the elliptical frame to a circular frame, calculating the electric fields in the circular frame, and then transforming the fields back to the elliptical frame. The procedure should give correct results for a uniformly charged elliptical beam.

IV. HEAVY ION FUSION ACCELERATOR DEVELOPMENT

A. The Combination of Ion Beams by Funneling

All proposed schemes for using rf linacs to produce heavy ion beams for inertial fusion require the beam current to be increased by sequentially combining linac output beams. To accomplish this increase, it has been proposed to funnel pairs of beams together in a manner that increases the beam current with no increase in radial emittance. For this latter step it is possible to use a time-varying electric deflector to interlace the microstructure pulses and to make them collinear. This combined beam then would be further accelerated in another linac that operates at twice the frequency of the first-linac stages.

Because the rf deflector is an important element of this system, a study[42] was made of a wide variety of possible arrangements. This study shows that appropriate deflectors can be designed. However, further overall work is needed to develop a system that provides the necessary radial focusing and bunching during the funneling process.

B. A High-Current, Four-Beam, Xenon Ion Source for Heavy Ion Fusion

With M. R. Shubaly, work was completed at Chalk River Nuclear Laboratories on the design and component testing of a four-beam, xenon ion injector for the four-channel RFQ accelerator, proposed here at Los Alamos as the initial stage of a heavy ion, inertial-confinement, fusion driver.[43] In this scheme, each channel of the RFQ would provide 25 mA of Xe^{+1} for funneling into a system of electrostatically and magnetically focused linear accelerators.

The RFQ has two advantages that greatly ease the injector design. It requires a relatively low injection energy (approximately 250 keV for Xe^{+1}) and has a 97% capture efficiency,[44] so that the injector need provide only 25 mA of Xe^{+1}. The four beams must be in a 10-cm square array to match the RFQ channel spacing. A source that provides a high (~90%) fraction of Xe^{+1} would make magnetic separation unnecessary and would permit a close-coupled design that would greatly ease beam transport. High source-gas efficiency is required to reduce charge-exchange losses and to reduce the gas load. High arc efficiency would ease the requirements for cooling and for power delivery to the high-voltage dome (at 245 kV). A high-current heavy ion duoPIGatron source, developed at the Chalk River Nuclear Laboratories,[45] provides an ideal ion source for this injector. This source has produced xenon beams of up to 100 mA, current densities of over 70 mA/cm^2, with low power and gas consumption.

C. Injector Description

The proposed injector uses four plasma sources on a 10-cm square array because a single source that would provide the desired current density over a large area would require an extremely high arc power. The four sources are mounted on a common extraction and acceleration column that uses an einzel lens to provide the required focusing. To provide consistent beam characteristics with different pulse lengths and duty cycles, the plasma sources operate

continuously and an extraction electrode is pulsed to give the desired pulse length and duty cycle. The ion sources essentially are a duplicate of the Chalk River sources, with minor mechanical modification to make them fit into the available space.

Figure 28 shows one quarter of the extraction and acceleration column and one plasma-source module. The first-column electrode holds the molybdenum plasma aperture plate with an 8-mm-diam shaped aperture. For convenience, the potential of this plate will be defined as zero. The next electrode is the extraction electrode, which is held at +30 V between pulses to prevent plasma flow into the column. During a pulse, it is at -45 kV to extract the beam. The next electrode is part of the einzel lens and is at -10 kV. The following electrodes are at -45, -145, and -245 kV with respect to the plasma aperture plate. The bottom electrode incorporates a magnetic electron-suppression element to prevent damage from backstreaming electrons during the pulse. As is shown, the vanes of the RFQ penetrate into the bottom of the column. The ceramics are convoluted to reduce surface tracking and are well shielded to reduce photoelectron production by bremsstrahlung radiation from backstreaming electrons. The active regions of all electrodes are of molybdenum to reduce beam-induced sparking. The outside of the column is insulated with low-pressure SF_6.

The extraction, focusing, and acceleration optics were designed using BEAM, an ion-beam-extraction and acceleration-modeling code being developed at Chalk River. Figure 29 shows the configuration of the central region of the electrodes and the calculated ion trajectories for a 29-mA beam. At tne entrance to the RFQ, the beam is 1.3 cm in diameter and slightly convergent. The extraction voltage and the voltage on the lens electrode can be varied to change the beam size and divergence, as required by the final RFQ design.

At Chalk River, tests of the system components have verified the feasibility of this injector concept.[46] Results of these tests have shown that the shimming to operate these ion sources in an array would be straightforward, and that the extrapolated normalized emittance for this configuration would be less than the specified 0.07π mm·mrad.

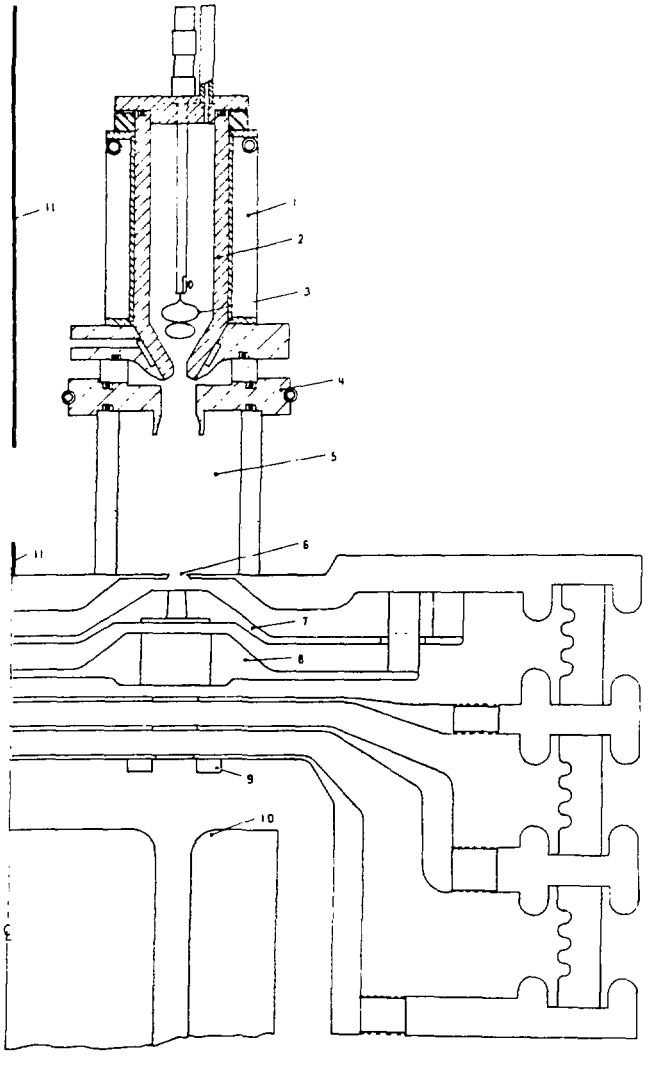

Fig. 28.
One quadrant of the injector showing (1) compressor coil, (2) iron intermediate electrode, (3) cathode, (4) anode, (5) PIG region, (6) extraction aperture, (7) extraction electrode, (8) lens electrode, (9) suppression magnet, (10) RFQ vanes, and (11) magnetic shielding.

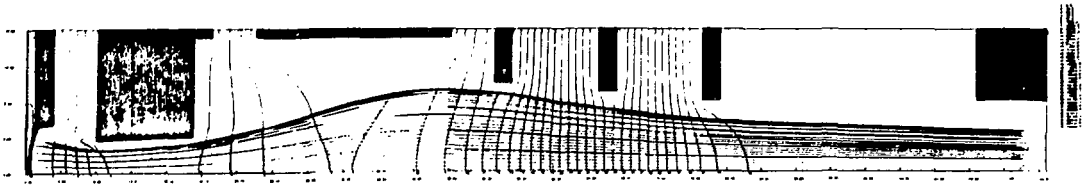

Fig. 29.
Computer simulation of ion beam optics in the injector.

A HEAVY ION LINAC FOR MEDICAL AND SCIENTIFIC RESEARCH

I. INTRODUCTION

The Electron Beam Ion Source (EBIS), because of its high charge-state ions and pulsed operation, is ideally suited as an injector for a heavy ion linac based on technology being developed at Los Alamos in the PIGMI program.[47] This combination would produce a small, efficient, heavy ion linac useful in relativistic heavy ion research or therapy. This section briefly describes the results of a design study for such a heavy ion facility.

The goal of this study was to present a conceptual design for an accelerator that would be an extension of the PIGMI design, for ions with a charge-to-mass ratio of 0.5 instead of protons. This accelerator could accelerate fully stripped ions from deuterons to calcium, but the emphasis would be on ions up to neon. This study considered only the accelerator system, because the beam transport and delivery system for medical therapy had been considered thoroughly in another study.[48] The system proposed here would meet the same medical requirements for ion-beam therapy and radiography as in the previous study. Emphasis is placed on using the technology currently being developed to make the accelerator system small and efficient.

The final 550-MeV/nucleon energy was assumed to give a range in tissue of greater than 30 cm for all ions from carbon through neon.[48] This energy also makes comparison with proposals for a synchrotron possible, because this is approximately the same value as that used in these proposals. The required beam intensities for obtaining a dose rate of 600 rad-ℓ/min in a 1-ℓ tissue volume, with a depth of 2.5 cm, are then from 3.4×10^9 particles for helium to 3.0×10^8 particles for neon. Because present medical requirements are for integrated doses, there is no direct requirement for a specific duty factor; therefore, it can be determined for optimum operation of the facility.

II. EBIS INJECTOR

The EBIS, shown schematically in Fig. 30, consists of a very dense, energetic, electron beam, magnetically confined within a series of insulated cylindrical electrodes along the axis of a solenoid. The space charge of the dense electron beam creates a radial potential well that traps ions as they

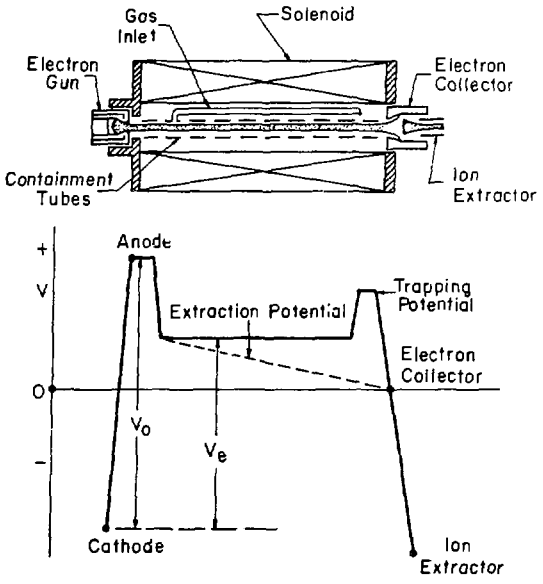

Fig. 30.
Schematic of the EBIS.

are created by ionization of atoms injected into the electron beam. A potential distribution, applied to the insulated electrodes, prevents the axial escape of the ions and they become highly ionized by successive electron impact ionizations. The ions are trapped within the electron beam until the production of a desired charge state has reached its optimum; they then are extracted by lowering the axial potential on the output end of the source. The total positive charge in the ion source cannot exceed the negative charge in the electron beam, and the ionization rate of the ions is dependent on the current density of the electron beam; thus, the total ion current extracted from the source in each pulse is proportional to the electron-beam current, whereas the confinement period to achieve a particular charge state is inversely proportional to the electron-beam-current density.

III. PROPOSED ACCELERATOR

The heavy ion linac proposed by combining the EBIS and PIGMI technologies is shown in Fig. 31. This system, designed for injection of fully stripped ions up to calcium ($q/m = 0.5$), is the optimum design for a low duty factor heavy ion linac. The maximum charge state for the ions (fully stripped) is attained in the injector by the use of the EBIS; the maximum acceptance possible into the accelerator (approximately unity) is attained by the use of the RFQ; and the maximum accelerating gradient and efficiency is attained in the accelerator (within the limits set by rf sparking) by the use of high frequencies and a low duty factor. In addition, the low duty factor employed in the accelerator system is a perfect match to the low duty factor required in

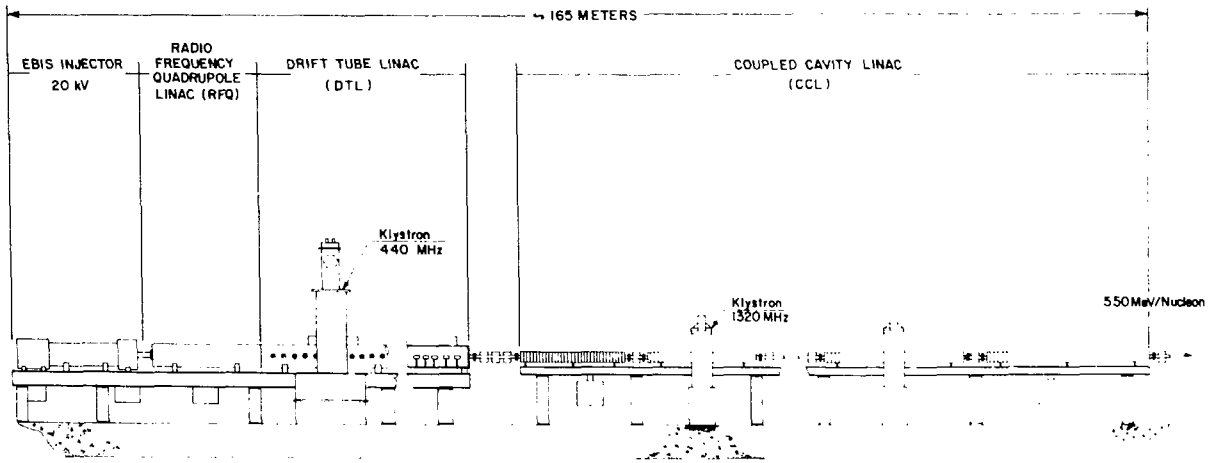

LINAC PARAMETERS

FREQUENCY	RFQ SECTION	440 MHz
	DTL SECTION	440 MHz
	CCL SECTION	1320 MHz
GRADIENT	DTL SECTION	6 MV/m
	CCL SECTION	12 MV/m
TRANSITION ENERGY	RFQ / DTL	1.5 MeV/Nucleon
	DTL / CCL	...0 MeV/Nucleon

BEAM PARAMETERS

INJECTOR VOLTAGE	20 kV
INJECTION ENERGY	10 keV/Nucleon
FINAL ENERGY	550 MeV/Nucleon
PEAK BEAM CURRENT	300-600 μA
PULSE LENGTH	30 μs
REPETITION RATE	30-120 Hz
AVERAGE BEAM CURRENT	1-3 μA

Fig. 31.
Heavy ion linac using the EBIS and PIGMI technologies.

the EBIS for production of the fully stripped ions. This low duty factor, combined with the large energy gain attained in the accelerator, minimizes the accelerator length and power consumption.

The accelerator system described above would use a cryogenic EBIS, such as CRYEBIS I,[49] for the injector. Because of the confinement time of the EBIS for the fully stripped ions required in this facility, the pulse repetition rate for the injector cannot exceed 140 Hz. The PIGMI duty factor (0.36%) can be obtained with twice the ac main cycle (120 Hz with a beam-pulse width of 30 μs); therefore, this repetition rate was chosen. Previous experimental data have shown that the ions can be extracted from an EBIS within the required beam-pulse duration, so the only work required to develop the source is to raise the pulse rate by a factor of 2 or 3 above that already obtained in CRYEBIS I, while maintaining the projected ion yield per pulse.

The use of the RFQ as the low-energy section of the accelerator would enable the ions to be injected with an injector voltage of 20 kV. This is approximately the extraction voltage used in an EBIS and can be obtained by elevating the source electrodes and electron gun, without having to use a large high-voltage dome and accelerating column. The RFQ is capable of accepting ions at this low energy and accelerating them to several million electron volts, with a very high capture efficiency, and without the aid of a separate bunching system. The RFQ beam dynamics and structure have been previously described,[18] as well as the experimental results from a structure tested on the PIGMI prototype accelerator.[14] The results of a beam-dynamics calculation for a $q/m = 0.5$ beam injected into a 440-MHz RFQ at 10 keV/nucleon are shown in Fig. 32. A yield of 10^{10} particles/pulse was assumed to be extracted from an EBIS during 30 μs. The experimental, measured, CRYEBIS I emittance of 1.2π mm·mrad was assumed for this beam, resulting in a greater than 99% capture efficiency for the structure. The final energy of 1.5 MeV/nucleon is attained with a structure that is only 3.3 m long, with a total peak rf power requirement of only 263 kW. The parameters of this RFQ are summarized in Table V.

This final energy for the RFQ makes the injection into a post-coupled DTL at the same frequency an easy technical task, because the first few drift tubes are long enough to easily use permanent-magnet-quadrupole focusing. The DTL in this accelerator is a simple extension of the PIGMI DTL to $q/m = 0.5$ particles, using the same acceleratin_ ,radient and rf source and having a

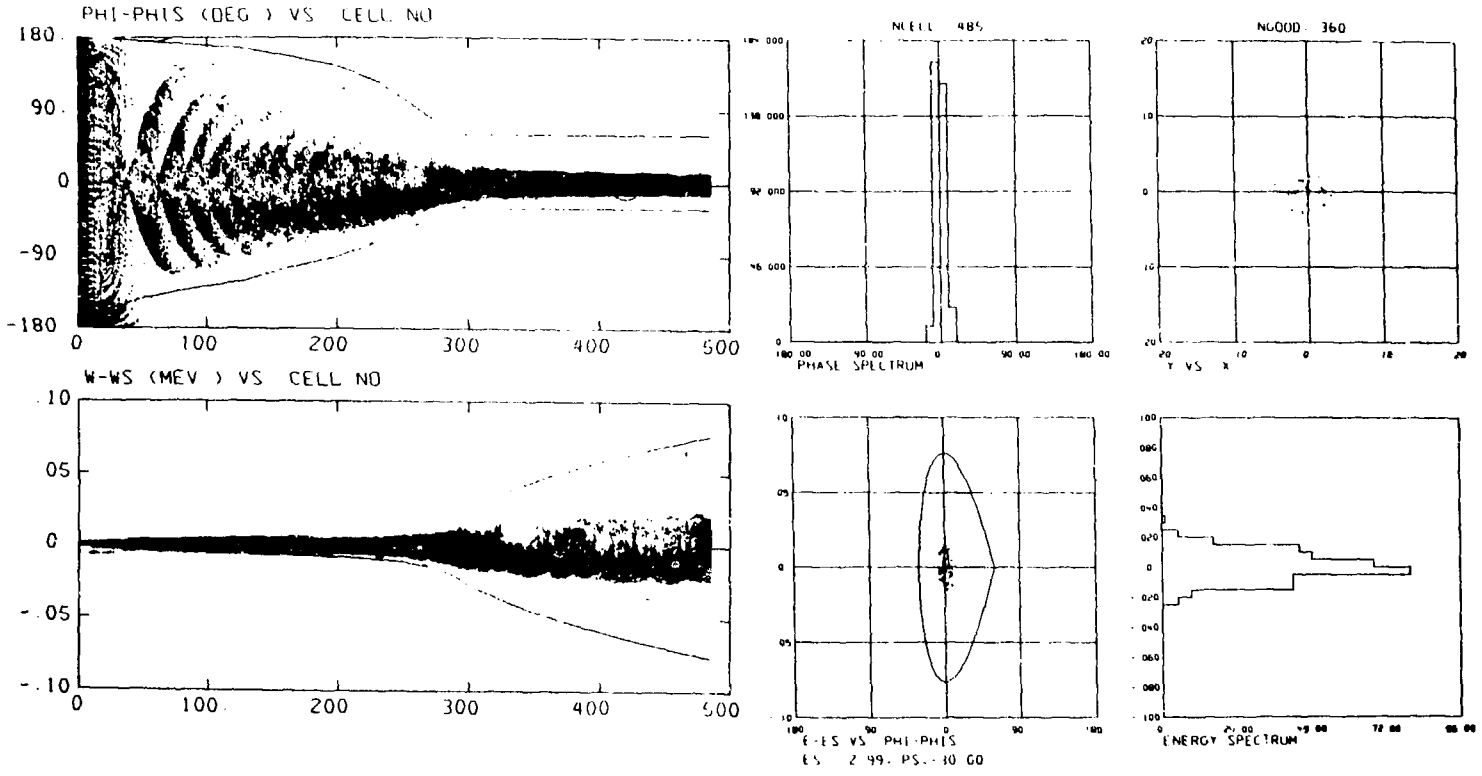

Fig. 32.
The RFQ beam dynamics for q/m = 0.5 ions.

TABLE V

HEAVY ION RFQ PARAMETERS

Injection voltage (V_i)	20 kV
Injection energy (W_i)	0.01 MeV/nucleon ($\beta\lambda$ = 0.316 cm)
Frequency (f)	440 MHz
Average bore radius (r_o)	0.187 cm
Final energy (W_f)	1.5 MeV/nucleon ($\beta\lambda$ = 3.84 cm)
Final radius (a_f)	0.147 cm
Structure length (ℓ)	3.28 cm
Final synchronous phase (ϕ_s)	-30°
Peak voltage between electrodes	56 kV
Peak rf power (including manifold)	80 kW/m

length of 38.5 m; however, to make the RFQ and DTL sections both powered by one 20-MW rf tube, the transition to the high-energy linac is made at 80 MeV/nucleon instead of at 125 MeV as in PIGMI. This energy is still a reasonable value for making this transition.

The final and largest component of the accelerator is the 118-m-long CCL, used as the high-energy portion. This linac uses the DAW structure developed in the PIGMI program and can accelerate the ions up to 550 MeV/nucleon. The only differences are that this structure would be for q/m = 0.5 ions instead of protons and would have a proposed accelerating gradient of 12 MV/m. This gradient is a very conservative extension of accelerating gradients currently used in operating medical electron linacs at somewhat higher frequencies.[50] This structure would be powered by 10 klystrons at 1320 MHz, and the peak rf power requirement would be 180 MW.

Thus, operating at 120 Hz with a 30-μs beam pulse, this accelerator would produce the required currents for medical therapy with an average power consumption of 720 kW. Assuming rf efficiencies of 35%, the total accelerator power requirement would be about 2 MW. A total operations and maintenance staff of 8 to 10 people would be required for such a system (just above the

PIGMI figure) because of the more complex injector and slightly longer machine. In addition, this system would use the same rf power sources and computer control systems as the PIGMI system. Both the 440-MHz klystron (Varian VA-812E) and the 1320-MHz klystron (Litton Industries L-5081) are commercially available tubes designed to operate with the approximate pulse width and duty factor required in this application.

TURBINE ENGINE LOADS SIMULATOR

The Turbine Engine Loads Simulator (TELS) is a turbine-engine test facility proposed for the Air Force by the Headquarters Arnold Engineering Development Center in Tennessee. This test facility would be capable of exposing operating turbine engines to simulated maneuver forces. An important part of the proposed facility is a radiographic system that would provide information regarding the effects of different loadings on the internal clearances and distortion of a gas turbine engine.

Turbine-engine radiography has been used successfully on stationary test stands of engine manufacturers for some years. Radiography has not been applied, however, to the study of turbine engines operating under simulated flight-maneuver conditions, where engine components are subjected to inertial forces. Depending on the location of the various accelerator components, all or part of these components must be capable of operating in an acoustical and mechanical environment generated near an operating turbine engine being subjected to facility-induced inertial loads of up to 21 g's.

The x-ray source requirements are

Bremsstrahlung spectrum	x-ray photons with energies to 10 MeV
Bremsstrahlung flux	a minimum of 3000 R/min at 1 m
X-ray pulse rate	variable from 50 to 350 pps
X-ray source size	1.25-mm diam

The most feasible choice for satisfying these requirements is an electron linear accelerator.

Los Alamos has contracted to perform a study of possible electron linear accelerators for the proposed application. Viable configurations of existing and developable S-band and C-band components will be studied and the advantages and disadvantages of each system will be established.

Systems in which the rf source is on the center of rotation, as well as those where the rf source is located on the gimbal near the turbine engine, will be included. The following characteristics are to be considered: radiation; reliability; size; weight; cost; susceptibility to inertial forces and vibration; support system requirements; and ease of operation, control, and maintenance. In addition, those critical components of each system that may need development will be identified and an estimate will be made of the developmental cost, time, and confidence. Where possible, the results of this study will be presented in matrix format for concise comparison. Finally, a recommendation for a system will be made with realistic estimates of cost, construction times, and performance.

FUSION MATERIALS IRRADIATION TEST PROJECT (FMIT)*

I. INTRODUCTION

The accelerator design activities for both the FMIT Facility and the FMIT prototype accelerator (FPA) continued during this reporting period. The contract for the FPA linac tank was awarded and the tank fabrication is progressing on schedule. The remainder of the FPA components are in final design. A preliminary design review of the FMIT accelerator occurred in August 1980 and was followed by additional reviews to address those problems identified at that time. Final design is well under way for all components of the FMIT accelerator.

To complete the construction package for the accelerator vault and support areas, the Los Alamos group worked closely with the architectural engineering firm responsible for the FMIT facility. This package was released for bid, the contract was awarded, and construction will begin in March 1981.

Effort for building the FPA was directed to three major areas: accelerator cooling system, facility control system, and rf-equipment installation. The contract for installation of the water-cooling system was awarded. The cooling tower with supply and return lines, was installed and the design of the water manifold up to connections to the accelerator was completed. The computer room, with associated utilities, was finished and the computer equipment was installed; this move was accomplished with minimal interruption of computer activities. The FPA building is being prepared to accept delivery of the rf equipment in the late spring of 1981. The design of the Phase C electrical-power distribution system for the rf-power amplifiers was completed. The bid cycle was started for a platform to support some of the rf equipment, and specifications were written for a 10-ton bridge crane. Award of the contract for the crane is expected to occur in January 1981.

Title II for the office building was completed. The construction contract was awarded and construction will start early in 1981.

*Work supported by the DOE Office of Fusion Energy in cooperation with the Hanford Engineering Development Laboratory (HEDL).

II. ACCELERATOR

A. Injector

Tests of the ion source and extractor geometries continued during this reporting period. The test-stand operation was significantly improved by the installation of the new 125-kV, 250-mA power supply for the FPA injector. This power supply uses vacuum tubes to achieve a voltage regulation of ±0.01%. Upon delivery, the power supply performed to specifications into a resistive load; however, sparking and ground-loop problems immediately arose when it was used on the test stand. These were eliminated by a modest redesign of the control and grounding circuits.

An attempt was made to increase the total extracted current to greater than 200 mA by increasing both the current density from the ion source and the areas of the apertures in the extractor. All tests run with the increased-area apertures (2.5 cm^2) yielded beams of substantially poorer quality (increased divergence, larger aberrations) than earlier 100-mA beams from 1 cm^2 apertures. It was assumed that the exit-lens effect at the extractor's ground electrode was dominating the beam characteristics. Additional problems were caused by increased beam impingement of the electron trap and by increased backflow of negative particles. The series of tests, using larger current densities and 1-cm^2 apertures, required higher electric field gradients inside the extractor; this, when coupled with power supply difficulties, led to frequent and unacceptable sparkdowns. Also, the ion source required high arc currents, which severely limited the filament lifetime and reduced the H_2^+ ion fraction.

As a result of the above tests, the last 4 months of the year were spent calculating spherically convergent extractor systems that would allow the use of a large aperture at the ion source (thus reducing the current density) and a much smaller aperture in the ground electrode (thus minimizing the exit-lens effect). Several preliminary designs were checked on the injector test stand before it was shut down in November; the shutdown was in deference to the installation and start up of the FPA injector. Calculations and experiments in December indicated a convergent geometry that promised to provide the desired source-extractor performance. The design was fabricated and will be tested as soon as the FPA injector is operational.

It was announced in August that the length of the FMIT RFQ linac could be reduced by at least 40% if the vane-tip electric fields were increased and if the injection energy were decreased. This prompted an investigation into the possiblity of operating the injector at a higher perveance value, that is, lower injection energy. A quick series of experiments indicated that there should be no fundamental problem except that of aberrations caused by the exit-lens effect at the extractor's ground electrode.

The ion source used throughout this period was the all-copper cusp-magnetic-field unit built more than 18 months earlier. Modified magnet placements were shown to improve overall source operation, that is, increased H_2^+ ion fraction with somewhat reduced source efficiency. To provide a cleaner operating ion source and to facilitate construction, an all-stainless-steel source was designed and fabricated.

Considerable effort was expended in assembling the vacuum system for the FPA injector, including the incorporation of an industrial programmable controller to provide versatile control and automatic sequencing of all injector vacuum pumps and valves.

A magnetic-deflection beam pulser was assembled between the extractor and analyzing magnet. A low-inductance magnet, consisting of a few turns of conductor on a ferrite core, was built. The magnet is powered using a series ballast resistor between the supply and the magnet and yields magnetic field rise-and-fall times of 0.25 ms. Pulsing of the beam with this magnet will be attempted as soon as possible.

B. Radio-Frequency Quadrupole Linac

1. Mechanical and Radio-Frequency Design Considerations. By the end of 1980 the beam-dynamics analysis and the rf design concept were developed to the point of fully specifying the parameters for the FMIT RFQ. Better understanding of RFQ beam dynamics produced a recommendation to reduce injection energy to below 100 keV. Another major development was the discovery of arcing damage in the POP RFQ that led to an important conclusion regarding a limit for the electric fields in the FMIT design. Finally, a good-quality beam-transport match allowed effective transmission of the beam from the RFQ into the DTL.

A design team consisting of one engineer, one technician, and two designers was organized to take over the RFQ design and to implement the analytical parameters. They attacked the outstanding mechanical problems of adequate cooling and of acceptable rf joints.

Subsequent estimates were made of the effects of vane-tip positioning errors on the RFQ's performance. It was determined that the beam performance is far more tolerant of such errors than the rf tuning; thus, fabrication-precision and vane-alignment tolerances are dictated more by rf considerations than by beam transmission. To accommodate the high level of alignment precision required to control capacitive coupling between the vane tips, the design appproach was shifted from rigid to flexible vane supports. This shift was contrary to decisions reached earlier in the year but was due to expanded analysis and a deeper appreciation of the critical nature of the required vane alignment.

The entire fabrication problem was greatly simplified by the decision to operate the RFQ at electric fields considerably above the Kilpatrick level (10.6 MV/m at 80 MHz). This decision was made after the discovery of arcing damage in the POP RFQ; the final field level selected was 1.7 times Kilpatrick (17.6 MV/m). These relatively high field levels permit the RFQ's length to be reduced considerably from that anticipated earlier in the year. The fixed length of the unit is about 4 m, which offers a major simplification to many fabrication problems.

2. Design Parameters - Beam Dynamics. The analysis of the RFQ's beam dynamics progressed to the point where the design parameters for the FMIT RFQ linac could be specified.

In the analysis (as has been stated previously) the maximum-surface electric field was allowed to increase above the nominal 1.5 times the Kilpatrick value that had been used in previous analyses. The dimensionless focusing parameter B was decreased linearly in the RFQ accelerator section, from an initial 6.823 value to a final 5.200 value, to facilitate radial matching into the DTL. This corresponds to a tapered increase of the average radius within the accelerator section.

Table VI lists the RFQ design parameters. The rf power estimate is based on a formula for the RFQ structure power. The RFQ structure power is multiplied by a factor of 1.5 to include actual copper losses and manifold losses. To this we add a beam power of 193 kW for a 100-mA beam. This results in a 491-kW total power.

Table VII lists the input conditions and Table VIII the calculated output. In these tables, W_i and W_f denote the beam energy at the input and output of the RFQ, respectively. The parameters α and β describe the emittance, and I is the beam current. Two computer programs, the T-code and the Z-code, were used to model the beam dynamics. Although the codes differ in the method of calculation, the results agree reassuringly.

TABLE VI

RFQ DESIGN PARAMETERS

Frequency	80 MHz
Ion	D^+
Number of cells	135
Length	388.11 cm
Vane voltage	184.5 kV
Average radius, r_o	1.423 cm
Final radius, a	0.998 cm
Final modulation, m_f	2.129
Initial synchronous phase, ϕ_i	-90°
Final synchronous phase, ϕ_f	-30°
Estimated rf power (including RFQ, manifold, and beam)	491 kW
Nominal current limit	205 mA
Nominal acceptance at 100 mA	0.73π cm·mrad (normalized)

TABLE VII

INPUT CONDITIONS

W_i	0.075 MeV
β	31.7 cm/rad
α	3.66
E_n (100%)	0.10π cm·mrad (normalized)
E_n (90%)	0.070π cm·mrad (normalized)
E_n (rms)	0.0167π cm·mrad (normalized)
I (mA)	108.3 (T-code); 106.1 (Z-code)

TABLE VIII

OUTPUT CONDITIONS

	T-Code Results	Z-Code Results
W_f (MeV)	2.00	2.00
E_n (90%)	0.17 π	0.16 π
E_n (rms)	0.038 π	0.036 π
Transmission	92.5%	94.1%
I (mA)	100	100

C. Beam Diagnostics

The beam-diagnostics activity was a three-pronged effort. First, considerable effort was directed toward understanding the underlying physics of the noninterceptive beam-diagnostic techniques. Second, computer programs were generated and recoded to be compatible with the FPA computer system; these computer programs will be used for data reduction, beam-emittance reconstruction, and optimizing the placement of the diagnostic sensors. Third, electronic hardware design and implementation were continued using an independent contractor. The mechanical design of much of the nonelectronic hardware was expedited by adding a mechanical engineer to the diagnostics group.

The development program was completed for high-bandwidth, radiation-hardened cabling and seals for the drift-tube beam-position monitors. The installation met all requirements, including ease of assembly.

Designs were essentially completed for the four-view-mirror optical system and the dc transductor for the low-energy beam-transport system. A design was completed, and a vendor located, for a fiber-optic imagescope to be used in those locations where there is insufficient space to install the mirror system.

A time loop and its associated fast electronics were ordered. These units are of a special design compatible with the requirements of the FMIT facility beam-diagnostics system.

D. The Radio-Frequency System

Work is proceeding in a number of areas on the prototype rf system for the FMIT project.

A preliminary design review was held at Continental Electronics in August, and the high-power rf-amplifier design was approved.

Dielectric Communication is supplying the 14-in. coaxial line for the FPA, FMIT, and the high-power test stands at Los Alamos and Continental Electronics. This contract is also proceeding satisfactorily.

A low-power (100-W maximum output) driver was designed, fabricated, tested, and shipped from Los Alamos to Continental Electronics in December 1980. This driver will power their high-power amplifier for testing purposes. The low-power driver is capable of fully testing their equipment in accordance with the specifications.

The FPA low-power rf system, including the feedback control systems, is in the final design phase.

The frequency control system that searches for, locks onto, and tracks the tank's resonant frequency as it approaches 80 MHz has been breadboarded and is presently being checked out. This system also controls the slug tuners, once the tank reaches 80 MHz, to maintain tank frequency.

The phase-and-amplitude feedback controllers were breadboarded and tested. Printed-circuit boards also were fabricated and tested.

Work is in progress on the linear digital phase detector. We are addressing some problems that have been encountered that involve resolution and bandwidth.

A single rf chain, up to the 100-W level (including feedback control systems), is being breadboarded and will be tested into a resonant load. This test should reveal any major design deficiencies. Changes then can be incorporated into the final FPA low-power rf system design.

A considerable effort has been spent by the Radio-Frequency Section to investigate experimentally the problem of rf field penetration from the linac into the vacuum-bellows region of the drift-tube support system. From information gained through tests using the quarter-scale model FPA linac, the problem appears to be quite serious. The rf section worked with the girder-design team on developing and testing a suitable rf seal for the drift-tube-stem/spanner-hatch-cover interface.

An rf window test section is being designed and fabricated. This consists of two ceramic rf windows, separated by 2 ft. of 9-in., 35-Ω, coaxial line that is evacuated. This window section will be taken to Varian, EIMAC Division, San Carlos, California, and tested at full power (600 kW) into a resistive load. This high-power test is designed to point out any deficiencies in the window design. Any problems can be corrected before window installation on the FPA tanks. This early testing is essential because of the long lead times required to obtain ceramic windows.

E. FMIT Facility Control System

1. Summary. The Facility Control System (FCS) for both the FMIT prototype accelerator and the FMIT facility is being designed and implemented by the combined Instrumentation and Control (I&C) Section from AT-4 and FMIT-HEDL. Additionally, the PSR I&C section has adopted much of our preliminary design and hardware selection to facilitate the design of that control system.

The FMIT FCS design calls for two computer systems: one in the central control room to drive a control console and one consisting of several remote data-collection and control stations [Instrumentation Subsystem (ISS)]. The FPA control room, containing the two main computers, is shown in Fig. 33; Fig. 34 shows the FPA console; Fig. 35 shows the FPA Injector ISS installation and local control equipment, with interface equipment and local CRT display terminal.

The control console contains two raster-scan graphic displays, two 12- by 40-character plasma panels with incremental shaft-encoding knobs, and

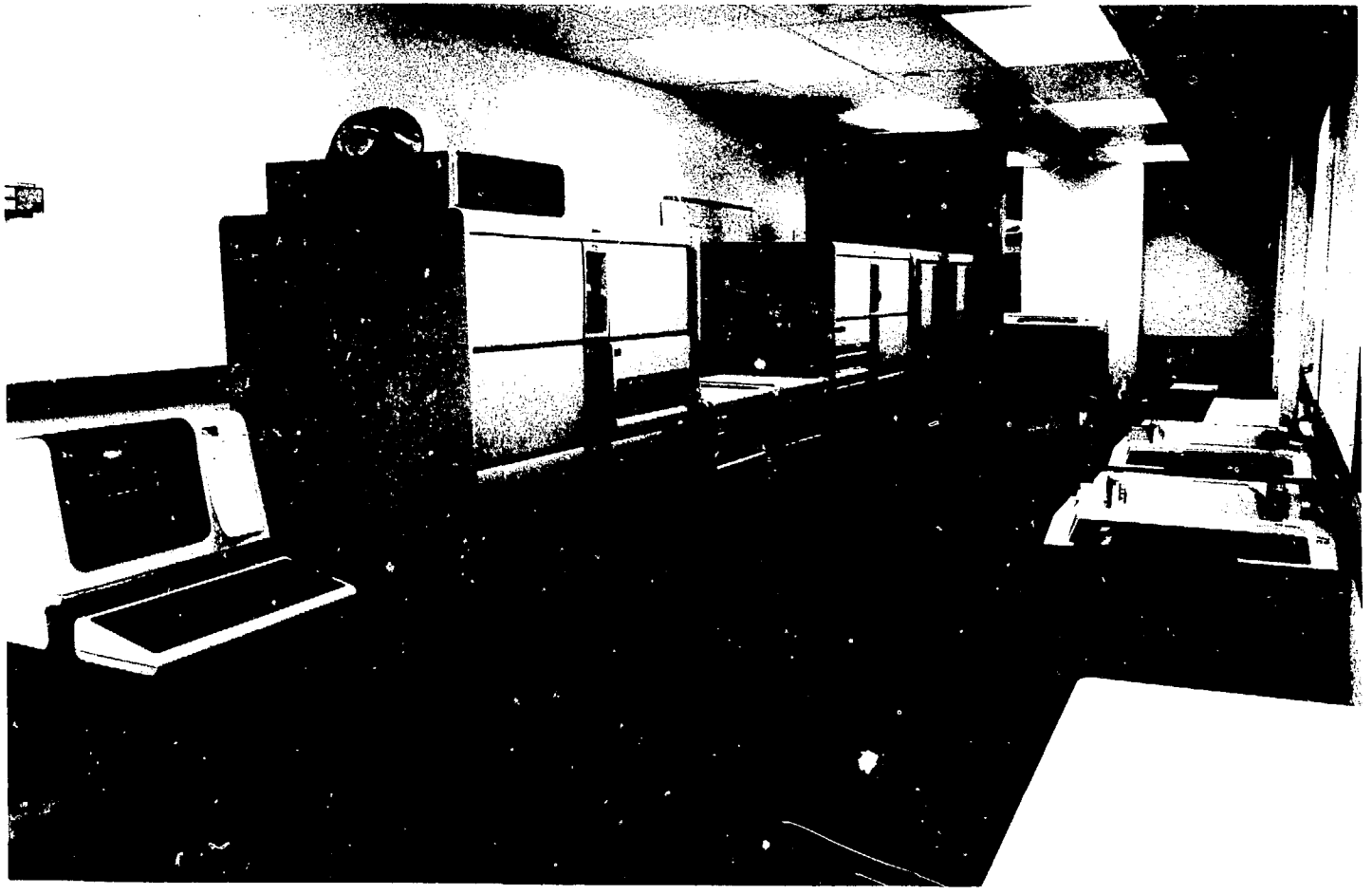

Fig. 33.
FPA control room.

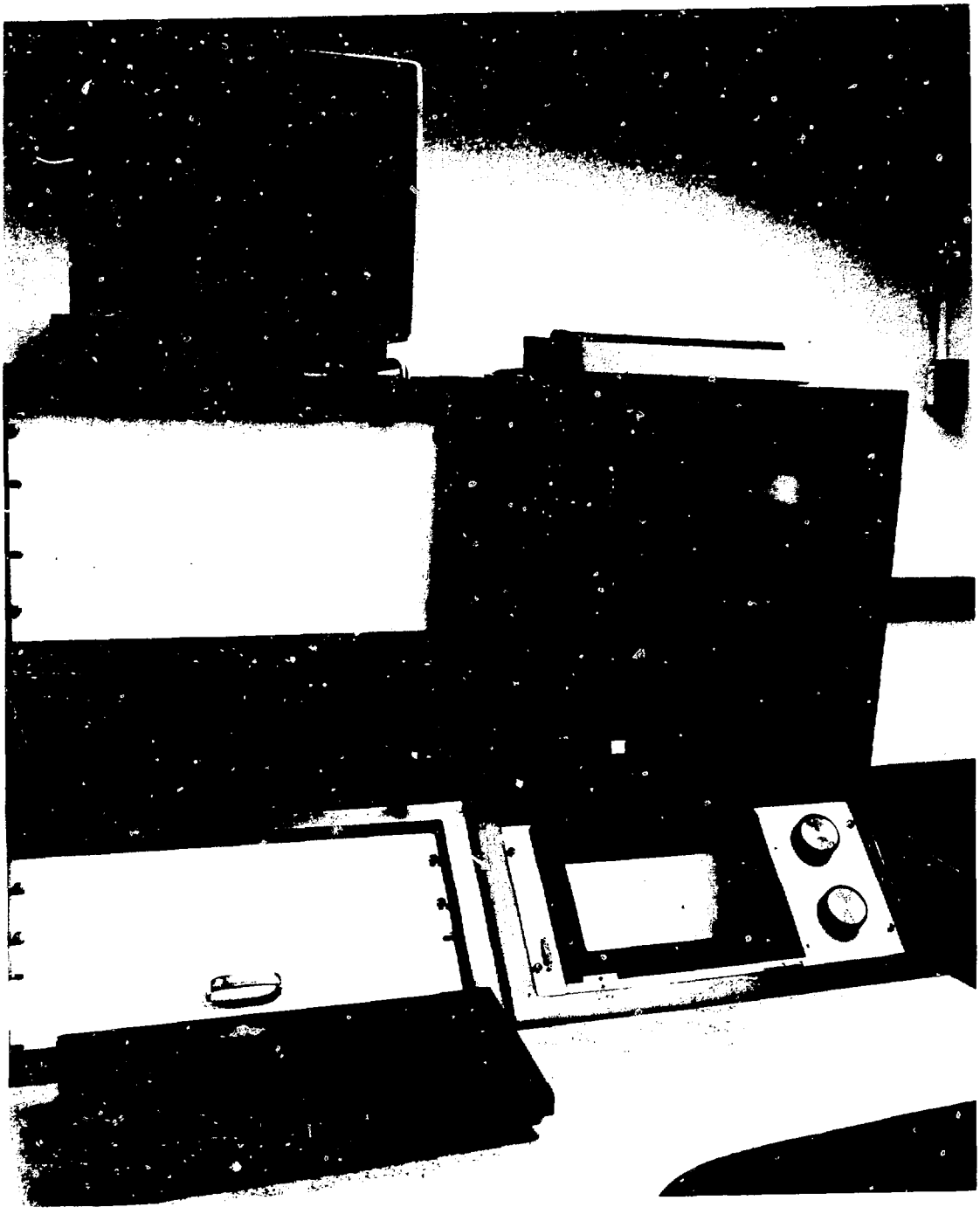

Fig. 34.
FPA console.

Fig. 35.
FPA injector ISS installation.

keyboard entry devices. The console also contains facility intercommunications: telephone, closed-circuit television monitor and analog oscilloscope, with patch connection to the facility proper.

The remote ISS equipment contains microcomputer processing hardware and interface modules connecting to the various controlled or monitored systems. A local CRT display will provide a way to communicate directly with the ISS hardware.

2. System Software. The main computers (DEC PDP-11/60 for the FPA) and the ISS processors (DEC LSI-11/23 microcomputer) both run under a real-time, multitasking operating system (called RSX-11M in the case of the main computers, and RSX-11S in the case of the ISS processor). A major evaluation was completed during this reporting period on the commercially supplied and supported data communication software program, proposed for use between our main computers and the ISS equipment. During the FCS Preliminary Design Review of December 1979, the FMIT Steering Committee expressed concern whether the vendor-supported network communications software (DECNET) was fast enough to support supervisory control requirements for the accelerator subsystems. The evaluation and demonstration were performed to provide the data for resolving this design question.

For the accelerator prototype, the evaluation used the computer control system that consists of two PDP 11/60 computers connected with data communication links to two LSI 11/23 microcomputers placed near the accelerator hardware.

A supervisory control system is required to give the operator a "real-time" feel for the system, to monitor the system, and to report any significant unrequested changes. Thus, the computer system must be able to execute an operator command over the data communication link and return a response in "human response time" while both the PDP 11/60 and the LSI 11/23 are executing other tasks. If a response to the command is updated four times per second, the human response time requirement is considered to have been met.

A control console was assembled consisting of two VT-52 compatible LCRTs, a plasma panel, two computer-interfaced incremental shaft-encoded control knobs, and a Tektronix 4014 graphics scope.

The most difficult control function, in the sense of operator reponse time, is the turning of a control knob to vary a control parameter. The knob is interfaced to the 11/60 by an RS-232 link and is software connected to the chosen control parameter through the plasma panel. A feedback channel is displayed on the plasma panel; if the feedback channel is displayed at least four times per second, the operator should feel that he is controlling the parameter in "real time." At the same time this control is being exercised, one or more displays of data should be updated at one time per second. Another task would be the request for data at random times, in addition to surveillance.

Several programs were written to demonstrate various control features, including the periodic logging of a set of data channels; the display of the channel data base on a CRT; the software connection of control knobs to form command channels; the display of several channel values on a CRT; and examples of reading data channels, making a calculation, and plotting the results on the Tektronix 4014. The results of these tests are subjective at best, but CRT displays of channels that are responding to command channels can be updated at least five times per second. Data arrays of 100 points for plotting can be read, transported over the link, and plotted in 2 to 3 s. These times are obtained while other tasks are running and requesting data.

The results of the evaluation showed that the DECNET communications software program, together with intelligent data link controllers located at each processor, can satisfy the requirements for control of an accelerator facility such as FMIT.

3. Application Software and Hardware. The remainder of the reporting period was spent in creating application software and hardware for the FPA injector and cooling systems.

The existing programs for the injector system were converted to FORTRAN code to run on the FMIT standard ISS processor. Work is now under way to convert these codes to the FMIT standard software structure, as defined in our preliminary software design.

Parallel to the software conversion effort, the injector ISS has been designed and was being installed as this reporting period closed. A programmable controller from the Gould Company was purchased for evaluating the injector vacuum system. This unit controls the logical turn-on and operation of the vacuum pumps and valves and will interface to the injector ISS soon.

Design description of the operator's console software and the cooling-system software was begun. These codes will be implemented during the next reporting period.

Much of the required hardware for the injector and cooling-system ISS, and for local interface equipment (racks, instrumentation power supplies, etc.) has been purchased and received. In addition, following the failure of one unit during this period, an extra 64-K word memory module for our main computers was purchased, to serve as an on-line spare.

The final implementation of our CATY interactive test software has been completed. The configuration operates on the FMIT standard ISS processor with a multicrate CAMAC Serial Highway. Test software need not know that the CATY system accesses other crates during an operation, and the software can be operated from the control console or from the local CRT terminal by involving the DECNET communication software features.

An interim hardware configuration has been created for the beam-diagnostics equipment because of the lack of software manpower to implement necessary code in an ISS processor. Until this software can be implemented the diagnostics data will enter our control computer by a separate, nonstandard route.

F. Drift-Tube Linac

1. Summary. A fabricator was chosen, and construction began for the prototype DTL tank. Only one major design feature remained somewhat uncertain, pending additional testing on the 363-MHz functional model. That feature was the positioning of the post-coupler ports. The present design places the upstream post coupler at the first free-hanging drift tube and advances down the linac in odd-numbered positions on alternating sides of the tank. Testing of the model will examine the tuning advantages of starting at the second drift tube. This apparently minor point may prove to have dramatic consequences in the effectiveness with which the prototype tank can be tuned.

Designs also were completed on the downstream end-closure bulkhead for the prototype tank; effective mechanisms were designed for both adjustment of the quadrupole magnet and strain adjustment of the tank's flexible end wall. Preliminary designs also were done on the bell housing that interfaces the RFQ to the tank; where possible, the bell-housing design will be FMIT compatible.

Design also was begun on the FMIT linac tanks and the intertank spacer. The same basic criteria apply to both the prototype and FMIT tank designs (that is, copper-clad steel, channelized single-pass counterflow cooling, rf peripherals, etc.), although differences in structural support, porthole design, and other features are present because of the more demanding requirements for FMIT.

A major accomplishment in the last half of 1980 was the completion of an operational post coupler. This unit allowed certain cost-saving decisions to be made regarding the method for vacuum sealing, as well as eliminating an expensive bellows. Concurrently, low-power testing of the 368-MHz model provided an accurate assessment of the gap-adjustment range for the prototype linac and will allow procurement of the FMIT post couplers to proceed on schedule. Another rf peripheral that progressed into the hardware phase was the slug tuner. Designs and reviews were completed, and construction of an operational model began. There were delays in fabricating the rf drive loops, because of important interface problems that had to be solved with the supplier of the coaxial drive lines. These problems (which centered around a semi-automated way of changing the rf windows) were solved, and final designs, plus material procurement for the prototype drive loop, went forward. The rf monitor loop was fabricated and approved. All of the above peripherals are required for both the prototype and FMIT. A nonprototypical peripheral, the intertank spacer, also moved into the mechanical design stage; the first problems solved were those involving interfaces with the two linac tanks, as well as problems with diagnostics.

2. Drift-Tube Girder Assemblies. Design of the structural support for the prototype drift tubes progressed in the latter part of 1980, with a strong design effort being applied to both the adjustable clamp for the drift-tube stems and the girder itself. A major technical difficulty continued to be the rf joint between the drift-tube stems and the spanner-hatch cover. All tests performed with high-power coaxial test cavities have been negative because of the presence of excessively high levels of TEM mode power in the region of the bellows. Thus, design has been directed toward a flexible-support, rf shorting collar as a backup, if the free-aperture choke joint does not work under realistic FMIT testing.

3. Drift Tubes and Quadrupoles. The drift-tube quadrupoles for the prototype were fabricated and given preliminary tests. Both Type A-2 (HiV Permendur pole tips) and Type A-1 will meet the field-intensity design goals predicted by beam-transport studies through the prototype linac. An important consideration addressed in late 1980 was that of developing radiation-hardened pottings for the FMIT quadrupoles. The quadrupole field coils for the prototype will be epoxy potted, but a more radiation-resistant method is required for FMIT; consultation with Los Alamos experts, as well as a developmental program to meet programmatic needs, was initiated.

Designs were completed for the drift-tube shells, and discussions were completed with HEDL concerning fabrication of the drift tubes for both the prototype and FMIT. A fabrication/assembly plan was developed that will be implemented for the prototype in 1981. All prototype drift tubes will be fabricated at HEDL, with the exception of the experimental drift tube, which is heavily instrumented and is being built at Los Alamos.

Alignment of the drift tubes in the girder assemblies is to be actively integrated with the alignment cart as soon as the girder design nears completion.

4. Beamstops. Good progress was made on design of the prototype and FMIT beamstop in late 1980. The design effort followed three parallel leads: activation analysis, investigation of brazing techniques, and testing. The graphite-clad copper, calorimetric design is being pursued. Activation studies by HEDL, based on the expected beam test profiles supplied by Los Alamos, have shown that a graphite sheath of sufficient thickness to exceed the range of 17.5-MeV protons is required to avoid extremely high activation of the copper calorimeter during the year of testing with H_2^+ envisioned at HEDL. A consultant from Aerojet General was invited to Los Alamos to discuss brazing techniques that will result in a good mechanical and thermal bond of the graphite to the copper over large areas. As a result of these discussions, it was decided to experiment with plates of at least 20 by 20 cm; this size represents a major increase over previous estimates of maximum feasible plate size. Finally, a test program was initiated to test the beamstop cooling system at power densities approaching those expected in the prototype beamstop (about 300 W/cm^2). Initial results of these tests, using radiant heating techniques

at about 80 W/cm^2, were very encouraging and tests are continuing in an effort to generate higher power densities.

5. High-Energy Beam Transport (HEBT) Mechanical Design. A large amount of conceptual development was completed in the HEBT mechanical design during late 1980. Most of this work involved a strong coordinating effort with R. M. Parsons Co., Pasadena, California. The primary thrust of this design was to develop a structural support for the HEBT that would be floor mounted, rather than ceiling mounted. This marked a major deviation from early FMIT designs and was prompted by concerns over maintenance and operational considerations, in light of HEDL studies of potential beamline activation. These activation studies revealed the need for elaborate collimating and shielding schemes that could not be completely assessed in terms of detailed mechanical design at this time, but that could result in considerably different loading of the HEBT modules than originally assumed. This uncertain loading potential could affect alignment in a detrimental way if the structural support were not extremely rigid. Furthermore, handling of highly activated HEBT modules is much facilitated by provision of a bridge crane. Thus, the concept of including both floor support and a bridge crane in the HEBT vault was developed. Ultimately, the floor-support design was further developed into a twin-floor concept to accommodate utility requirements in a shielded environment. The final design now includes a reasonably complete concept for purposes of maintenance and shielding.

Parallel to this effort, detailed optical design of the beamline was developed within the building constraints to provide optimum beam transport. Requirements for the quadrupoles and bending magnets were further developed, and mechanical designs for both 25- and 30-cm effective field-length designs were completed.

The magnet elements, as well as diagnostic and vacuum components, have been incorporated into a continuing series of HEBT beamline layouts, as the optics design continues to undergo changes.

In addition to the FMIT work, layouts of the prototype HEBT were completed. The prototype HEBT requires two quadrupoles, and it is intended to use FMIT quads for this purpose to fully qualify the FMIT designs in the prototype. No bending magnets are required. The supporting structure for the prototype HEBT will use steel pedestals; a preliminary design for this is complete.

6. Cooling System. Work on FMIT cooling systems during this period consisted of reviews of construction drawings to insure compatibility with the accelerator design, but most of the effort was concentrated on the FPA cooling system. A contract was let and construction was started on an FPA facility cooling system. Although this system is not identical to that of FMIT, it is sufficiently prototypic to verify the cooling and control concepts. It is to be available in the spring of 1981 for use in rf amplifier testing. The cooling-system instrumentation and its interfaces with the FCS were identified on Piping and Instrumentation Diagrams (P&ID).

Work was started on the definition of cooling-control algorithms through simulation of cooling-system dynamics on an analog computer. A local control box was designed to provide the electronics that interface between the control computer and the ac motors of control valves. The low-power, "logic-level" signals from the computer are converted to high-power ac signals by solid-state relays in the local control box. Variable-speed operation of the valves is achieved by a pulse train from the computer of variable duty cycle. This concept was breadboarded and tested on all control-valve types to be used in the FPA cooling facility.

7. The dc Power Systems. As the design of beam transport and matching has matured, requirements for magnet power supplies have changed, as has the configuration of the dc power system. In particular, the required gradients of adjacent quadrupoles have, in some cases, differed sufficiently to make it impractical to supply the current from a common power supply without shunting hundreds of amperes. These changes have resulted in the addition of six new power supplies.

Wiring connections to each quadrupole were extended to junction boxes outside the linac vault, facilitating connection of shunts and horizontal steering to any point in the beamline where start-up testing indicates the need for adjustment. Detailed schematic drawings of all dc power, steering, and shunt connections to the linac were completed and sent to Parsons and were coordinated as the basis for conduit design in Work Package No. 4.

The power-distribution and installation drawings were completed for the Phase C installation of rf power rectifiers and switchgear for the FPA building.

A magnet test stand was completed; this included a dc power supply, water-cooling source, water and temperature interlock, and a quadrupole. The quadrupole was powered during a Bitter-figure alignment test.

8. Vacuum System. An accelerator vacuum system modeled after LAMPF had been proposed for FMIT. LAMPF uses ion pumps exclusively for beam-on conditions. At the design review in August, reviewers felt that more detailed consideration should be given to alternative pump types before a final decision is made. A study was therefore performed that compared the merits of ion pumps, cryopumps, diffusion pumps, and turbopumps for use on the accelerator and HEBT high-vacuum systems. That study confirmed the original decision to use ion pumps on the accelerator tanks, provided the pump isolation valves were deleted to reduce costs.

While the study was under way, a decision was made to provide radiation shields in the HEBT, increasing the isolation between vacuum pumps and the beamline. The required pumping speed was greatly increased to overcome the increased impedence of connecting piping. The study pointed out that the most economical way to realize the high pumping speed, while meeting the other performance requirements, was with cryogenic vacuum pumps. Figure 36 shows the proposed FMIT vacuum system with both high-vacuum and roughing pumps for the accelerator and HEBT.

Vacuum pumps for the FPA have been received. These include the 1342-cfm Roots Blower with mechanical backing pumps, the 150-cfm Roots Blower with backing pump, two 26.8-cfm mechanical pumps, two 1500-ℓ/s turbomolecular pumps, one 500-ℓ/s ion pump, and one 2000-ℓ/s ion pump. Three 2000-ℓ/s ion pumps are on order. Valves and instrumentation have been identified and are to be ordered as funding is made available.

9. HEBT Design - Beam Dynamics.

a. FMIT. In July, the FMIT HEBT consisted of a periodic front leg, periodic bend system (BM = 17.3 kG), and a transport to the target with four quads focusing the beam to a 1- by 3-cm spot on the target. Working with E. Colton of Argonne National Laboratory (ANL), computer codes were rewritten to provide the proper input Gaussian beam to the third-order code RAYTRACE. New RAYTRACE runs were done that showed no significant aberrations in the

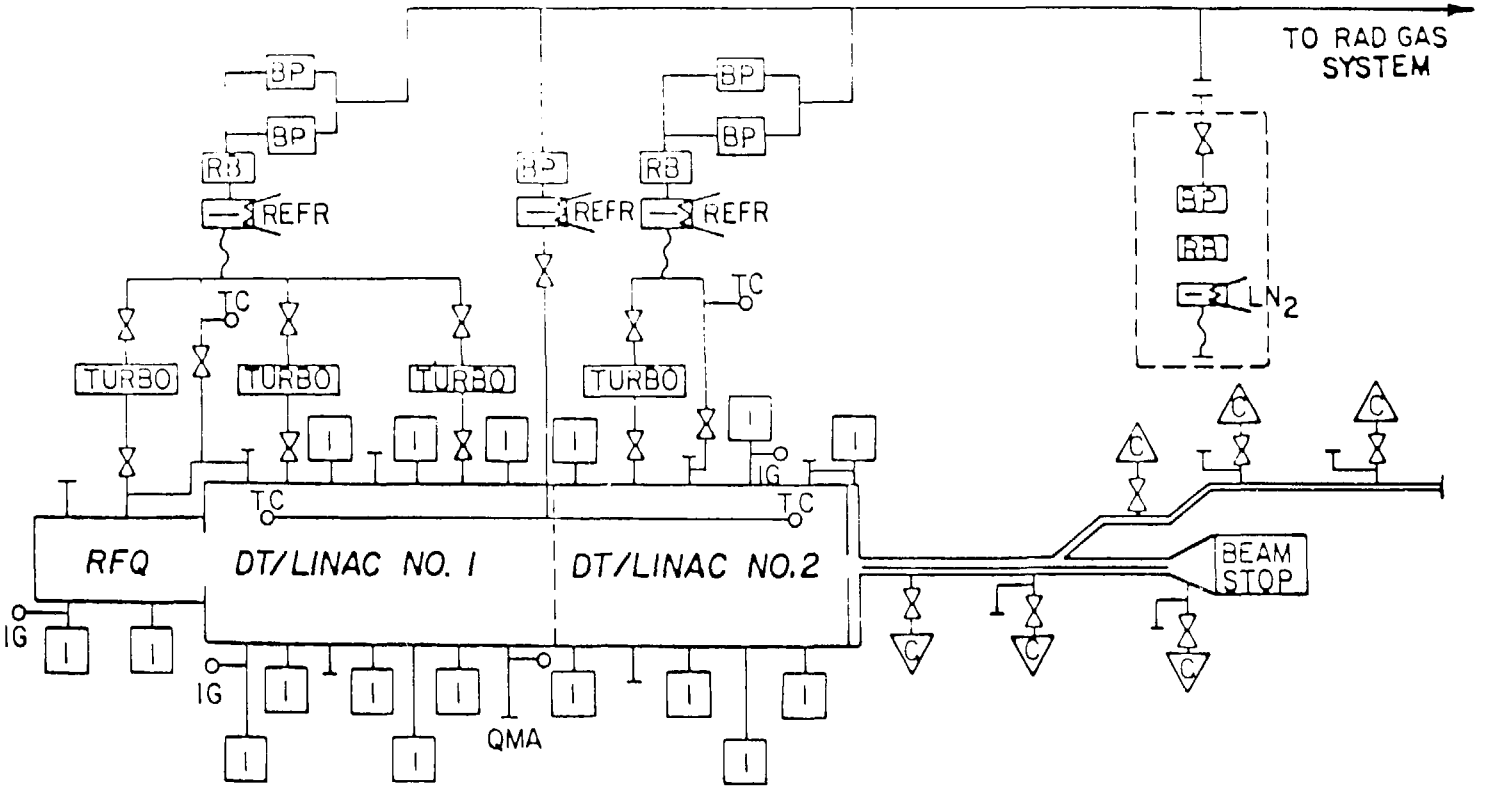

LEGEND:

I – ION PUMP
BP – BACKING PUMP
IG – IONIZATION GAUGE
TC – THERMOCOUPLE GAUGE
RB – ROOTS BLOWER

TURBO – TURBOPUMP
QMA – QUADRUPOLE MASS ANALYZER
LN_2 – LIQUID NITROGEN TRAP
REFR – REFRIGERATED TRAP

Fig. 36.
Proposed FMIT vacuum system.

target spot for a distance of 1.0 m. Error studies were performed for 20- and 35-MeV beamlines to specify location accuracy of quads and bending magnets, design parameters, tolerances, and power-supply stability. Studies were performed with TURTLE to investigate the potential usefulness of scrapers, and discussions were held between Los Alamos and HEDL. An agreement was reached to include scrapers in the front leg (to pick up low-energy particles) and at the target (to protect the target structure). Further studies to precisely position these scrapers have been postponed until a decision on the HEBT configuration is made.

The HEBT optics design was presented at the FMIT preliminary design review. After that review, the periodic bend system was redesigned with 16-kG (at 35-MeV) bending-magnet fields. This redesign increased the test-cell separation 0.76 m, the overall HEBT length 0.76 m, and decreased the required bending-magnet fields. The reduction in magnetic field eliminated the saturation effects in the bending-magnet steel. To provide quad gradients that would properly focus the 1- by 3-cm FWHM spot on target, computer runs were done at target distances of 1.00, 1.25, and 1.50 m from the last quad. Because of a request for the target distance to be increased to 1.5 m, TRANSPORT, TURTLE, and PARMILA runs were evaluated by Los Alamos and E. Colton of ANL. They found the aberrations were small enough so that the distance from the last quad to the target could be increased from 1.0 to 1.5 m. Error studies were performed on the new system.

The evaluation of these error studies showed the nonbend plane focusing to be undesirable. To correct this problem, the bend system was redesigned, using a quadrupole instead of the bending-magnet exit-edge angle. This also reduced the bending-magnet field to 14.8 kG at 35 MeV for the same building size. This system was studied for both 35- and 20.395-MeV beams; at the end of 1980, both error studies and a study of space-charge effects were under way.

b. Prototype. The prototype beamline was reinvestigated as new RFQ information became available. A range of possible beamstop spot sizes was investigated, and provided, to aid the beamstop design.

c. General. The program TRACE was modified to calculate the betatron phase-shift angle μ;

$$\mu = \int_{z_1}^{z_2} \frac{dz}{\beta} \quad ,$$

where β is the Courant-Snyder beta related to beam size. The phase shift can be calculated between any two beamline elements and displayed by a simple command. This calculation is expected to be useful in determining the position of diagnostic elements.

10. Beam Dynamics. Several new codes were written during this period. They include codes to analyze the output beams from the RFQ, the DTL, and the HEBT. These codes allow us to understand the beams we are working with and to improve system performance.

Several codes were put on, or optimized for, the CRAY-1. These included both versions of the RFQ PARMILA (T-Code and Z-Code), the standard drift-tube PARMILA, and the matching codes. The speed of execution is now four to six times faster in the CRAY than the 7600 for comparable numbers of particles. When larger numbers of particles are used, the time per particle improves in most cases. The shift to the CRAY has allowed the use of either more particles for the same cost, and with better results, or the running of the same number of particles at less cost. Furthermore, the use of the CRAY enables more particles to be used per run than is possible on the 7600, thus yielding a better assessment of the beam loss.

a. RFQ, DTL, Prototype, and HEBT. Matching studies were made for two RFQ/DTL combinations. It is necessary to match the RFQ to the DTL so that excessive quad gradients are not required, the beam size in the DTL is minimized, and the beam size and matching gradients are insensitive to small variations in the input parameters. This matching is accomplished by varying the output flare in the accelerating section of the RFQ and by adjusting the first four DTL quads, until acceptable properties are found.

Following the selection of the flare, particle runs were made with groups numbering more than 40 000 particles to estimate the power deposited in the first sections of the DTL by out-of-bucket particles emerging from the RFQ.

The particles do not represent a serious radiation problem, because they are not accelerated. No lost particle has been seen with an energy as high as 4 MeV.

RFQ-generated beams were passed through the DTL and used for brief evaluations of the HEBT design. They also were used to study the DTL's performance when it was operated with the rf turned off in the second tank and to study prototype operation with, and without, the rf.

b. Quadrupole Design. Results from the measurements of the Type A quad prototype were used to develop a computer code to estimate quad-end leakage. Preliminary designs were made for the B and C quads. Predicted performance graphs were made for these designs, using the leakage code.

I. WIGGLER DESIGN AND CONSTRUCTION FOR THE FEL AMPLIFIER EXPERIMENT*

A. Introduction

The Los Alamos National Laboratory has proposed a three-phase program[51] to build an efficient high-power FEL laser operating at 10.6 μm. In the first phase, now in progress, we will demonstrate light amplification at moderate efficiency and high power levels. The major goal of this phase is to demonstrate the special advantage of a tapered wiggler[52] over a uniform one, that is, its good energy-extraction efficiency. An important second goal is to provide diagnostic facilities, for both electron and light beams, extensive enough to allow detailed confirmation of the effect of optical gain on both beams and to help unravel unexpected problems. We are not aiming for the highest possible efficiency. Therefore we have attempted to develop a design that (1) simultaneously satisfies our two major goals listed above; (2) allows for anticipated modifications in the wiggler's key parameters; and (3) is basically simple, conservative, and reliable. Below we will describe the wiggler designed to meet these requirements. This section is divided into five parts: choice of the key parameters of the wiggler, its performance, anticipated problem areas, construction details, and its present status.

B. Key Parameters

The starting point for our design is the characteristics of the electron and laser beams we will use. The laser beam must be powerful enough to cause a significant (>1%) transfer of energy from the electron to light beams. Our laser has a peak power of 10^9 W at 10.6 μm and is assumed to be ideal, except that (because of aberrations in the optics) its area at the focus is twice as large as the ideal value. We chose an electron beam with a 20-MeV energy and other properties that do not significantly degrade its ability to interact ideally with the laser beam in the wiggler. In particular, the energy spread

*Work performed under the auspices of the US Department of Energy with the support of the Air Force Office of Scientific Research, the Defense Advanced Research Projects Agency, and the Naval Air Systems Command.

of the beam is about 1% and its emittance about 2π mm·mrad; these values are low enough to allow the electrons readily to be trapped, held by buckets, and contained everywhere within the envelope of the laser beam. The electron beam current is 20 A. This choice does not directly affect the energy-extraction efficiency of the wiggler but does provide an optical gain large enough to allow the wiggler to be operated in an oscillator configuration later on.

Five important decisions were made about the wiggler before its design began: to use $SmCo_5$ permanent magnets to provide the wiggler field; to use the arrangement of magnets shown in Fig. 37; to taper the wavelength of the wiggler's field, rather than its amplitude; to arrange the magnets with a uniform gap, rather than tailoring the gap to follow the diameter of the laser beam; and to mount the magnets inside the vacuum envelope. These decisions were based on the need to achieve high magnetic fields, to simplify the design, and to make better provisions for diagnostics.

The major design goal was to provide both a large laser field and a large wiggler field over a long length of the electron beam. This could not be accomplished merely by designing a long wiggler, because the laser beam cannot be sharply focused over a long path. Instead, there must be careful optimization of three strongly interacting parameters: the magnet gap, the wiggler length, and the characteristic Rayleigh length z_0 that describes the laser beam. After testing many different combinations of these parameters, the values listed in Table IX were chosen.

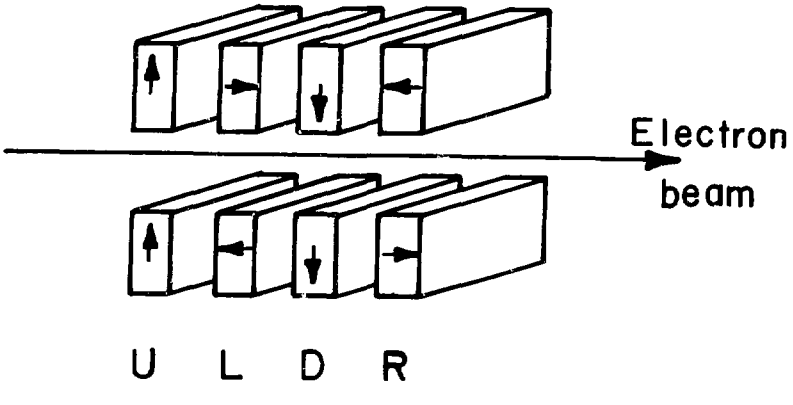

Fig. 37.
Magnets used to generate one wavelength of wiggler field.

TABLE IX

CHARACTERISTICS OF WIGGLER

Optical	
Wavelength	10.6 μm
Design optical power	1000 MW
Strehl ratio	0.5
Rayleigh length	400 cm
Radius of focus	0.16 cm
Electron Beam	
Design electron current	20 A
Electron energy	20 MeV
Energy spread	±1%
Emittance	2π mm·mrad
Wiggler	
Wiggler length	100 cm
Length of exit/entrance regions	5.0 cm
Taper in wavelength	12%
Max/min wavelength	2.7/2.4 cm
Number of wiggler cycles	40
Total number of magnets	314
Magnet size	0.5 by 0.5 by 3.5 cm^3
Gap between magnets	0.88 cm
Peak magnetic field	0.3 T
Performance	
Design energy-extraction efficiency	2.8 %
Design optical gain	1.1 %
Small signal gain	1.4 %

The taper of the wiggler was determined by a computer program.[53] This program solves the usual wiggler equations for a group of several-hundred electrons and evaluates (among other things) the wiggler's wavelength as a function of position, the size and locations of the magnets, the efficiency of the resulting wiggler in converting electron energy to light, and the energy

distribution of the electrons leaving the wiggler. The program takes into account the initial energy spread of the electron beam and the aberrations of the laser beam, calculates the local fields of the magnets, and increases the laser field (down the wiggler) to reflect the optical gain. The program varies the local wiggler wavelength to achieve a constant resonant phase angle of 40°, under the design conditions. The resulting taper in wavelength is not strictly uniform but varies from 9% near the entrance to 12% near the exit. This taper gives a somewhat higher efficiency than does a constant one.

C. Wiggler Performance

The characteristics of our prototype wiggler are given in Table IX, and typical performances are shown in Figs. 38 through 41. Figure 38 shows the optical gain and energy-extraction efficiency as a function of optical power. These parameters have been calculated for various values of wavelength around 10.6 μm, the design value. Figure 38 shows the maximum values found; these occur at wavelengths that are usually slightly shifted from 10.6 μm. Figure 39

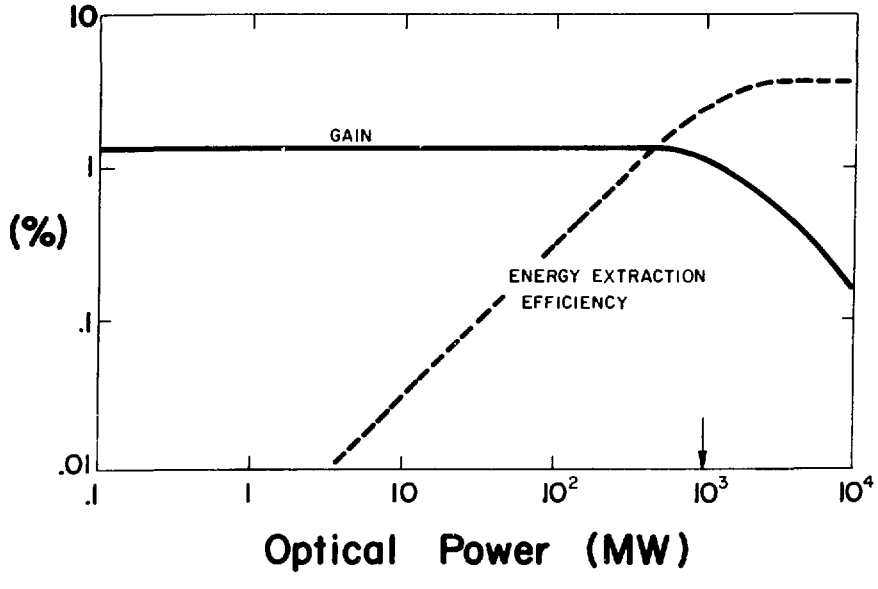

Fig. 38.
Optical gain and electron energy-extraction efficiency as a function of optical power.

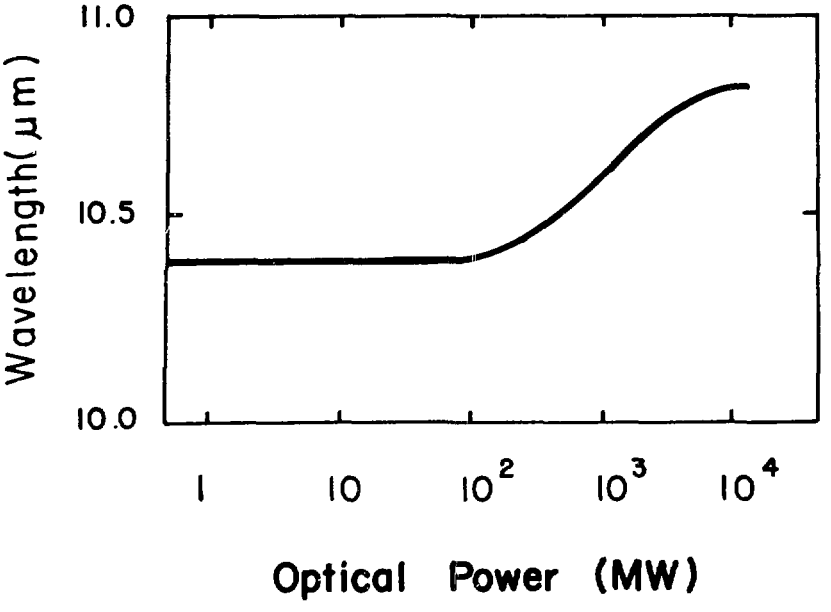

Fig. 39.
Optical wavelength for maximum gain as a function of optical power.

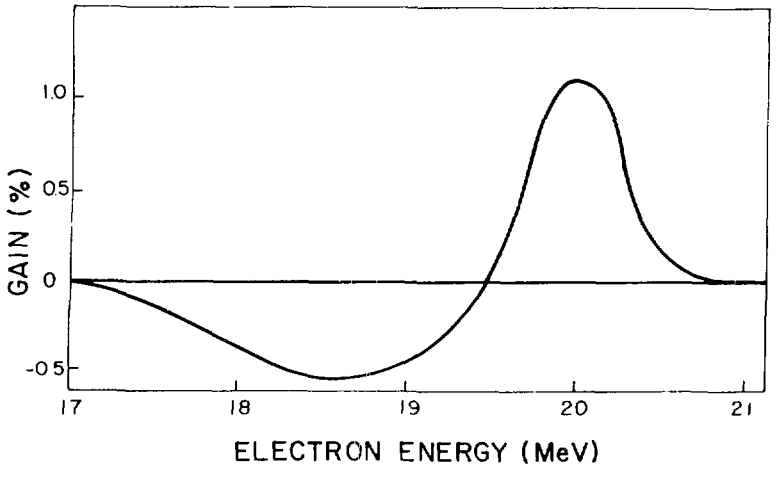

Fig. 40.
Optical gain as a function of electron energy.

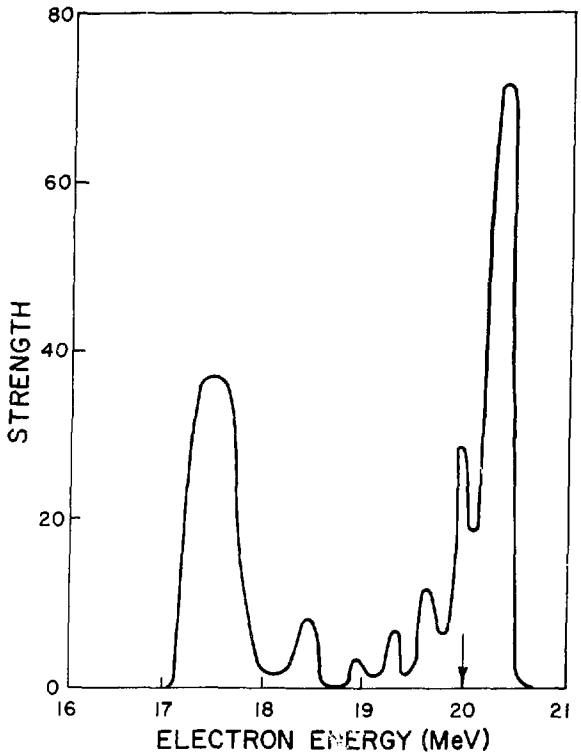

Fig. 41.
Electron energy-distribution function at the wiggler's exit.

shows the shift in the optical frequency for which the gain is a maximum, as a function of optical power. The shift from 10.6 μm is important; it may have a significant effect upon the wiggler's operation in an oscillator configuration. In such an arrangement, the wiggler must operate over a wide range of optical powers, and the shift discussed above may reduce the rate at which the optical power builds up from noise. Figures 40 and 41 show two other important characteristics of the prototype wiggler: the shape of its gain curve, and a curve of the typical energy-distribution function of the electrons leaving the wiggler. The latter curve clearly demonstrates a distribution split into one part that was captured by the wiggler's buckets and decelerated and another part that was neither captured nor decelerated.

D. Problem Areas

The wiggler's performance, presented above, should be obtained under ideal circumstances, but there are several particularly important design problems that could make circumstances less than ideal. These problems are related to the electron beam and its reaction to the wiggler fields. In order of importance, they concern designing the wiggler so that

(1) the electron beam passes through the wiggler without striking its walls,

(2) the electron beam overlaps the light beam and the wiggler's axis well enough to assure a strong interaction, and

(3) the buckets move smoothly through the wiggler without shaking free any of the captured electrons.

To handle these problems, we have devoted major attention to three areas:

(1) devising workable ways to generate a wiggler field that deflects the electron beam in the desired way,

(2) devising accurate and convenient ways to align the two beams with the wiggler's axis, and

(3) providing adequate diagnostics to show the positions of the two beams at several points down the wiggler.

We will discuss briefly these three subjects.

In the wiggler, 157 magnets lie on each side of the electron beam. A single magnet creates a bend in an electron's path of about 4 mrad. If uncompensated, such a bend generates an electron displacement of 4 mm over 1 m of path. Ideally, the displacements caused by all the magnets should cancel exactly at the exit to the wiggler. We have performed random-walk-type calculations to estimate the magnitude of the deviations from this ideal, caused by small random variations in the fields of all 314 magnets. These calculations show that random variations in strength must be held well below 1%; however, our magnets* vary more than this amount.

We considered two techniques to reduce the effect of such large variations: first, carefully measure each magnet's field and then select and group several magnets together, so that each one compensates for the errors of its neighbors; and second, provide an adjustable mount for each magnet, so that each one could be moved closer to or farther from the axis of the wiggler, thus compensating for its weaker or stronger fields. We have chosen the first of these alternatives.

Convenient, sure alignment of the laser and electron beams, with each other and with the axis of the wiggler, is an essential part of the experiment. Although final peaking will undoubtedly be done by maximizing some output signal, preliminary alignment must be provided to bring the beams very close to their preferred positions. The technique we employ avoids many problems common to alignment systems by introducing a third reference beam, a low-power helium-neon laser. The three critical systems (the wiggler, the CO_2 laser,

*Hicorex 90B, available from Hitachi Magnetics Corp., Edmore, MI 48829.

and the electron beam) are then aligned to each other in an indirect manner by being separately aligned to the reference beam.

The wiggler is aligned by maximizing the transmission of the reference beam through apertures placed on the wiggler's axis at its entrance and exit. The CO_2 laser is aligned by superimposing it with the reference beam before the two beams enter the wiggler. The CO_2 beam's position can be monitored thereafter by observing the reference beam. The electron beam is aligned by observing the fluorescence it causes on the three screens that can be inserted into the wiggler. The spot generated by light scattered from the reference beam also can be seen on the same screens. Alignment occurs when the two spots are superimposed on all three screens.

E. Wiggler Construction

The wiggler system includes four major parts: the magnet support structure, the vacuum envelope, the trim coils, and the shield. The trim coils and shield are supported on the outside of the vacuum envelope; the support structure is suspended on the inside of the vacuum envelope.

1. Magnet Support Structure. Figure 42 shows the central part of the magnet support structure; note that some of the magnets are not yet assembled. The rectangular port on the near side will be used when inserting a fluorescent screen into the center of the wiggler. The structure is built of 6061-aluminum members held together by nonmagnetic stainless-steel pins and bolts. The members are dimensioned to resist sagging from their own and the magnets' weight. The structure is supported within the vacuum envelope solely by spring-loaded pins that do not transfer bending or twisting movements to the structure.

The magnets are located by toothed bars running the length of the wiggler. The teeth engage slots that are cut into the ends of each magnet. A second slot cut into each magnet's ends, perpendicular to the first slot, allows short splines to be inserted into each magnet and (simultaneously) into a longitudinal slot in the toothed bar. The splines fix the magnets in place and resist forces of several pounds, either toward the center of the wiggler or away from it.

The entrance and exit sections of the wiggler each are composed of a single pair of normal magnets, spaced from each other and the wiggler proper by distances calculated to ensure almost zero deflection of the electron beam.

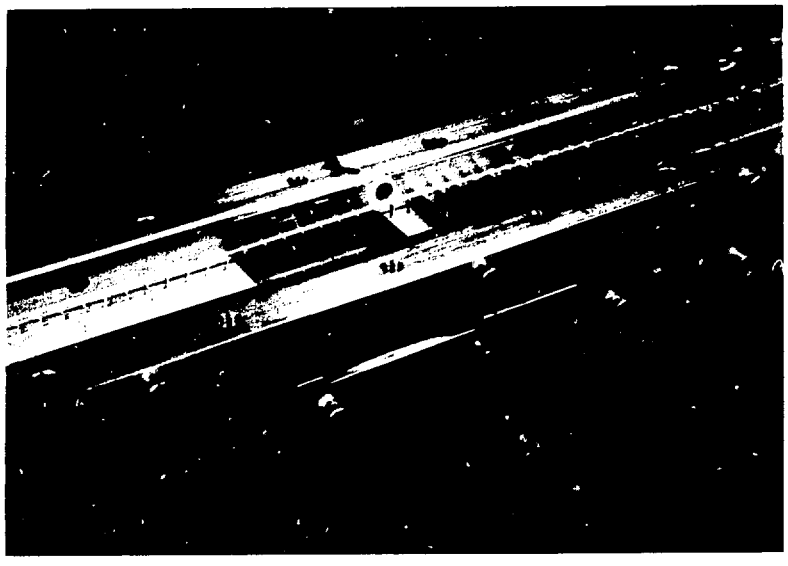

Fig. 42.
Central part of the wiggler, showing the magnets, the toothed location bar, spacer plates separating the top and bottom halves, and the fluorescent-screen insertion and viewing ports.

The magnet strengths are actually about 10% too high. Final trimming of their effects is accomplished by rotating each pair by a small angle from the upright setting. Figure 43 shows a view of one of these magnets in its holder.

An important feature of the support structure is its adaptability to changes. Anticipated changes are of three kinds: the use of new, higher strength magnet material, a change in the taper, and a change in the magnet gap. If required, these changes would be accomplished by the following means: (1) if a new set of magnets were to be inserted, each new magnet would first be measured and characterized and (2) compensated groups then would be chosen and loaded into the wiggler. This whole process would take about a week. If a new taper were desired, a new set of toothed locating bars would be machined and the magnets reloaded on them. If a new gap were to be used, the spacer plate separating the upper and lower halves of the wiggler (visible in Fig. 43) would be removed or replaced. Provisions have been made for jacking the upper and lower halves apart, to permit this replacement without removing the magnets.

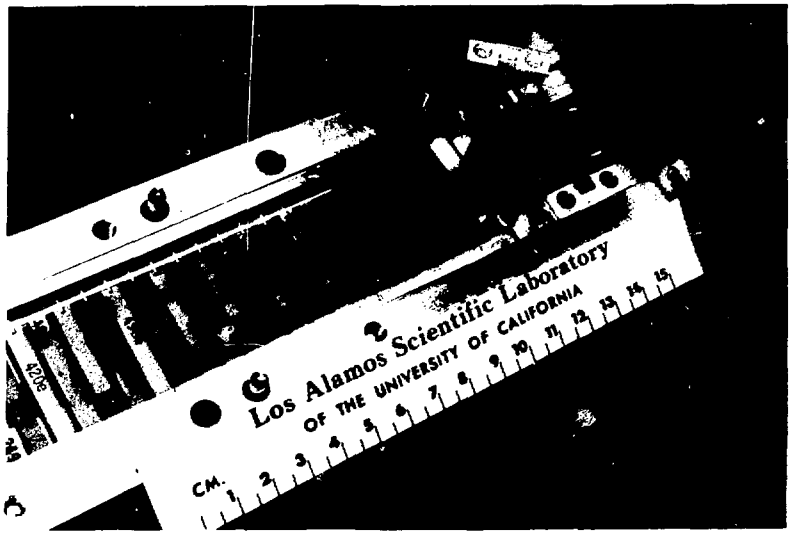

Fig. 43.
The entrance of the wiggler, showing a rotating holder for one of the entrance magnets, and one of the end pins that support the wiggler within its vacuum enclosure.

2. Vacuum Envelope. The vacuum envelope is built of nonmagnetic stainless steel and is characterized by 10 diagnostic penetrations, some of which are shown in Fig. 44. Four of these penetrations allow alignment apertures of two different sizes to be inserted near the ends of the wiggler. Three allow fluorescent screens to be inserted at either end or at the center. The remaining three penetrations serve two purposes: they contain windows to allow vidicon cameras to view the fluorescent screens, and they serve as pump-out ports for the vacuum system. All of the motion required to move the screens and apertures is provided by pneumatic cylinders that operate through metallic bellows. None of the devices penetrating the vacuum envelope actually touch the support structure, thus avoiding the possibility of deflection of the support structure itself.

An interesting feature of our design is the use of sintered $SmCO_5$ magnets inside the vacuum system. This approach was chosen because of the ruggedness it gives to the vacuum enclosure and the ease of inserting diagnostics at the center of the wiggler. A serious question has been raised about the

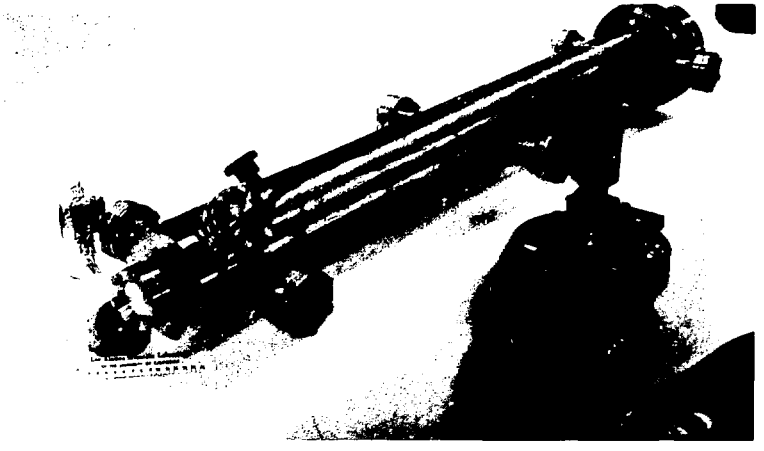

Fig. 44.
Vacuum enclosure being evacuated, showing some of its diagnostic sidearms.

suitability of this porous material in a high-vacuum system, but recent tests show that the vacuum properties of both the complex support structure and the magnets are good enough to eliminate concern.

3. Trim Coils. The trim coils are mounted on a split aluminum tube, fastened directly to the vacuum envelope. There are 20 coils, consisting of 5 pairs that develop a horizontal deflection of the electron beam and 5 that develop a vertical deflection. One segment containing 10 coils is shown in Fig. 45. Without overheating, each pair of coils can produce a field of about 3 mT and can develop an angular deflection to the beam of about

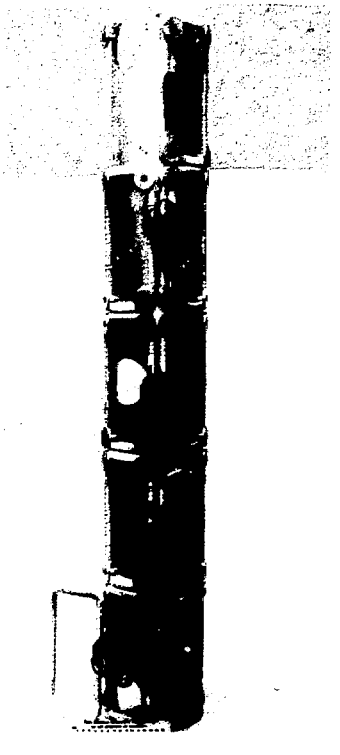

Fig. 45.
Trim coils on supporting segment.

8 mrad, more than enough to compensate for the anticipated residual field errors. These coils will be used in two ways: first, a preliminary adjustment of their fields will be chosen to compensate for residual field errors; and second, a final peaking will be realized in the presence of the electron beam, to maximize the performance of the wiggler.

The preliminary adjustment now has been performed. A fine current-carrying copper wire was used to simulate the electron beam. When the tension and current in the wire are correctly chosen,[54] the deflections of the wire exactly match those of the electron beam. The deflections of the wire were first monitored without current in the trim coils, to assess the field errors of the wiggler magnets alone and also to assist in the adjustment of the entrance and exit magnets. The coil currents then were adjusted until the net deflections of the wire were acceptably small. An attractive feature of this technique is that it can be used with all the components (vacuum envelope, trim coils, and shield) in place. Any unexpected contributions to the net field (caused, for example, by remnant magnetism in the shield) can be detected and corrected.

4. Shield. The shield is composed of a 1/4-in.-thick tube of soft iron, completely surrounding the trim-coil system. This acts as a cradle to hold all of the parts, shields the wiggler from external fields, acts as a low-reluctance return path for the field of the trim coils, and reduces fringing fields generated by them. If necessary, its shielding function will be supplemented by thin layers of a low-reluctance material placed on its outer surface.

F. Status

This section is an accounting of work in progress. All wiggler-system components, discussed above, have been built and now are being tested. In particular, the wiggler has been completely loaded with magnets and has passed our vacuum tests. Measurements of its field, using both a Hall probe and a wire to simulate the electron beam, have been completed. The compensation techniques employed are good enough so that no current is needed in the trim coils to achieve a satisfactory field distribution. Tests are now being conducted on the alignment and diagnostic systems.

II. PROGRESS ON THE FEL RADIO-FREQUENCY SYSTEM

A block diagram of an rf system to deliver ≈6 MW of peak rf power at 1300 MHz for 100-μs pulses was designed. The rf system will use an L-3707 klystron and a LAMPF floating-deck modulator. The modulator was built and operated with an L-3707 at 86 kV in an existing test stand. An overall view of the klystron and modulator is shown in Fig. 46. The klystron was operated at 86 kV and ≈40-A beam current for 100-μs pulses at 120-Hz repetition rate. Because of the lack of a 1300-MHz driver, only a few watts of 1300-MHz output power were produced. The gain of the tube was 30 dB, and the klystron is excellent electrically.

Los Alamos has a total of six L-3707 klystrons, but only one is operable. Two others are physically undamaged but have small leaks that have destroyed the vacuum. These two klystrons were shipped to the original manufacturer, and only one is in good enough condition to be rebuilt economically. One klystron is being rebuilt as a spare for the project.

Several components of the rf system have been fabricated, including four of the klystron-magnet power supplies, the ion-pump power supply, and klystron running-time meters. Essentially all of the major procurement for the rf system has been completed, and the klystron power supply and high-power phase shifters have been delivered. Very little engineering design remains to be done, but substantial system integration and documentation remain for the current year.

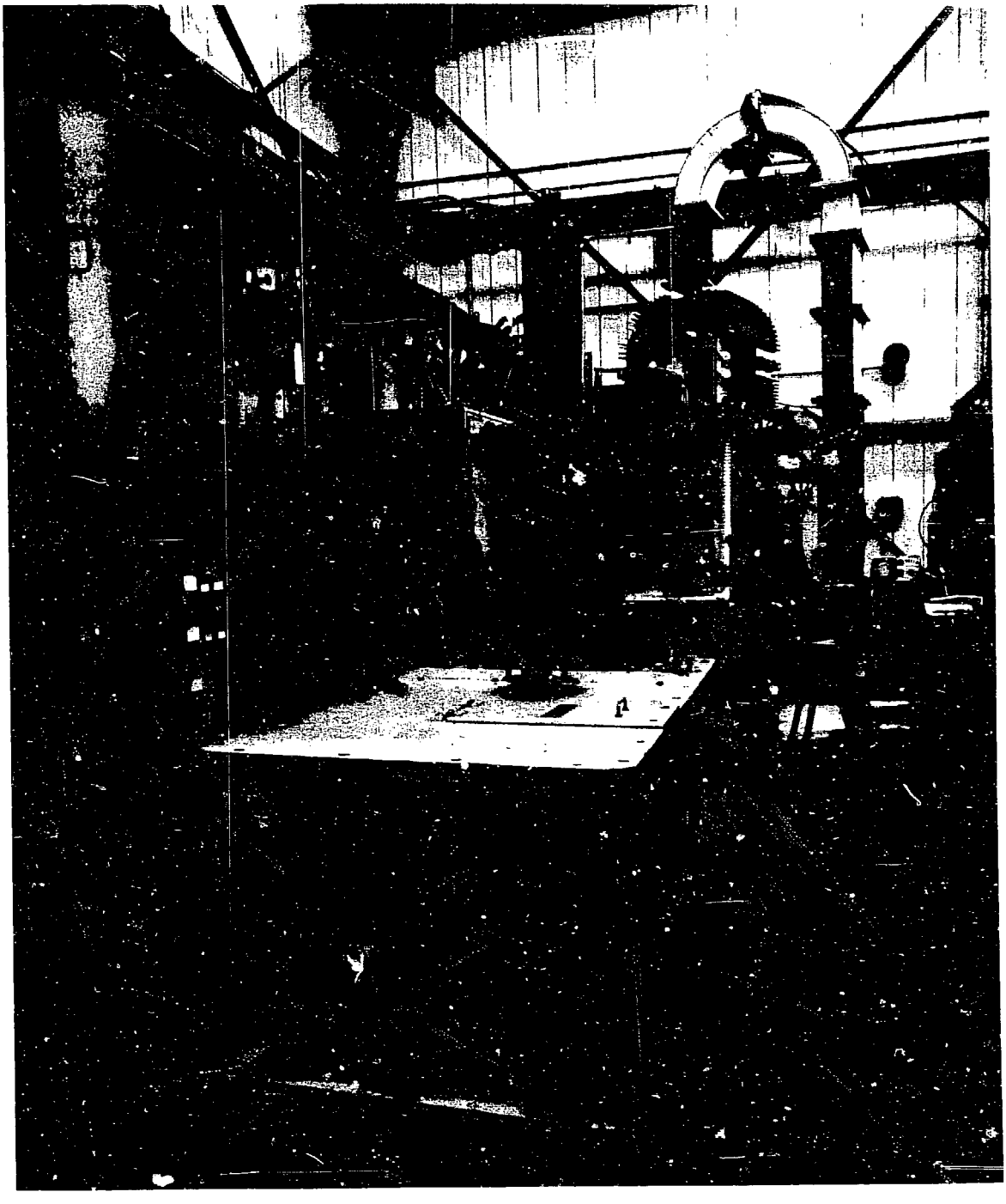

Fig. 46.
L-3707 klystron, solenoid, and modulator before 86-kV tests.

THE LOS ALAMOS-NBS cw MICROTRON

I. INTRODUCTION

The Los Alamos-NBS racetrack microtron (RTM) is a joint research project of the National Bureau of Standards (NBS) and the Los Alamos National Laboratory. The project has two goals: first to determine the feasibility of building a 1- to 2-GeV, high-current, continuous-beam electron accelerator;[55-57] and second, to develop the necessary technology for building it. To achieve these goals, a demonstration accelerator will be designed, constructed, and tested. Some of the parameters of the demonstration RTM[58] are 5-MeV injection energy, 12-MeV energy gain per pass, 15 passes, 185-MeV final beam energy, and 550-μA maximum current.

The RTM offers a number of unique advantages as an electron accelerator for energies above 50 MeV. It should be cheaper to build and operate than a conventional pulsed rf linac of the same maximum energy and average beam power. It is possible to build a continuous wave (cw) microtron with available high-power rf techniques. The RTM will have better beam quality and a continuous beam--qualities that are essential for nuclear physics experiments requiring coincidence measurements between emitted particles.

Three recirculating cw electron accelerators are now in operation: MUSL-2,[59] a 66-MeV, 6-pass RTM (at the University of Illinois) that uses a superconducting accelerating section; MAMI-1,[60] a 14-MeV, 20-pass RTM (at Mainz, West Germany) that uses a room-temperature rf accelerating structure; and a 155-MeV, 4-pass recyclotron[61] (at Stanford University) that uses several superconducting accelerating sections operating with a duty factor of about 75%. Our project is using a room-temperature DAW rf accelerating structure.[62,63] We expect to achieve beam currents of several hundred microamperes, limited by beam blowup. Another of our project's goals is to determine the beam-blowup-imposed current limit of such a machine by a combination of measurements and calculations.

Initial funding for the Los Alamos-NBS microtron was received in September 1979. The conceptual design of the RTM was completed in June 1980.* In

*S. Penner and L. M. Young, "NBS-LASL Microtron Design," National Bureau of Standards unpublished report.

addition to development of the injection and control system and end-magnet design described in this section, our efforts have concentrated on the procurement of long-lead items such as klystrons, power supplies, the control-system computer, and electron gun. The 1-MW klystron power supply was received in December 1980. We expect delivery of the first klystron in July 1981 and the first high-power test of the accelerating structure to take place in August 1981. Our schedule calls for the first operation of the injector linac in August 1982, and completion of the entire accelerator by June 1983.

II. INJECTION SYSTEM

The injection system uses a 100-keV modulating anode-type electron gun with a 5-mA current capability. A focusing lens system, with two physical apertures, limits the beam's transverse emittance to $\varepsilon_t = 4\pi$ mm·mrad, at 100 keV. The apertures are followed by a two-cavity chopper system that limits the longitudinal beam emittance ε_L to less than 3π keV·deg, with little effect on the transverse phase space. Following the second chopper cavity, the beam is bunched by a single-cavity klystron buncher before entering the capture section of the injection linac. The design of the injection linac has been analyzed with the aid of the computer programs PARMELA and SUPERFISH.

Our original design consisted of a 2-m-long, tapered-β capture section with an average accelerating gradient of 1.0 MV/m and a 2-m-long preacceleration section with a 1.5 MV/m gradient. PARMELA showed that this design would not meet the specifications for the beam from the injection linac. The beam's design specifications from the injection linac at 5 MeV and 550 μA include a normalized transverse emittance of ($\varepsilon_n = 5\pi$ mm·mr) ($\varepsilon_T = 0.47\pi$ mm·mrad) and a longitudinal emittance of 20π keV·deg for a 2° phase-bunch length.

The new design for the injection linac meets these specifications. It consists of a 1-m-long tapered-β capture section with a uniform accelerating gradient of 1.5 MV/m and a 2.4-m-long preaccelerating section, also with a uniform accelerating gradient of 1.5 MV/m. The computer program SUPERFISH showed it was possible to construct a tapered-β DAW accelerating structure with a uniform accelerating gradient.

III. END-MAGNET DESIGN

An RTM's beam quality and operating ease are critically dependent on the properties of the end magnets. Furthermore, the end-magnets' cost will be a large part of the overall cost of a 1- to 2-GeV microtron. For these reasons the design of the end magnets for the demonstration RTM must meet the performance requirements at the least possible cost. A novel and economical magnet design has been developed at NBS[63] having a calculated field uniformity of better than two parts in 10^4. The design incorporates a Purcell filter into a half-picture-frame magnet and provides a 25% reduction in weight from an equivalent C-magnet. The design of the RTM end magnets is shown in Fig. 47, and some pertinent parameters are given in Table X. The gap is large (relative to the beam size) to allow space for an independent vacuum chamber and for corrective windings that will reduce the effect of gap variation on field homogeneity. Spacers are used to maintain the gap in the presence of magnetic forces. Inaccuracies in fabrication and inhomogeneities in the iron are expected to cause local field inhomogeneities of about one part in 10^3. After field mapping, such inhomogeneities will be reduced by an order of magnitude, using low-power printed-circuit board surface windings.

TABLE X
END MAGNET PARAMETERS AT 1 T

Gap dimensions, cm	6 by 71 by 158
Mass of steel, kg	29 000
Mass of copper, kg	420
Main coil	
Turns	64
Nickel, A-turns	58 000
Power, kW	42
Current density, A/cm^2	
Reversing coil	
Nickel, A-turns	7 200

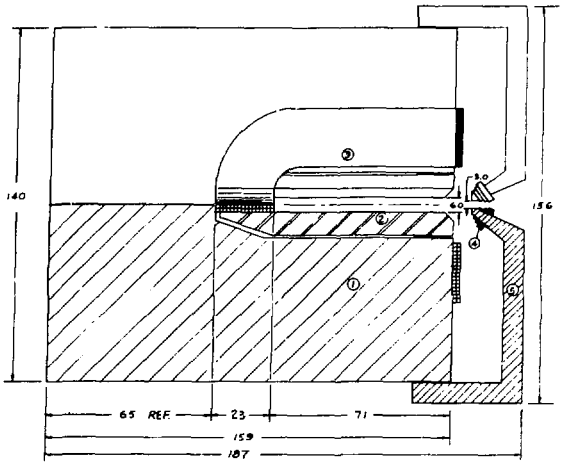

Fig. 47.
Side view/section of end magnet. Parts are (1) yoke, (2) pole, (3) main coil, (4) reversing coil, and (5) field clamp. Dimensions are in centimeters. Width perpendicular to this view is 158 cm, resulting in an approximately cubic magnet.

The end-magnet fringe fields must be treated carefully because of the unwanted (and potentially very strong) defocusing perpendicular to the magnet's plane. We will use active field clamps along the entire entrance edge of the end magnets and will provide a reverse field (~30% of the main field) to nullify the fringe fields' defocusing effect.[64] This method of nullifying the fringe-field defocusing of the RTM's end magnets has been used successfully on MUSL-1[65] and MUSL-2[59] (at the University of Illinois) and MAMI-1 (at Mainz, West Germany).

IV. CONTROL SYSTEM

A. Architecture

The architecture chosen for the control system is based on considerations of the specific requirements of this project. First, the number of devices to be controlled and monitored is large. Second, development of the subsystems of the accelerator will proceed simultaneously at Los Alamos and NBS, requiring each subsystem to have an independently operable local control system. Third, cost and manpower limitations require that we hold hardware costs to a minimum and reduce our programming and engineering effort by using, to the greatest possible extent, the best commercially available control technology.

The control system will be based on distributed, intelligent, secondary stations. The secondary stations will consist of a Multibus* crate with one or more single-board computers (SBC), analog and digital interface equipment,

*Multibus is a trademark of the Intel Corporation.

CRT terminal, and several switches and two knobs. A communication link using RS-232 serial-data link or a 1-Mbaud DMA Megalink* (a Multibus compatible interface) will be used to link the local stations to the primary station. The primary station will be interfaced also to the main control computer and to the central control console. Each secondary station will consist of a powered Multibus crate with several card slots. Each crate will contain a similar SBC, plus other analog- and digital-interface cards as needed for control and monitoring. The crate could contain additional SBCs, if the process being controlled requires a dedicated processor.

The software in the SBC will consist of an operating system that handles the link communications and the local control console, plus the applications programs. The operating system will be the same in all secondary stations. The applications programs will be unique to each process being controlled and monitored. Where there are many similar devices being controlled and monitored, one application program, having a data array containing entries for each individual device, will be used.

The central control computer will be a PDP/11/44, a new medium-sized minicomputer with a multiuser-disk operating system. This computer will be used for storage and retrieval of the accelerator data, for generating displays of this data, for simulating the operation of the accelerator, and for developing programs for the secondary station SBCs. The computer also will be used for calculating and setting the values in the digital-to-analog converters (DAC).

The central control console will have several knobs and a keyboard for manual control of the DACs or for input to the simulation programs. A high-resolution graphics terminal and an alphanumeric color display also will be available. The knobs, keyboard, and alphanumeric color display will be interfaced to the primary station, which will have an additional SBC to control these devices; this will prevent complicating the communication link software in the primary SBC. The primary station will be interfaced to the central control computer either through a Computrol Megalink board or a high-speed RS-232 serial-data link. The interfacing of key elements of the control console to the primary station will give us the advantage of uninterrupted control of the accelerator when the central control computer is "down" or

*Megalink is a trademark of the Computrol Corporation.

otherwise occupied, as during system generation. Another advantage of this scheme is speed. For example, data from the knobs do not need to be processed by the central control computer, with its high software overhead inherent in the multiuser-disk operating system.

A high-resolution graphics terminal such as the Tektronix 4014 will be interfaced to the central control computer to take advantage of the computing power available for generating more complex displays.

The RTM will have hundreds of separate steering coils, quadrupoles, and bending magnets. Most of these elements will require only small dc power supplies; therefore, a few large dc power supplies will be used to supply current to many current regulators. Each current will be controlled by a DAC. The conventional method would use a card plugged into the bus of the local station and would send the analog voltage to the power supply through cables. Cards with eight DACs per card are available; however, because hundreds of DACs are needed, many cards and hundreds of connecting cables also would be required.

A simpler, less expensive method for the low-power devices places the DAC on the power-supply card and controls the DAC with an addressable asynchronous receiver/transmitter. This device receives and sends data on a serial line that can service up to 128 units. The power-supply cards would plug into a card cage having as many slots as practical. Each card will have a large air-cooled heat sink on it; therefore, a practical limit on the number of power-supply cards per cage probably will be about eight. All connections to the power-supply card would be made through the card-edge connector; if one failed, it could be replaced by another card, with no need to disturb the wiring.

The serial line can be driven directly by the SBC through an asynchronous communications interface adapter (ACIA) or through a communications-controller card plugged into the local station bus. This card has four ACIAs on it; therefore, with only one extra card, one secondary station could control several sets of 128 power supplies.

B. Diagnostics

A large number and variety of analog signals must be monitored by the control system. These include the currents of all the power supplies controlled by DACs, temperature sensors on the accelerating structures, analog voltages in the rf control system, currents in ion-pump power supplies, and

many others. Commercially available multiplexed analog-to-digital converter (ADC) cards will be used; these have up to 64 inputs per card (32 differential) that plug directly into the secondary-control-station bus.

C. Beam Analyzers

Several types of devices will be used for beam analysis. View screens will be viewed by TV cameras and displayed to the operator on a TV monitor. This information will not be available to the computer for analysis or control. Positioning (in/out) of the view screens will be set and monitored through the control system. The other beam-monitoring devices (the wire scanners and the rf position, phase, and current monitors) will be analyzed by the computer and displayed on the high-resolution graphics terminal or on the color display. The analog data from these devices will be analyzed by high-speed ADCs; the digitized data will be preprocessed on the local microprocessor, or by the control console microprocessor, for quick analysis and display on the central control computer.

The method used to measure the position, phase, and current of the beam (on each pass through the linac in the RTM) is to send a 40-ns beam pulse through the RTM. This pulse length is less than the recirculation time of the machine. One set of rf beam-monitor cavities will be placed at each end of the linac. Four analog signals contain the horizontal and vertical position, phase, and current information for each set of rf beam-monitor cavities. Each analog signal will consist of up to 16 pulses, ~40 ns long, with a period of ~80 ns. The amplitudes of these pulses will be analyzed with an 8-bit, 20-MHz, video ADC with Sample and Hold. The 8-bit word will be stored in fast 16-word memory for later access and analysis by the microprocessor.

PROTON STORAGE RING (PSR)

I. PROJECT CONCEPT AND SCOPE

The Los Alamos Weapons Neutron Research (WNR) facility,[66] operational since 1977, is a pulsed polyenergetic neutron source driven by bursts of 800-MeV protons generated by the LAMPF linear accelerator. Each proton produces 15 neutrons by nuclear fragmentation when it passes through a thick tungsten target. The primary spectrum ranges from hundreds of MeV to 100 keV; with hydrogenous material surrounding the target, the spectrum can be extended into the thermal and epithermal region (0.01-10 eV). Fast neutrons are used for nuclear-physics measurements, whereas slow neutrons are used to study the dynamics and structure of materials. Experimenters at both ends of the spectrum use time-of-flight methods to distinguish neutrons according to energy. To obtain good energy resolution without sacrificing flux, the neutrons must be generated in intense pulses of short lengths compared with characteristic flight times. The PSR meets this need by acting as a proton accumulator; it converts long (100- to 750-μs) linac pulses, which are unsuitable for driving the neutron source, into appropriately short, very intense bursts, without losing particles in the process. To accomplish this, the Ring operates in two distinct accumulation modes, each independently optimized to provide the desired neutron-source pulse structure for nuclear-physics and materials-research programs.

The PSR has been authorized for construction and is now in the design stage. It will be located in a tunnel adjacent to, and below the level of, the existing beam line (D) that serves the WNR facility. A plan view of the Ring and tunnel, showing component locations, is given in Fig. 48. Beam enters the Ring from Line D; after accumulation, it returns to Line D, through which it is transported to the WNR neutron production target. Connections with Line D are made by short, sloped, beam-transport channels. Above the Ring tunnel, and on top of a 4.9-m-thick earth shield, a 750-m^2 building houses power supplies and control systems. Also included in the project is a 930-m^2 building for component development and assembly.

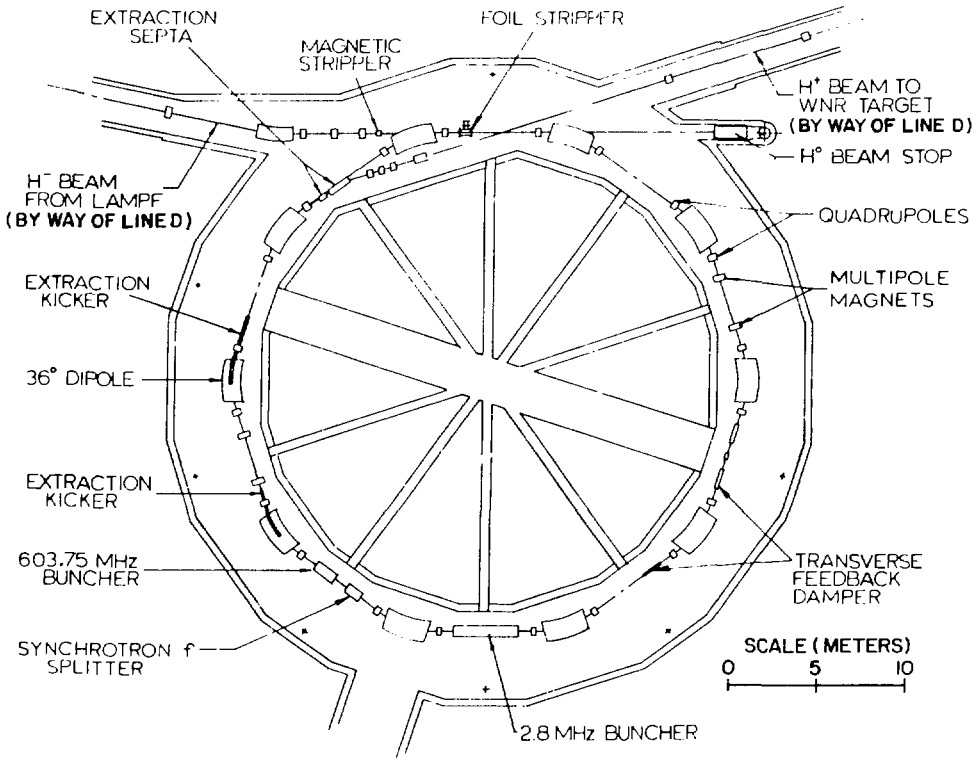

Fig. 48.
Plan view of Storage Ring.

A. Operating Modes

Operational characteristics of the two PSR storage modes are summarized in Table XI. In the short-bunch high-frequency (SBHF) mode, protons are accumulated in six, equally spaced 1-ns bunches during each LAMPF beam cycle (macropulse). The bunches are individually extracted by a fast kicker during the 8.2-ms interval between injection periods. Because the linac macropulse frequency is 120 Hz, this produces an extraction rate of 720 pps. The last 108 μs of each macropulse is modified by a chopper-buncher system in the low-energy linac transport to form a sequence of micropulses spaced at 60-ns intervals. The Ring circulation period is chosen so that this injected pulse train is synchronized with the six bunches already stored; each incoming micropulse, containing 3.33×10^8 protons, merges with a Ring bunch. Before extraction begins,

TABLE XI

PSR OPERATING-MODE CHARACTERISTICS

Parameter	Short Bunch High Frequency Nuclear physics	Long Bunch Low Frequency Materials science
Number of bunches in Ring	6	1
Bunch length in Ring	1 ns	270 ns
Bunch interval in Ring	59.63 ns	-
Buncher frequency	603.75 MHz	2.795 MHz
Protons/bunch accumulated	1×10^{11}	5.2×10^{13}
Accumulated turns	300	2100
Injection rate	120 bursts/s	12 pps
Filling time	108 μs	750 μs
Extraction rate	720 pps	12 pps
Peak circulating current	24.0 A	46.3 A
Average current	12 μA	100 μA

300 micropulses are accumulated in each Ring bunch. The narrow bunch width in this mode is maintained by a high-frequency buncher located in the Ring.

In the long-bunch low-frequency (LBLF) mode, the Ring accumulates entire linac macropulses (5.2×10^{13} protons) in a single 270-ns bunch. Each stored bunch is extracted immediately after completion of the injection cycle, with a maximum delay of 4 ms. Cycle repetition rate is 12/s. Peak current, assuming a parabolic longitudinal charge distribution, is 46.3 A; average circulating current is 100 μA. A slow-wave chopper in the linac low-energy transport carves each macropulse selected for the Ring into a continuous sequence of 270-ns pulses separated by 90-ns intervals. The Ring period is 360 ns, which permits entering pulses to be phase matched with those already stored. A first-harmonic buncher keeps the 90-ns interval clear of protons to facilitate low-loss extraction. After accumulation is complete, the Ring is emptied in a single turn by the fast-extraction kicker.

TABLE XII

STRUCTURAL PARAMETERS

Orbit circumference	90.2 m	Dipole field	1.20 T
Focusing structure	DOFO	Bend radius	4.06 m
Lattice type	Separated function	Dipole aperture	10.5 cm by 28 cm
Number of periods	10	Quadrupole gradients	3.76, -2.29 T/m
Free straight section	4.7 m/cell	Quadrupole aperture	11.4 cm
Dipole length	2.55 m	Quadrupole length	0.5 m

B. Ring Design

PSR structural parameters are listed in Table XII and dynamical parameters in Table XIII. The present design differs somewhat from an earlier concept[6] in that the circumference has been increased to 90.2 m, and the number of periods from 8 to 10. The circumference is dictated by (a) the need for a first-harmonic bunch length that is short, compared to thermal neutron generation times in the WNR target (1 to 10 μs) and (b) the need for a lattice large enough to provide straight sections for injection, extraction, and bunching, as well as space for future upgrades. A separated-function lattice was chosen to allow a wide tune range and for simplicity of construction. The nominal horizontal and vertical tunes of 3.25 and 2.25 were chosen to decouple vertical and horizontal motions, to minimize radial beam size at extraction, and to locate the transition energy well above the particle energy. The focusing structure is a perfectly symmetric 10-cell DOFO sequence, which provides many moderate-length straight sections, eliminates structure resonance effects below fourth order, and produces reasonable-amplitude betatron functions.

TABLE XIII

DYNAMICAL PARAMETERS

Circulation period	357.7 ns	$\Delta p/p$ (injection/extraction)	±0.001/±0.003
Proton kinetic E	797.0 MeV	Emittance, injected beam	0.05 cm·mrad
Proton β, γ	0.842, 1.849	Emittance, extracted beam	2.0 cm·mrad
Proton rigidity	4.869 Tm	Phase advance/cell	
Transition γ	3.02	horizontal	117°
Tunes (Q_H, Q_V, nom.)	3.25, 2 25	vertical	81°

The natural chromaticity of the lattice is negative (about -0.5) in both planes, which should eliminate the need for sextupoles to suppress the head-tail instability. However, four multipole magnets are included in the Ring design, so that sextupole field components can be introduced if required. Figure 49 shows the radial and vertical betatron functions and the off-momentum function η for a single period.

The ten 36° dipoles have a 10.5-cm vertical aperture to allow for a large emittance in the LBLF mode, which permits a high space-charge limit. Based on the Laslett expression for the incoherent space-charge limit, assuming a maximum tune shift of 0.2, the acceptance aperture of the Ring would be filled by 4×10^{14} protons in a 270-ns parabolic longitudinal charge distribution. The design goal in the LBLF mode is 5.2×10^{13} protons in such a pulse.

The dipoles will be made from one-piece laminations of 1.6 mm-thick steel to ensure adequate magnet-to-magnet reproducibility and to minimize random multipole errors. The pole-face contour is designed to produce a field uniformity of 5×10^{-4} within a 10.5-cm-diam circular section. Pole ends are parallel to simplify lamination stacking.

C. Injection

Multiturn injection into the Ring in both operating modes is by charge changing of an intense H^- beam.[68] To provide the required H^- beam intensity and pulse sequences to the PSR with minimum perturbation of other LAMPF experimental areas, some components of the accelerator must be modified. Funds for this are provided in the Ring construction budget. Significant changes include (a) installation of a high-current, surface-ionization, H^- source, (b) alteration of the H^- low-energy transport, (c) independent steering of H^- and H^+ beams in the linac, and (d) reconstruction of the front end of the switchyard. These

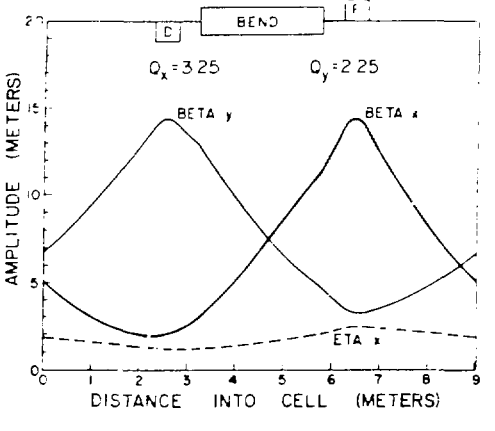

Fig. 49.
Radial (Beta x) and vertical (Beta y) betatron functions and off-momentum function (Eta x) for a single period.

changes will be accomplished during scheduled LAMPF shutdowns and will be completed by March 1985.

The H^- beam is carried to the PSR from Line D by an achromatic transport system. Immediately before entering the Ring, the beam passes through a strong transverse magnetic field (1.8 T) that converts it with 100% efficiency to H^0 atoms.[69] The magnet is specially designed to minimize the angular dispersion accompanying this process. The neutral beam then passes unperturbed through a Ring dipole, and subsequently through a thin (200-$\mu g/cm^2$) carbon foil that converts it to H^+ with 98% efficiency. At this point the incoming particles merge with previously stored protons. A beamstop downstream from the next Ring dipole collects the unstripped H^0 atoms.

The injected H^- beam emittance is 40 times smaller than that of the stored beam at the end of the accumulation cycle. This permits the stored beam phase-space distribution to be arbitrarily adjusted during injection by suitable programming of the relative coordinates of the incoming and circulating beams.[68] Control in the horizontal plane is implemented by a time-dependent closed-orbit distortion near the foil stripper, produced by a four-element pulsed magnet (bumper) system. Vertical control is accomplished concurrently by pulsed steering magnets in the injection transport line. Figure 50 illustrates the injection scheme.

D. Capture and Bunching

Beam bunches entering the Ring are synchronized in both operating modes to merge with bunches already accumulated. In the SBHF mode, entering bunches will be about 200 ps long and will have a maximum energy variation of ±0.6 MeV. Bunch structure is maintained by a cw bunching system operating at a 603.75-MHz frequency. The buncher cavity is a 2-m-long DAW structure. A modified TV transmitter package supplies the cavity with up to 100 kW of rf power. Bunching rf amplitude is 1.5 MV. Effects of high beam loading and step-load changes, caused by individual extraction of the six stored bunches, are handled at extraction time by electronically detuning the cavity and rapidly adjusting the low-level rf drive phase and amplitude.[70]

In the LBLF mode, the 270-ns-long injected beam bunches are captured by a first-harmonic, 2.795-MHz bunching system. To minimize energy spread during capture, the cavity gap voltage is linearly ramped during the injection cycle to pace the accumulated charge. Maximum rf amplitude and average drive power

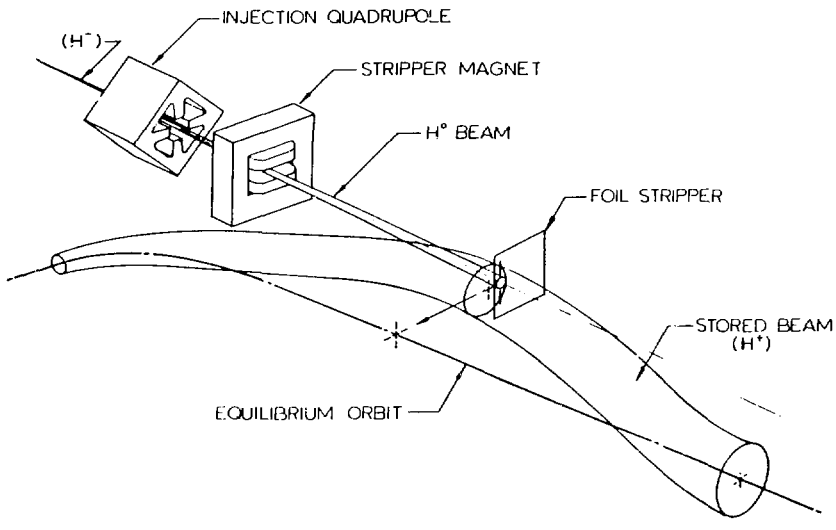

Fig. 50.
Injection scheme, showing stripper magnet, foil, and orbit bump.

are 10 kV and 30 kW, respectively. Power is coupled to the beam by a single-gap, 2-m-long, ferrite-loaded cavity. Because beam-loading effects would be severe for a conventional high-output-impedance drive, the cavity will be driven by a low-impedance (10-Ω) output stage configured as a power follower. In the SBHF mode, the first-harmonic cavity will be mechanically shorted.

E. Extraction

Beam extraction is in the horizontal plane and is accomplished by two 4-m, parallel-plate, transmission-line kickers, located as shown in Fig. 48. These provide (sequentially) 6.6-mrad radially outward and 3.3-mrad radially inward deflections that add because of the betatron phase difference between them. The kicked beam enters the aperture of a 0.5-T dc septum magnet, which in turn deflects it into the extraction channel. Radial separation between stored and kicked beams is 10 cm at the septum entrance. Figure 51 displays the beam envelopes of the kicked and unperturbed beams. Extracted beam is conducted to a reinsertion point in Line D by a transport system designed for high currents.

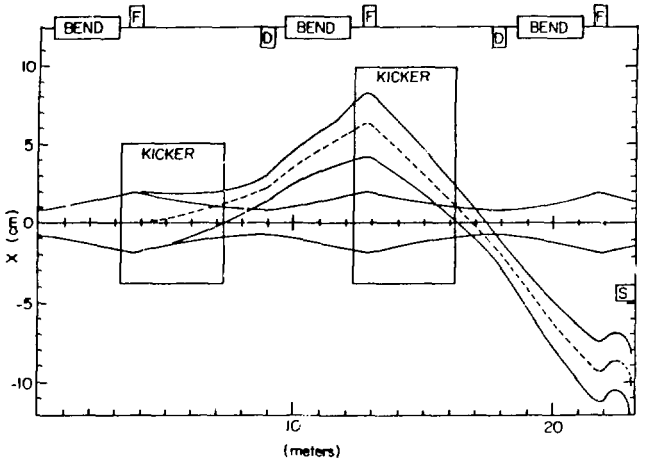

Fig. 51.
Beam envelopes of the kicked and unperturbed beams.

The kicker pulse is propagated opposite to the beam to obtain additive deflections from electric and magnetic fields of the TEM wave. Pulses are provided by a thyratron-switched ferrite-isolated Blumlein PFN.[71] Rise-and-fall times are 30 ns in the SBHF mode, with a total base width of 115 ns. These stringent requirements are set by the need to extract individual bunches without disturbing those remaining in the Ring. Pulse amplitudes are ±50 kV, and peak power is 100 MW, with a 4.3-kW average power. Pulse repetition rate is 720/s. The unusually high rates, coupled with the short transition times, stretch the state of the art in switch-tube technology. Long-bunch kicker requirements are not as demanding, because repetition rates are much lower and pulse fall time is not critical. However, a different energy store is required.

F. Instabilities and Control

Growth times and thresholds for coherent instabilities in the PSR have been previously investigated by Neil and Cooper [72] and also by Courant, Smith, and Neil.[73] Because of exceptionally high circulating currents, low energy spread, and relatively low energy, PSR operation might appear to be threatened by many instabilities; however, because storage times are short (a few milliseconds at most), only instabilities with growth times of that order are

important. This radically improves the situation. Further advantages inherent in the PSR design are (a) operation well below transition, which eliminates the negative mass instability; (b) a large aperture; and (c) good vacuum (3×10^{-9} torr).

The transverse resistive wall instability has submillisecond growth times for the LBLF operating mode. A high-power, wide band, active damping system is therefore incorporated into the Ring to suppress it. Bandwidth is sufficient for control of growth modes up to n = 20. The system is similar in design to those in use at Fermilab.[74] If necessary, the four multipole magnets of the Ring can be energized as octupoles to raise the threshold for onset of this instability.

The longitudinal resistive wall instability has an n = 1 growth time (LBLF mode) of ~1 s and therefore would seem to present no problem. However, the local Keil-Schnell criterion applied at the ends of the bunch indicates the possibility of fast-growing instability in these regions. To study the details of longitudinal motion expected in the Ring during injection and capture, as well as thereafter, a computer code was written that numerically integrates the Vlasov equation for the appropriate distribution function. The calculation[75] includes longitudinal forces caused by wall currents and space charge, finite wall resistance, and rf cavities. No evidence of instability appears, even after 2000 turns. The injection process was initiated with the 2.795-MHz rf cavity gap voltage at 2.5 kV; rf amplitude then was ramped linearly to a 10.5-kV final value.

The amplitude of coupled-bunch longitudinal oscillations (SBHF mode) is not known at this time; provision has been made to install a synchrotron-frequency splitting cavity in the Ring to eliminate this problem should it occur. The Ring also is being constructed to minimize both transverse and longitudinal coupling impedances.

In the SBHF mode, the high bunching voltage (1.5 MV) demands a high shunt impedance to keep rf power requirements reasonable. The relatively high beam current (I = 0.53 A at h = 216) thus induces a substantial cavity voltage, and the Robinson instability must be considered. The effects of this instability have been calculated[76] and the 603.75-MHz rf system is being designed accordingly.

Two vacuum-related instabilities also have been considered. These are (a) beam-induced electron multipactoring[77] and (b) the beam-induced ion-wall

instability, initially observed in the CERN Intersecting Storage Ring (ISR). The first involves acceleration of electrons into the vacuum wall by the time-dependent radial electric field of the circulating bunched beam. For pulse frequencies and intensities expected in the PSR, calculations suggested that the process could rapidly escalate; this would lead to pressure rise, diagnostics blinding, and beam loss. However, a simulation experiment indicated that if baked stainless steel surfaces are used in the vacuum system, there should be no multipactoring near PSR bunch frequencies.

The second, the ion-wall instability, is caused by gas evolution from the vacuum walls produced by energetic ions accelerated in the radial electric field of the stored beam. The ion-wall instability also can escalate rapidly, leading to pressure rise and beam loss. Detailed calculations for PSR operating modes showed that, because of short storage times, PSR peak currents are at least an order of magnitude below the critical currents for onset of this effect.

II. PROJECT STATUS

During this reporting period the design, performance goals, and cost estimate of the PSR project have been extensively reviewed. At the same time, considerable progress was made on the design of equipment and buildings and on development of prototypes for key advanced-technology devices, such as the fast-extraction kickers.

A. Reviews

The overall PSR project design and planned performance objectives were examined in June by a DOE panel chaired by R. Neal of Stanford Linear Accelerator Center (SLAC). The review was one segment of a comprehensive comparison of the two competing United States pulsed spallation neutron sources--the PSR/WNR at Los Alamos and the Intense Pulsed Neutron Source-I (IPNS-I) at ANL. Both projects were carefully scrutinized with reference to their present capabilities and future potential as thermal neutron sources (intensities, usage factors, operating costs), and also with reference to the planned materials-science research programs. The chief aim of the review essentially was to determine which spallation neutron source, in a severely constrained United States materials-science budget, should receive future support.

The Neal committee concluded that the PSR design was realistic, practical, and well thought out and also that the performance objectives were readily achievable, assuming the usual machine commissioning period. A subsequent comprehensive neutron-source review body (now referred to as the Brinkman Panel) recommended that the PSR/WNR at Los Alamos should receive strong future support.

At the request of DOE, the PSR cost estimate was re-examined in detail during August and September, taking particular account of recent and anticipated equipment-cost escalation and the latest building-cost estimates furnished by the project's architect/engineer. Increased costs of modifying the LAMPF accelerator to provide beam to the PSR were also closely examined. The firm of William Brobeck, Inc., of Berkeley, California, was engaged as engineering consultant to help with equipment estimates. The new estimate turned out to be significantly higher than the then-current total estimated cost (TEC) of $19 M, and a Laboratory committee, composed of senior staff with construction-project experience, was formed to audit the estimate and assess the situation. This committee found that, except for somewhat low allowances for I&C software and for project management, the estimate was complete and correct. They found nothing significant to delete or add. A new construction TEC of $21.8 M was proposed to (and eventually accepted by) DOE, and the Laboratory agreed to furnish an additional $1.5 M in R&D funds to augment the budget for development of advanced PSR special equipment.

B. Buildings

Designs for the PSR staging building were completed. The low bid was $0.791 M, 20% below the estimate. Construction began on January 1, 1981, and will be completed by summer of 1981. The staging building, which is fully equipped with substantial electric power, closed-loop cooling water, and other essential services, will provide the PSR project with 12 500 square feet of much-needed, on-site, laboratory and equipment-assembly space.

Design of the Ring tunnel and equipment buildings has begun. Initial radiation-shielding studies are being reviewed to provide final specification on the thickness of tuff between the buried tunnel and the equipment building. An air-flow scheme for purging and ventilating the tunnel has been worked out.

Preliminary layouts of the water-cooling systems have been made. A surplus 8-MW cooling tower, more than adequate to handle the Ring heat load, has been found in West Virginia; arrangements have been made for it to be shipped to Los Alamos.

C. Equipment Design and Development

Summarizing the status of equipment design and development, ordered by major systems, we can make the following remarks.

1. Injection System. Injection transport optics have been optimized, and the locations and parameters of the magnetic elements have been specified. The line has been designed to cancel beam-momentum dispersion at the Ring injection point and to handle any of several possible injection programming (phase-space filling) schemes. Studies of these programming modes are continuing; the object is to select one and specify its appropriate hardware within the next few months. We have studied a foil-based, beam-halo removal scheme in the injection line. This halo stripper will clean off most of the unwanted edges of the beam (beyond 3σ in transverse dimension) before it enters the Ring, thereby considerably reducing activation of Ring components. About 2% of the beam may be removed in this process. The injection-line quadrupoles have been specified and put out for bids. Drive requirements for the programmed fast-injection steerers have been specified, and a first look at a pulsed-power-supply design for these units has been completed. A circuit that uses power field-effect transistors (FETs) appears attractive. An improved high-speed driver for the low-energy beam chopper also has been investigated, although the final design requirements for this device are not yet known.

2. Storage-Ring Passive Elements. Preliminary design for the 4-in.-aperture main Ring dipoles has been completed. The magnet cores are to be fabricated from parallel laminations that are slipped with respect to each other to follow the curve of the beam trajectory. We intend to have these magnets fabricated by industry. This procurement (which will approximate $1 M, including the power supply) will be the largest single equipment order. Design of the main Ring quadrupoles has been postponed until the extraction beam-dynamics problems have been ironed out. A prototype trim-coil power supply for the main dipoles has been completed and performs as required.

We have taken a first look at a scheme for scraping the edges of the stored beam, using foil scatterers and downstream, scattered-proton collectors. Possible scatterer and collector locations have been identified.

The vacuum-system design is well along. Studies of pumping and flow for representative segments of the Ring vacuum system have been performed, and desired base operating pressures (in the 10^{-9} torr range) have been achieved. Outgassing measurements have been made for sample dielectric materials intended for service in the Ring.

3. Storage-Ring Active Elements. System requirements for the 2.8-MHz rf buncher have been outlined, and preliminary buncher-cavity parameters worked out. Possible rf power sources also have been studied, with emphasis on modeling a low-output-impedance power follower. This rf drive would radically reduce the effects of beam loading, which for the more conventional high-impedance source, are a very serious problem.

Construction of a prototype 20-tube distributed power amplifier for the transverse damper has made good progress. Several important low-power prototype components of the damper electronics package have been fabricated and successfully tested. The order for the Eimac power tetrodes needed for the final version of the distributed amplifier is on hold, pending availability of funds.

General requirements for the low-level rf system have been outlined. The principles of operation for a special phase-stabilized cable, which carries the 201.15-Mhz reference signal from LAMPF to the PSR, have been successfully demonstrated.

Specifications for the 603.75-MHz rf system have been set down. Various options have been examined, with particular attention being focused on the problem of how to handle the high beam loading, and step changes in beam loading, as bunches are individually extracted from the Ring. The currently favored solution calls for fast mechanical tuning of the bunching cavities and relatively modest (100-kW) rf drive power, provided by two 55-kW commercial TV transmitter packages.

4. Extraction System. Dynamics of the extraction process have been studied extensively, with the objective of increasing to 10 cm the kicked-beam displacement at the extraction septum. The scheme now specified requires two

4-m-long stripline kicker magnets, located in the two straight sections preceding the septum. Beam is first kicked radially outwards and then, after a 180° phase advance, is kicked radially inward across the septum.

Construction of the short-bunch kicker modulator prototype is complete, and testing of critical components has begun. The long-bunch modulator test stand is about 50% complete. A contract with industry to develop a magnetic-modulator alternative approach to the extraction-kicker power supply has been terminated, because of difficulties in fabricating suitable low-inductance cores. The program is being continued as a low level in-house project by the Electronics (E) Division.

Considerable effort has been devoted to optical design of the extraction transport system. This system is required to put the beam onto the WNR target through a large existing 90° bending magnet, which has a rather restrictive aperture and is highly dispersive. The system also must handle the very large momentum spread and very high initial momentum dispersion of beam that leaves the Ring and very high levels of space charge. Several solutions have been studied; so far, the most promising is a short-wavelength focusing system that achieves partial cancellation of momentum dispersion. Details will be worked out during the next few months.

In the extraction process, it may be advantageous to use a special septum-quadrupole magnet in the Ring, as an alternative to the septum dipole. Figure 52 shows a possible septum quadrupole configuration made by modifying an existing quadrupole design. Note that the number of excitation coils is high, the geometry is complicated, and the quadrupole size is large.

A better conceptual design for a septum quadrupole is shown in Fig. 53, where all excitation coils are of small size and the septum return conductor is incorporated into the excitation coils. Figure 54 shows the actual conductor configuration. The conductor extending beyond the poles of the quadrupole is meant to shape the fringing fields, to avoid introducing other multipole moments; extended septa are used in much the same way to linearize the end fields of dipole septum magnets. Calculated magnetic fields for the septum quadrupole are shown in Fig. 55. The septum-conductor current-density variation was crudely simulated by splitting the septum conductor into three sections, each with the proper currents. With even this crude simulation, the field gradient is uniform to within 2% and the "field-free" region has a residual field of ~2 G. Figure 56 shows the kicked and stored beams when a septum

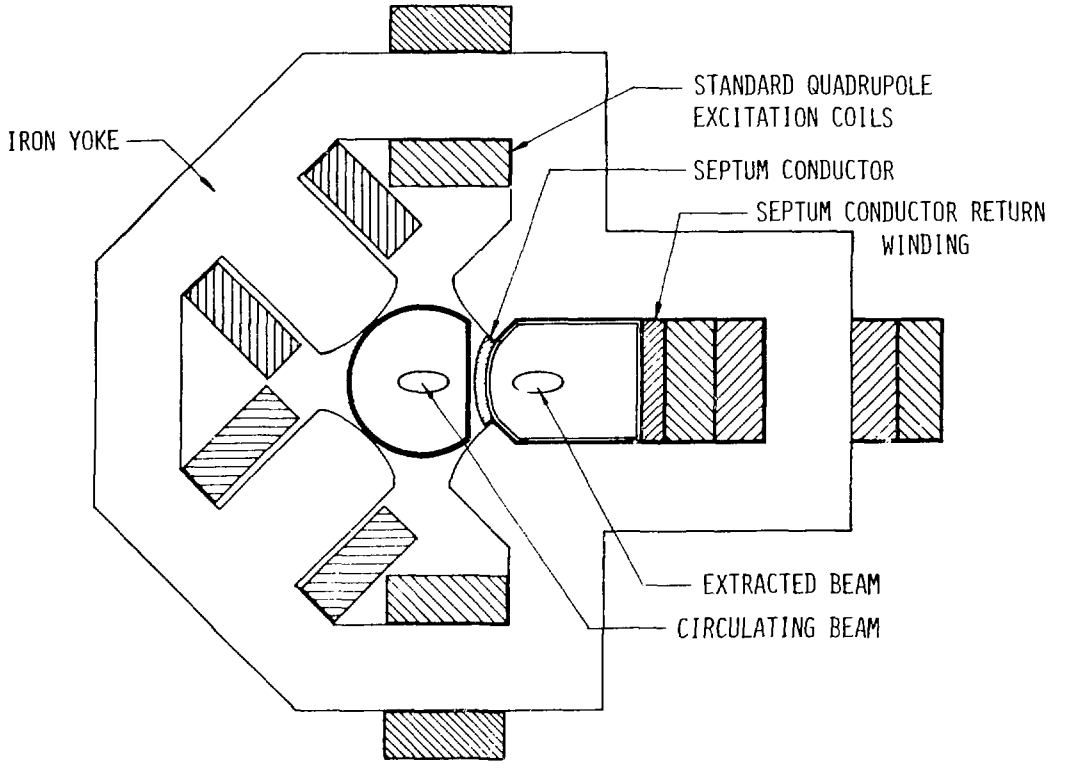

Fig. 52.
Cross section of standard quadrupole modified to a septum quadrupole.

quadrupole is used in the extraction straight section. Note that the beams are separated quite well in the middle of the straight section and that the extracted-beam diameter increases rapidly.

5. Instrumentation and Control. A start has been made on overall design of the PSR I&C system and on staffing of the I&C section. A central feature of the design is commonality with the FMIT project I&C hardware, as well as cooperative development of the system software with FMIT staff. Progress has been made toward defining and ordering the central control computer; at present, a member of the VAX family, manufactured by Digital Equipment Corporation, looks likely. As much as possible, the I&C system is to be based on

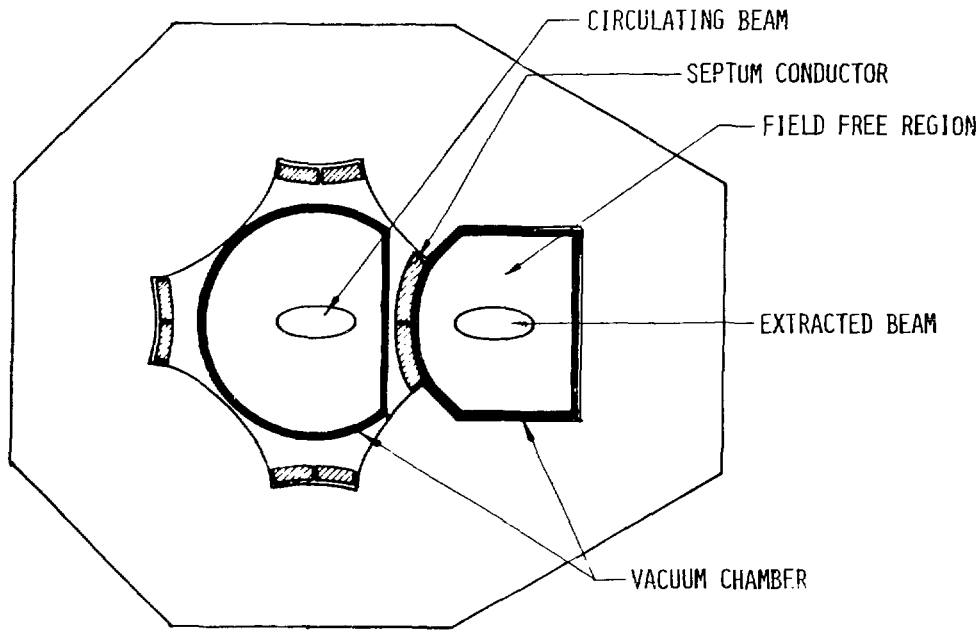

Fig. 53.
Septum quadrupole cross section.

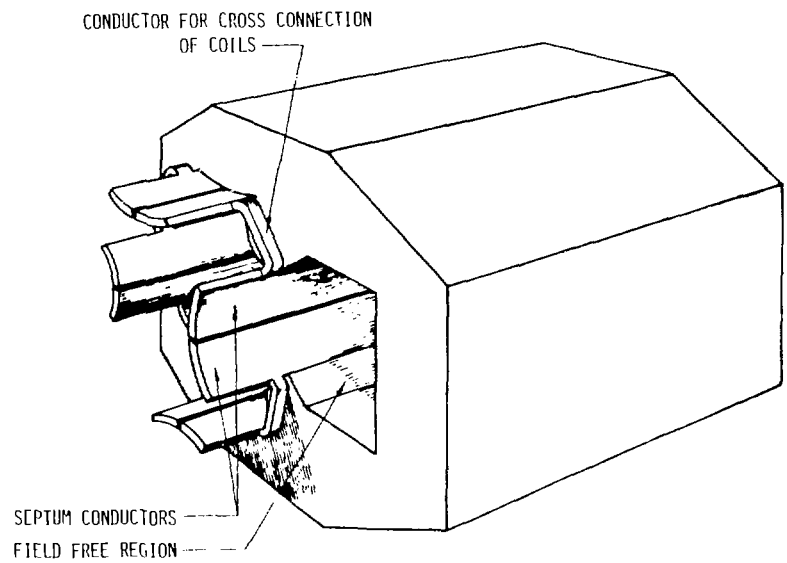

Fig. 54.
Septum quadrupole isometric view.

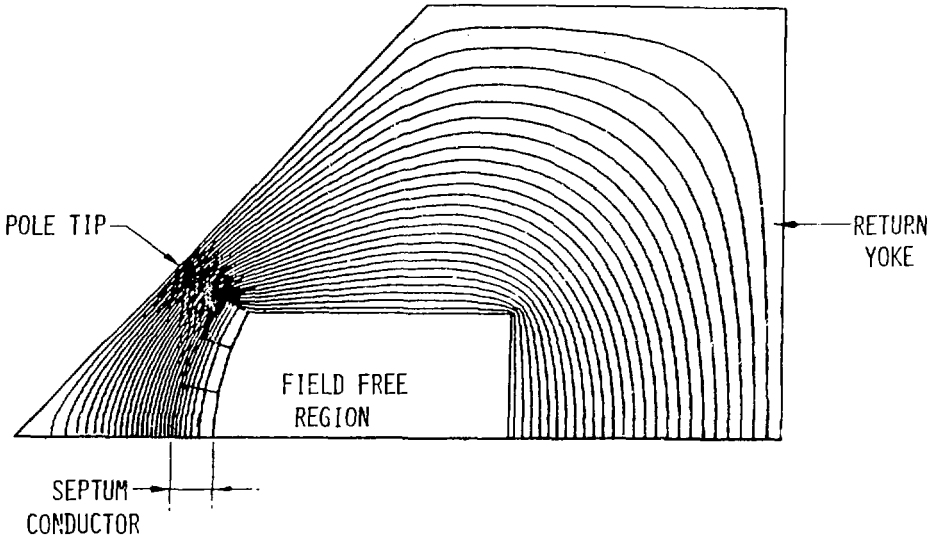

Fig. 55.
Plot of magnetic field in septum quadrupole (one octant).

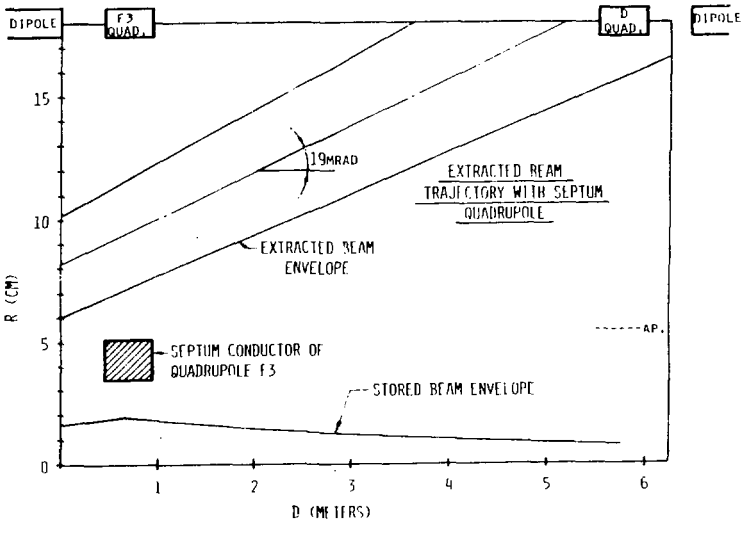

Fig. 56.
Schematic drawing of the kicked and stored beams for the septum quadrupole configuration.

standard available CAMAC modules; some hardware has been ordered for system-development studies. A preliminary study has been made of the operators' console, and the PSR signal-timing system has received initial attention.

H^- ION SOURCE, INJECTOR, AND ACCELERATOR TEST-STAND STUDIES

I. ION-SOURCE RESEARCH

The following performance has been achieved for various surface-plasma-source (SPS) configurations during this reporting period.

A. Dudnikov Configuration (Pulsed Operation)

Maximum extracted H^- current is 160 mA with a 0.5- by 10-mm emission slit having a 0.5-mm anode web.

At H^- current of 80 mA, the upper bounds for the normalized emittances* of $\varepsilon_x = 0.041\pi$ cm·mrad and $\varepsilon_y = 0.027\pi$ cm·mrad have been measured, and a lower bound on the normalized brightness (B) of 14.6 $A/cm^2 \cdot mrad^2$ has been determined with a 0.5- by 10-mm emission slit and a 0.5-mm anode web.

The ribbon-emission-slit dimensions were changed from 0.5 by 10 mm^2 to 1- by 5-mm^2 to measure the change, if any, in ε_x and ε_y. For a 51-mA beam from the 1- by 5-mm^2 slit, the upper bounds on the normalized emittance are $\varepsilon_x = 0.026\pi$ cm·mrad and $\varepsilon_y = 0.029\pi$ cm·mrad, resulting in a lower bound on the brightness of 13.7 $A/cm \cdot mrad^2$. Note that the x- and y-plane emittances are symmetrized by this simple change in the ribbon-slit geometry.

B. General SPS Research

1. Arc Noise Versus Emittance Studies. Measurements in the Dudnikov configuration of the beam emittance, with quiet- and noisy-arc discharges, clearly indicated an improvement by a factor of 3 in beam emittance for a quiet arc, compared to a noisy arc. The exact origin of the arc noise is uncertain, although hydrogen gas flow, cesium flow, and the source magnetic field all seem to affect the amplitude of the arc noise. This research demonstrated H^- beams in the 10- to 20-mA range with $\varepsilon_x \simeq \varepsilon_y < 0.008\pi$ cm·mrad, and $B \simeq 31$ $A/cm^2 \cdot mrad^2$.

---

*The emittance numbers reported here are those that contain 63% of the current in each direction.

2. Source-Emittance Distribution Theory. A simple ion-source emittance-distribution theory, which assumes a uniform current distribution and a Boltzman distribution of transverse ion velocities at the source plasma boundary, has been partially developed. The theory relates the beam emittance to the fraction of the beam contained within the emittance contour. The one free parameter is the ion temperature used in the Boltzman distribution. The shape of the measured curve for an 80-mA beam is fairly well represented by the theory, although not as well as for a low-current (~10-mA) beam.

Other calculations done this year considered the theoretical space-charge limit for extracting H^- ions through circular emission-extractor geometries. Details of the ion-source research are reported in Refs. 78 through 81.

II. ACCELERATOR TEST STAND

The ATS work completed or in progress, and its status at the end of the reporting period, is described in the following section.

A. Facilities

The Accelerator Technology Laboratory (ATL) building was completed in November. Preparations have been made to begin installation of the remaining high-power electrical utility circuits for the ATS, its rf-power source, and other general laboratory circuits. Figure 57 shows the system layout.

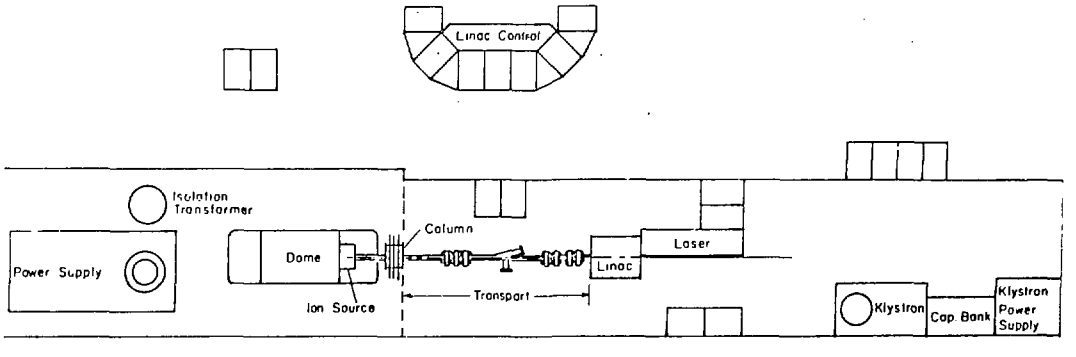

Fig. 57.
Experimental equipment layout.

B. ATS Control System

A master clock, providing control signals to all subsystems of the ATS, has been designed, fabricated, and tested. The clock is synchronized to the 60-Hz ac line to provide accurately reproducible rf-power time profiles. The signals are a time-zero pulse for reference, gas and arc pulses to the source, a pulse of variable delay and duration to the rf system, trigger to the laser, and trigger to the diagnostic. The design permits computer-control additions at a later time.

C. Laser Diagnostics

The laser for the laser diagnostic is installed on the ATS. Its safety enclosure and interlock system are complete. The last element of the picosecond timing system (10-ps resolution, 5-ps jitter), which measures the time of the laser pulse relative to the rf, has been delivered by the commercial vendor. Acceptance tests have begun for establishing reliability of the device. Optics for transporting the laser beam from the laser to the diagnostic region are on hand but are not yet installed.

Stepping-motor positioners, capable of one-, two-, or three-dimensional operation in high vacuum, were designed and built. Initial tests revealed that hardening the lead screws by heating produced unacceptably large deformations. A nonhardened lead screw was made and is being tested.

III. THEORY

A. ATS Injector-Column Calculations

We have recalculated the ATS injector-column beam dynamics for the case of a 100-mA, 100-keV H^- beam. Initial phase space is taken from recent emittance measurements on a pulsed 80-mA H^- beam. Additional calculations will be done on the column beam dynamics next year.

B. RFQ Design-Error Analysis

We performed an analysis of the effects of beam mismatch into the final design RFQ for the ATS. The design specification is given below. We found that the following actions taken with the input beam typically nad a 10% effect on the current and emittance of the output beam: ±0.15-cm off-axis beam displacement, ±3-keV error in input energy (out of 100 keV), ±1.5° offset in

Design Parameters		Input Conditions	
Frequency	424 MHz	W_i	0.10 MeV
Ion	H^-	ε_n(100%)	0.10π cm·mr (normalized)
Number of cells	360		
Length	2.886 m	ε_n(90%)	0.070π cm·mr (normalized)
Vane voltage	120.5 kV		
Average radius, (r_o)	0.409 cm	ε_n (rms)	0.016π cm·mr (normalized)
Final radius (a)	0.297 cm		
Initial modulation, M_i	1.000	I	105 mA
Final modulation, M_f	1.688		
Initial synchronous phase, ϕ_i	-90°	Output Conditions	
Final synchronous phase, ϕ_f	-30°	W_f	2.00 MeV
		ε_n(90%)	0.075π cm·mr (normalized)
RF power (including RFQ, manifold, and beam)	1.15 MW	ε_n (rms)	0.0184π cm·mr (normalized)
		Transmission	96.1
		I	101 mA

dx/dz, and a 25% error in beam size. The beam transmission efficiency (nominally 96%) and output emittance (nominally 0.0184π cm·mrad rms) were insensitive to ±40-mA fluctuations in input current, assuming a matched current of 105 mA. We also have run calculations using asymmetrical input emittances, such as those produced by the Dudnikov source with a rectangular emission slit. The results are quite interesting in that the RFQ output emittance is symmetrical, and for reasonable input beams $(\varepsilon_x + \varepsilon_y)_{input} \approx (\varepsilon_x + \varepsilon_y)_{output}$. This implies that the RFQ does not require a symmetrical input emittance. Table XIV tabulates the results of the error studies.

TABLE XIV

RFQ ERROR STUDIES

Run No.	I_{out} x 10^{-3} amp	Trans Eff I_{out}/I_{in}	Normalized Output Emittance X_{rms}	$X_{90\%}$	Y_{rms}	$Y_{90\%}$	Comments
0	101	0.96	0.0185	0.0722	0.0183	0.0785	Nominal Parameters
4	93	0.89	0.0228	0.1009	0.0188	0.0822	Ribbon beam; ε_x = 3 x nominal emittance, ε_y = 1/3 nominal emittance
5	51	0.49	0.0228	0.1425	0.0258	0.1142	Input energy 10% high (110 keV)
6	87	0.83	0.0215	0.0884	0.0217	0.0980	Input energy 5% high (105 keV)
7	82	0.78	0.0216	0.0932	0.0216	0.0951	Input energy 5% low (95 keV)
8	100	0.96	0.0188	0.0830	0.0176	0.0756	0.05 cm off axis displacement
9	96	0.92	0.0234	0.1078	0.0218	0.0967	0.10 cm off axis displacement
10	89	0.85	0.0243	0.1017	0.0232	0.1005	0.15 cm off axis displacement
11	82	0 78	0.0275	0.1218	0.0238	0.1125	0.20 cm off axis displacement
12	69	0.66	0.0276	0.1153	0.0215	0.0929	0.25 cm off axis displacement
15	71	0.68	0.0250	0.1016	0.0240	0.1120	0.05 radian error in dx/dz
16	94	0.89	0.0244	0.1051	0.0223	0.0947	0.025 radian error in dx/dz
18	122	0.94	0.0187	0.0764	0.0176	0.0779	Current mismatch - I_{in} = 0.130 A
19	137	0.86	0.0186	0.0819	0.0205	0.085?	Current mismatch - I_{in} = 0.160 A
20	144	0.80	0.0186	0.0842	0.0215	0.0942	Current mismatch - I_{in} = 0.180 A
21	48	0.97	0.0172	0.0737	0.0186	0.0842	Current mismatch - I_{in} = 0.050 A
22	0	0.99	0.0212	0.1013	0.0218	0.0956	Current mismatch - I_{in} = 0.0 A
23	95	0.91	0.0174	0.0738	0.0171	0.0696	Beam size mismatch - 0.86 x nominal
24	89	0.84	0.0186	0.0814	0.0187	0.0720	Beam size mismatch - 0.77 x nominal
25	77	0.73	0.0210	0.0841	0.0213	0.0925	Beam size mismatch - 0.67 x nominal
26	95	0.91	0.0193	0.0856	0.0192	0.0773	Beam size mismatch - 1.22 x nominal
27	86	0.82	0.0197	0.1011	0.0191	0.0820	Beam size mismatch - 1.41 x nominal
29	72	0.90	0.0296	0.1202	0.0281	0.1197	Dudnikov source; 0.080 A in, E_x^{rms} = 0.041, E_y^{rms} = 0.027
30	68	0.85	0.0316	0.1185	0.0260	0.1120	Dudnikov source error; 0.10 cm off axis displacement in X
31	70	0.88	0.0306	0.1270	0.0287	0.1233	Dudnikov source error; 0.10 cm off axis displacement in Y
32	68	0.85	0.0301	0.1295	0.0304	0.1349	Dudnikov source error; 0.025 radian error in dx/dz
33	69	0.86	0.0261	0.1099	0.0307	0.1280	Dudnikov source error; 0.025 radian error in dy/dz
34	61	0.76	0.0329	0.1319	0.0314	0.1223	Dudnikov source error; input energy 5 keV high
35	60	0.75	0.0289	0.1281	0.0342	0.1448	Dudnikov source error; input energy 5 keV low
36	62	0.78	0.0285	0.1130	0.0295	0.1242	Dudnikov source error; size mismatch - 0.77 x nominal
37	64	0.81	0.0278	0.1109	0.0278	0.1100	Dudnikov source error; size mismatch - 1.22 x nominal

C. Detailed Matching

A numerical procedure was developed for generating phase-space distributions matched to nonlinear periodic focusing systems. This procedure uses a version of the particle-tracing code HOT, which starts in a smooth-focusing configuration for which a matched distribution can be calculated by the RZED79 code. Such a distribution is followed in the tracing code, while adiabatically deforming the focusing forces until an alternating gradient configuration is reached. The final distribution function is periodic with the structure period; that is, the distribution is matched to the final configuration. Computer simulations show it is possible to match into highly nonlinear focusing forces by producing a large beam matched to an accelerator operating near the $2\sigma_x + \sigma_z = 360^\circ$ resonance, which is excited by the first harmonic of the rf

coupling forces. These calculations do not include space-charge effects. We expect the procedure to work similarly when the three-dimensional space-charge calculation is included in the particle-tracing code. This work is described and discussed in more detail in report LA-8442-MS, Ref. 82.

We believe that the adiabatic transition occurring in an RFQ structure is responsible for its excellent performance. It is worthy of note that the detailed matching theory was instrumental in providing the impetus to build the POP RFQ.

D. Ellipse Fitting

This year we tested and completed the documentation on a computer program that will fit a hyperellipse to a set of phase-space points in as many as six dimensions. An added feature of this program from a previous version is that we can vary the weight assigned to the phase-space points as a function of their distance from the centroid of the distribution. By varying the weight, we can determine whether there is a difference in ellipse orientation between inner and outer particles.

The program is useful in studying the effects of longitudinal and transverse phase-space couplings. The documentation is included in Refs. 83 and 84.

E. Mismatch Emittance Growth

In the design and construction of accelerators there are two major goals: obtaining sufficient current of adequate quality (emittance) and, for some devices, avoiding even low levels of particle loss. Effects from beam space charge place important limitations on achievable performance.

In circular accelerators the requirement of single-particle stability in a strictly periodic system limits the beam-plasma frequency to much less than the transverse-oscillation frequencies. In addition, the long time scales usually involved, together with the small plasma frequency, imply that the most important space-charge effects are instabilities, and these have been investigated extensively.[85]

On the other hand, in linear accelerators the lack of strict periodicity means that plasma frequency can equal or exceed particle oscillation frequencies, and operation in this high-density regime is required to meet the design goals of several planned linear accelerators. Because beams are in linear

accelerators for only a short time span, instabilities, though still quite important, may no longer be the dominant effect of space charge on beam behavior. In fact, evidence from computer simulations[86,17] suggests that mismatch (that is, injecting the beam into the accelerator, or a portion of the accelerator, in the wrong state) is largely responsible for the observed degradation of beam quality.

The problem of emittance growth (degradation of beam quality) caused by mismatch has been treated theoretically in this period. The method of attack is outlined here; the full analysis will be published separately. Particle losses, the possibly important influence of machine errors, and instabilities are ignored. Note, however, that even if we are operating in a regime where instabilities do occur, it is necessary (to study the instabilities accurately) to separate the effects of mismatch. Therefore, the purpose of our study was to understand what types of mismatch are most common or important so that possibly they can be avoided.

In attacking this problem there are four major difficulties. Our problem is fully three-dimensional, both in external forces and in beam configuration. In some cases beams are very long, and thus effectively are two-dimensional; but in many cases of interest all beam dimensions are comparable. The inhomogeneity scale length is the same as the mean oscillation amplitude of particles, so that no uniform density approximation is valid. Note also that the inhomogeneity scale lengths are comparable in all three directions. We see that both external forces and beam configuration are time dependent. A multiplicity of time scales of significant phenomena occur. Of course, all of these difficulties affect computer simulations also, making them both difficult to do and hard to interpret.

The fastest time scale in our problem is the accelerator period; because almost all accelerators are made up of repeating configurations of focusing, defocusing, and accelerating elements, whose properties repeat with small variation (as seen in the beam frame) along the accelerator, it makes sense to talk about an accelerator period. A somewhat longer time scale, by a factor of 3 or 4 (for high-intensity beams), is the plasma period. Somewhat longer still, by a factor of 2 to 4, is the single-particle oscillation (betatron) period. (Note that when we refer to betatron period we always mean the effective oscillation period in the presence of the beam's space charge.)

Our approach to this problem is to make a multiple time-scale expansion so that we correctly can include the effect of the rapid fluctuations on the slower time evolution (the ponderomotive force) while ignoring the details of the rapid fluctuations, and thus also leaving out the possibility of parametric instabilities driven by the fluctuating external force. We first use the multiple time-scale expansion to derive equations for both the slowly and the rapidly varying parts of the match. We then examine the time evolution of perturbations about the match and divide this time evolution into rapidly and slowly varying parts. Finally, we assume that only the slowly varying part of the time evolution of the perturbation is significant, an assumption that is violated if parametric instabilities also occur.

All of our equations are written for the beam frame of reference, so that all external forces depend on both space and time. In this frame of reference we assume that the particle motion is nonrelativistic: an approximation that, for the particles we are interested in (protons and heavier particles), is always very good. In addition, because space-charge effects are most important at low beam velocity, the electrostatic approximation is well justified. Also, we assume free-space boundary conditions, thus ignoring the effects of the wall--an approximation that may not be completely justified. We also use the transport approximation; that is, we assume that the accelerator period structure is changing so slowly from period to period that we can ignore the change. Accelerators often are designed so that, from the beam frame of reference, this approximation is very good. In addition to time periodicity, we make no assumption about the external forces, allowing arbitrary dependence on space and time (consistent with net focusing). Using these approximations, we can elucidate the qualitative mechanisms of emittance growth as a function of time.

The analysis proceeds as follows. We make a multiple time-scale expansion of a single particle's motion in a rapidly fluctuating force. The force is allowed to be fully three-dimensional, with arbitrary spatial dependence. These results are used to derive, from the full Vlasov equation, a set of equations for the rapidly and slowly varying parts of the match; in other words, we make a multiple time-scale expansion of the Vlasov equation. We then examine the initial value problem for perturbations away from the matched solution. We split this time evolution into slowly and rapidly varying parts

and derive a linearized Vlasov equation for the slowly varying piece; the relation to the "smooth" approximation that is often used is seen at this step. The short-time, or high-density, limit of the Vlasov equation is examined, and some qualitative results about the mechanisms of emittance growth are presented. A systematic expansion around the high-density solutions is developed and the solutions, including first-order corrections, are explicitly given. In addition, the long-time behavior is discussed qualitatively. We define and derive expressions for the rms emittances and give approximate formulae for these emittances. We compare our theory to one set of computer simulations, while examining the hypothesis that one type of mismatch is primarily responsible for the simulation results. We obtain reasonable agreement between theory and simulations. Finally, we review the results of the theory and discuss limitations and possible extensions of this work.

REFERENCES

1. E. A. Knapp and J. N. Bradbury, "Medical Linac Design Possibilities," Proc. 3rd Conf. on Applications of Small Accelerators, Denton, Texas, November 6-8, 1974 (National Technical Information Service, Springfield, Virginia, 1975), CONF-741040, p. 304.

2. J. N. Bradbury, E. A. Knapp, and D. E. Nagle, "Light Ion Linacs for Medical Application," Proc. 1975 Particle Accelerator Conf., Washington, DC, March 12-14, 1975, IEEE Trans. Nucl. Sci. 22, p. 1755 (1975).

3. E. A. Knapp. J. N. Bradbury, and D. A. Swenson, "Proposal for Development of a Pion Generator for Medical Application," Los Alamos Scientific Laboratory Proposal No. P-540 (September 1975).

4. E. A. Knapp and D. A. Swenson, "The PIGMI Program at Los Alamos Scientific Laboratory," 1976 Proton Linear Accelerator Conf., Chalk River, Ontario, September 14-17, 1976, Chalk River Nuclear Laboratory report AECL-5677, p. 230 (1977).

5. L. D. Hansborough, R. W. Hamm, J. E. Stovall, and D. A. Swenson, "An Optimized Design for PIGMI," Proc. 6th Conf. on Applications of Accelerators in Research and Industry, Denton, Texas, November 3-5, 1980, IEEE Trans. Nucl. Sci. 28, p. 1511 (1981).

6. D. A. Swenson, "Low-Beta Linac Structures," Proc. 10th Linear Accelerator Conf., Montauk, New York, September 10-14, 1979, Brookhaven National Laboratory report BNL-51134, p. 129 (1980).

7. S. O. Schriber, "High-Beta Linac Structures," Proc. 10th Linear Accelerator Conf., Montauk, New York, September 10-14, 1979, Brookhaven National Laboratory report BNL-51134, p. 164 (1980).

8. V. E. Hart, "PIGMI Mechanical Fabrication," 1976 Proton Linear Accelerator Conf., Chalk River, Ontario, September 14-17, 1976, Chalk River Nuclear Laboratory report AECL-5677, p. 230 (1977).

9. R. W. Goodwin and M. F. Shea, "A Distributed Linac Control System Featuring SDLC Loop Communications," Proc. 10th Linear Accelerator Conf., Montauk, New York, September 10-14, 1979, Brookhaven National Laboratory report BNL-51134, p. 274 (1980).

10. R. W. Hamm, R. R. Stevens, Jr., D. W. Mueller, and H. M. Lederer, "A Compact 250-kV Injector System for PIGMI," Proc. 5th Conf. on Applications of Small Accelerators in Research and Industry, Denton, Texas, November 6-8, 1978, IEEE Trans. Nucl. Sci. 26, p. 1493 (1979).

11. R. W. Hamm, "30-kV Injector for PIGMI Prime Prototype," Los Alamos Scientific Laboratory, Accelerator Technology Division, Group AT-1 memorandum No. AT-1-270 (September 11, 1980).

12. T. P. Wangler and R. H. Stokes, "The Radio-Frequency Quadrupole Linear Accelerator," Proc. 6th Conf. on Applications of Accelerators in Research and Industry, Denton, Texas, November 3-5, 1980, IEEE Trans. Nucl. Sci. 28, p. 1484 (1981).

13. R. H. Stokes, K. R. Crandall, R. W. Hamm, F. J. Humphry, R. A. Jameson, E. A. Knapp, J. M. Potter, G. W. Rodenz, J. E. Stovall, D. A. Swenson, and T. P. Wangler, "The Radio-Frequency Quadrupole: General Properties and Specific Applications," Proc. 11th Int. Conf. on High-Energy Accelerators, CERN, Geneva, July 7-11, 1980, Experimentia: Supplement 40, p. 399 (1981).

14. R. W. Hamm, K. R. Crandall, L. D. Hansborough, J. M. Potter, G. W. Rodenz, R. H. Stokes, J. E. Stovall, D. A. Swenson, T. P. Wangler, C. W. Fuller, M. D. Machalek, R. A. Jameson, E. A. Knapp, and S. W. Williams, "The RF Quadrupole Linac: A New Low-Energy Accelerator," Proc. 2nd Int. Conf. on Low-Energy Ion Beams, Bath, England, April 14-17, 1980 (Inst. of Phys., Bristol, 1981), Conf. Ser. 54, p. 54.

15. J. M. Potter, S. W. Williams, F. J. Humphry, and G. W. Rodenz, "Radio-Frequency Quadrupole Accelerating Structure Research at Los Alamos," Proc. 1979 Particle Accelerator Conf., San Francisco, California, March 12-14, 1979, IEEE Trans. Nucl. Sci. 26, p. 3745 (1979).

16. J. E. Stovall, K. R. Crandall, and R. W. Hamm, "Performance Characteristics of a 425-MHz RFQ Linac," Proc. 6th Conf. on Applications of Accelerators in Research and Industry, Denton, Texas, November 3-5, 1980, IEEE Trans. Nucl. Sci. 28, p. 1508 (1981).

17. R. A. Jameson and R. S. Mills, "On Emittance Growth in Linear Accelerators," Proc. 10th Linear Accelerator Conf., Montauk, New York, September 10-14, 1979, Brookhaven National Laboratory report BNL-51134, p. 231 (1980).

18. K. R. Crandall, R. H. Stokes, and T. P. Wangler, "RF Quadrupole Beam-Dynamics Design Studies," Proc. 10th Linear Accelerator Conf., Montauk, New York, September 10-14, 1979, Brookhaven National Laboratory report BNL-51134, p. 205 (1980).

19. J. M. Potter, "An RF Power Manifold for the Radio-Frequency Quadrupole Linear Accelerator," Proc. 10th Linear Accelerator Conf., Montauk, New York, September 10-14, 1979, Brookhaven National Laboratory report BNL-51134, p. 138 (1980).

20. D. A. Swenson, "Resonant Coupling of an RFQ Manifold to a Drift-Tube Linac Cavity," Los Alamos Scientific Laboratory, Accelerator Technology Division, Group AT-1 memorandum No. AT-1-197 (June 26, 1980).

21. D. A. Swenson, E. A. Knapp, J. M. Potter, and E. J. Schneider, "Stabilization of the Drift-Tube Linac by Operation in the $\pi/2$ Cavity Mode," Proc. 6th Int. Conf. on High-Energy Accelerators, Cambridge, Massachusetts, September 11-16, 1967, Cambridge Electron Accelerator Laboratory report CEAL-2000, p. 167 (1967).

22. L. D. Hansborough, E. D. Bush, and V. E. Hart, "Mechanical Description of PIGMI," Proc. 5th Conf. on Applications of Small Accelerators in Research and Industry, Denton, Texas, November 6-8, 1978, IEEE Trans. Nucl. Sci. 26, p. 1464 (1979).

23. R. F. Holsinger, "The Drift-Tube and Beam-Line Quadrupole Permanent Magnets for the New Proton Linac," Proc. 10th Linear Accelerator Conf., Montauk, New York, September 10-14, 1979, Brookhaven National Laboratory report BNL-51134, p. 373 (1980).

24. N. V. Lazarev and V. S. Skachkov, "Tipless Permanent-Magnet Quadrupole Lenses," Proc. 10th Linear Accelerator Conf., Montauk, New York, September 10-14, 1979, Brookhaven National Laboratory report BNL-51134, p. 380 (1980).

25. D. E. Nagle, E. A. Knapp, and B. C. Knapp, "Coupled Resonator Model for Standing-Wave Accelerator Tanks," Rev. Sci. Instrum. 38 (11), p. 1583 (1967).

26. E. A. Knapp, B. C. Knapp, and J. M. Potter, "Standing-Wave High-Energy Linear Accelerator Structures," Rev. Sci. Instrum. 39, p. 979 (1968).

27. J. J. Manca, E. A. Knapp, and D. A. Swenson, "High-Energy Accelerating Structures for High-Gradient Proton Linac Applications," IEEE Trans. Nucl. Sci. 24, p. 1087 (1977).

28. K. Halbach and R. F. Holsinger, "SUPERFISH - A Computer Program for Evaluation of RF Cavities with Cylindrical Symmetry," Particle Accelerators 7, p. 213 (1976).

29. K. Halbach, R. F. Holsinger, W. E. Jule, and D. A. Swenson, "Properties of the Cylindrical RF Cavity Evaluation Code SUPERFISH," 1976 Proton Linear Accelerator Conf., Chalk River, Ontario, September 14-17, 1976, Chalk River Nuclear Laboratory report AECL-5677, p. 122 (1977).

30. D. A. Swenson and J. M. Potter, "Resonantly Coupled Bridge Couplers for the Disk-and-Washer Linac Structure," Los Alamos Scientific Laboratory, Accelerator Technology Division, Group AT-1 memorandum No. AT-1-186 (June 16, 1980).

31. S. O. Schriber, "Room-Temperature Cavities for High-Beta Accelerating Structures," Proc. Conf. on Future Possibilities for Electron Accelerators, Charlottesville, Virginia, January 8-10, 1979 (University of Virginia, Charlottesville, Virginia, 1979), p. L-1.

32. T. P. Wangler and R. H. Stokes, "How FMIT RFQ Designs Depend on Injection Energy," Los Alamos Scientific Laboratory, Accelerator Technology Division, Group AT-1 memorandum No. AT-1-241 (August 25, 1980).

33. T. P. Wangler and R. H. Stokes, "FMIT RFQ with Optimum Surface Fields," Los Alamos Scientific Laboratory, Accelerator Technology Division, Group AT-1 memorandum No. AT-1-231 (August 12, 1980).

34. K. R. Crandall, R. H. Stokes, and T. P. Wangler, "Design of PIGMI Prototype RFQ," Los Alamos National Laboratory, Accelerator Technology Division, Group AT-1 memorandum No. AT-1-81-11 (January 7, 1981).

35. K. R. Crandall, R. H. Stokes, and T. P. Wangler, "Design of an RFQ for PIGMI Report," Los Alamos Scientific Laboratory, Accelerator Technology Division, Group AT-1 memorandum No. AT-1-317 (October 22, 1980).

36. G. P. Boicourt, K. R. Crandall, R. H. Stokes, and T. P. Wangler, "FMIT PROTOTYPE: RFQ Design, Matching to DTL, and RFQ-DTL Performance," Los Alamos Scientific Laboratory, Accelerator Technology Division, Group AT-1 memorandum No. AT-1-403 (December 30, 1980).

37. R. H. Stokes and T. P. Wangler, "Preliminary Design of an RFQ for Group AT-2," Los Alamos Scientific Laboratory, Accelerator Technology Division, Group AT-1 memorandum No. AT-1-247 (August 25, 1980).

38. R. H. Stokes, T. P. Wangler, and K. R. Crandall, "Radio-Frequency Quadrupole Linear Accelerator for High-Current Applications," Department of Energy Workshop on the Formation and Acceleration of High-Energy Neutral Beams for Magnetic Fusion, Washington, DC, December 11-12, 1980, US Department of Energy report DOE/TIC-11371 (1981).

39. E. L. Alten, "Advanced Design Research, Heavy Ion Medical Accelerator," Lawrence Berkeley Laboratory report PUB-5047 (1981).

40. T. P. Wangler, "Space-Charge Limits in Linear Accelerators," Los Alamos Scientific Laboratory report LA-8388 (December 1980).

41. K. R. Crandall, "Improved Space-Charge Calculations for Beams Having Elliptical Cross-Sections," Los Alamos Scientific Laboratory, Accelerator Technology Division, Group AT-1 memorandum No. AT-1-237 (September 2, 1980).

42. K. Bongardt, "Calculation of the Transfer Matrix T in Six Dimensions for an rf-Deflector Element," Los Alamos National Laboratory report LA-8668-MS (January 1981).

43. D. A. Swenson, "RF Linac Approach to Heavy Ion Fusion," Proc. Heavy Ion Fusion Accelerator Study, Berkeley, California, October 29-November 9, 1979, Lawrence Berkeley Laboratory report LBL-10301, p. 239 (1980).

44. T. P. Wangler and R. H. Stokes, "Application of the RF Quadrupole in Linear Accelerators for Heavy Ion Fusion," Proc. Heavy Ion Fusion Accelerator Study, Berkeley, California, October 29-November 9, 1979, Lawrence Berkeley Laboratory report LBL-10301, p. 21 (1980).

45. M. R. Shubaly, "A High-Current dc Heavy-Ion Source," Proc. 2nd Int. Conf. on Low-Energy Ion Beams, Bath, England, April 14-17, 1980 (Inst. Physics, Bristol, 1981), Conf. Ser. 54, p. 333.

46. M. R. Shubaly and R. W. Hamm, "A High-Current Four-Beam Xenon Ion Source for Heavy-Ion Fusion," Proc. 6th Conf. on Applications of Accelerators in Research and Industry, Denton, Texas, November 3-5, 1980, IEEE Trans. Nucl. Sci. 28, p. 1316 (1981).

47. J. E. Stovall, "The PIGMI Program at the Los Alamos Scientific Laboratory," Los Alamos Scientific Laboratory report LA-8525-SR (September 1980).

48. "Dedicated Medical Ion Accelerator Design Study," Lawrence Berkeley Laboratory and University of Arizona, Lawrence Berkeley Laboratory final report LBL-7230 (1977).

49. J. Arianer, A. Cabrespine, and C. Goldstein, "CRYEBIS, A Multi-Purpose EBIS for the Synchrotron Saturne II," Proc. 1979 Particle Accelerator Conf., San Francisco, California, March 12-14, 1979, IEEE Trans. Nucl. Sci. 26, p. 3713.

50. V. A Vaguine, "Standing-Wave High-Gradient Accelerator Structure," Proc. 1977 Particle Accelerator Conf., Chicago, Illinois, March 16-18, 1977, IEEE Trans. Nucl. Sci. 24, p. 1084 (1977).

51. R. W. Warren, "FEL Development Program at Los Alamos Scientific Laboratory," Proc. Conf. Int. School of Quantum Electronics, August 1980, Ettore Majorana Center for Scientific Culture, Erice, Sicily, S. Martellucci and A. N. Chester, Eds., forthcoming; also W. E. Stein, C. A. Brau, B. E. Newnam, R. W. Warren, and J. G. Winston, "LASL Free Electron Laser Experiments," Proc. 6th Conf. on Applications of Accelerators in Research and Industry, Denton, Texas, November 3-5, 1980, IEEE Trans. Nucl. Sci. 28, p. 1522 (1981).

52. For general discussions on tapered wigglers, see Physics of Quantum Electronics, Vol. 7, S. F. Jacobs, M. O. Scully, and M. Sargent, Eds.; also Free-Electron Generators of Coherent Radiation, S. F. Jacobs, H. S. Pilloff, M. O. Scully, M. Sargent, and R. Spitzer, Eds. (Addison-Wesley Publishing Co., Reading, Massachusetts, 1980).

53. FELMOV, a computer program written by R. K. Cooper, Los Alamos National Laboratory, Accelerator Technology Division, Group AT-3.

54. R. B. Neal, Ed., The Stanford Two-Mile Accelerator (W. A. Benjamin, Inc., Menlo Park, California, 1968), p. 5725.

55. "Future of Nuclear Science," monogram of the Ad Hoc Panel on the Future of Nuclear Science, G. Friedlander, Chmn., National Academy of Sciences, Washington, DC (1977).

56. "The Role of Electron Accelerators in U. S. Medium-Energy Nuclear Science," report of the DOE/NSP Study Group, R. S. Livingston, Chmn., Oak Ridge National Laboratory report ORNL/PPA-77/4 (1977).

57. "A Long-Range Plan for Nuclear Science," report of the NSP Nuclear Science Advisory Committee, H. Feshback, Chmn. (1979).

58. S. Penner, R. I. Cutler, P. H. Debenham, E. R. Lindstrom, D. L. Mohr, M. A. D. Wilson, N. R. Yoder, L. M. Young, T. J. Boyd, E. A. Knapp, R. E. Martin, J. M. Potter, C. M. Snyder, D. A. Swenson, and P. J. Tallerico, "The NBS-LASL CW Microtron," Proc. 6th Conf. on Applications of Accelerators in Research and Industry, Denton, Texas, November 3-5, 1980, IEEE Trans. Nucl. Sci. 28, p. 1526 (1981).

59. P. Axel, L. S. Cardman, H. D. Graef, A. O. Hanson, R. A. Hoffswell, D. Jamnik, D. C. Sutton, R. H. Taylor, and L. M. Young, "Operating Experiences with MUSL-2," Proc. 1979 Particle Accelerator Conf., San Francisco, California, March 12-14, 1979, IEEE Trans. Nucl. Sci. 26, p. 3143 (1979).

60. H. Herminghaus, A. Feder, K. H. Kaiser, W. Manz, and H. V. D. Schmitt, "The Design of a Cascaded 800-MeV Normal Conducting CW Race Track Microtron," Nucl. Instrum. Methods 138, p. 1 (1976).

61. C. M. Lyneis, M. S. McAshan, R. E. Rand, H. A. Schwettman, T. I. Smith, and J. P. Turneaure, "The Stanford Superconducting Recyclotron," Proc. 1979 Particle Accelerator Conf., San Francisco, California, March 12-14, 1979, IEEE Trans. Nucl. Sci. 26, p. 3246 (1979).

62. S. O. Schriber and J. M. Potter, "Limitations of the Disk-and-Washer Structure," Proc. 10th Linear Accelerator Conf., Montauk, New York, September 10-14, 1979, Brookhaven National Laboratory report BNL-51134, p. 176 (1980).

63. P. H. Debenham, "End-Magnet Design for the NBS-LASL CW Microtron," Proc. 1981 Particle Accelerator Conference, Washington, DC, March 11-13, 1981, IEEE Trans. Nucl. Sci. 28, p. 2885 (1981).

64. H. Babic and M. Sedlacek, "A Method for Stabilizing Particle Orbits in a Racetrack Microtron," Nucl. Instrum. Methods 56, p. 170 (1967).

65. L. M. Young, "Experience in Recirculating Electrons through a Superconducting Linac," Proc. 1973 Particle Accelerator Conf., San Francisco, California, March 3-5, 1973, IEEE Trans. on Nucl. Sci. 20, p. 81 (1973).

66. G. J. Russell, P. W. Lisowski, and N. S. P. King, "A Pulsed Spallation Neutron Source at the Los Alamos Scientific Laboratory," Los Alamos Scientific Laboratory preprint, talk given at Harwell, England, September, 1978 (LA-UR-78-2451).

67. R. K. Cooper and G. P. Lawrence, "The Design of the WNR Proton Storage Ring Lattice," Proc. 1977 Particle Accelerator Conf., Chicago, Illinois, March 16, 1977, IEEE Trans. Nucl. Sci. 24, p. 1073 (1977).

68. D. W. Hudgings and A. J. Jason, "Injection System for the Proton Storage Ring at LASL," Proc. 11th Int. Conf. on High-Energy Accelerators, CERN, Geneva, July 7-11, 1980, Experimentia: Supplement 40, p. 277 (1981).

69. A. J. Jason and D. W. Hudgings, "The H^- Field Ionization Experiment; Preliminary Results," Los Alamos Scientific Laboratory, Accelerator Technology Division, Group AT-3 Technical Note No. 45 (January 1980).

70. M. Donald, "Fundamental Mode Beam Loading in the 603.75-MHz RF System," Los Alamos Scientific Laboratory, Accelerator Technology Division, Group AT-3 Technical Note No. 35 (May 1979).

71. W. C. Nunnally, D. W. Hudgings, and W. J. Sarjeant, "Fast-Extraction Modulators for Los Alamos Scientific Laboratory Proton Storage Ring," Proc. 14th Pulse-Power Modulator Symp., Orlando, Florida, June 1980. (IEEE, Piscataway, New Jersey, 1980), p. 292.

72. V. K. Neil and R. K. Cooper, "Possible Coherent Electromagnetic Effects in the Los Alamos Proton Storage Ring," Lawrence Livermore National Laboratory report UCID-16299 (1973).

73. R. K. Cooper and G. P. Lawrence, Eds., "Proton Storage Ring Summer Workshop, The Los Alamos Scientific Laboratory, August 16-20, 1976," Los Alamos Scientific Laboratory report LA-6749-C, p. 31 (October 1977).

74. E. F. Higgins, Jr., Q. Kerns, H. Miller, B. Prichard, R. Stiening, and G. Tool, "The Fermilab Transverse Instability Active Damping System," IEEE Trans. Nucl. Sci. 22, p. 1473 (1975).

75. R. K. Cooper and V. K. Neil, "Proton Accumulator-Ring Injection Studies," Proc. 10th Int. Conf. on High-Energy Accelerators, Protvino, USSR, July 1977, Vol. II, p. 294.

76. R. K. Cooper and P. L. Morton, "RF Stability for the PSR," Los Alamos Scientific Laboratory, Accelerator Technology Division, Group AT-3 Technical Note No. 17 (May 1979).

77. O. Grobner, "Bunch-Induced Multipactoring," Proc. 10th Int. Conf. on High-Energy Accelerators, Protvino, USSR, July 1977, Vol. II, p. 277.

78. P. W. Allison, H. V. Smith, Jr., and J. D. Sherman, "H^- Ion-Source Research at Los Alamos," Proc. 2nd Int. Symp. on the Production and Neutralization of Negative Hydrogen Ions and Beams, Upton, New York, October 6-10, 1980, Brookhaven National Laboratory report BNL-51304, p. 171 (1981).

79. P. W. Allison, J. D. Sherman, and H. V. Smith, Jr., "Comparison of Measured Emittance of an H^- Ion Beam with a Simple Theory," Los Alamos National Laboratory report LA-8808-MS (June 1981).

80. H. V. Smith, Jr., J. D. Sherman, and P. W. Allison, "A Rotating Penning Surface-Plasma Source for DC H^- Beams," Proc. 2nd Int. Symp. on the Production and Neutralization of Negative Hydrogen Ions and Beams, Upton, New York, October 6-10, 1980, Brookhaven National Laboratory report BNL-51304, p. 178 (1981).

81. J. D. Sherman, P. W. Allison, and H. V. Smith, Jr., "H^- Beam Formation from a Penning Surface Plasma Source Using Circular Emission-Extractor Electrodes," Proc. 2nd Int. Symp. on the Production and Neutralization of Negative Hydrogen Ions and Beams, Upton, New York, October 6-10, 1980, Brookhaven National Laboratory report BNL-51304, p. 184 (1981).

82. W. P. Lysenko, "Matching Bunched Beams to Alternating-Gradient Focusing Systems," Proc. 1975 Particle Accelerator Conf., Washington, DC, March 12-14, 1975, IEEE Trans. Nucl. Sci. 22, p. 2516 (1975), and Los Alamos Scientific Laboratory report LA-8442-MS (July 1980).

83. E. A. Wadlinger, "General Least-Squares Fitting Procedures to Minimize the Volume of a Hyperellipsoid," Proc. 10th Linear Accelerator Conf., Montauk, New York, September 10-14, 1979, Brookhaven National Laboratory report BNL-51134, p. 242 (1980).

84. E. A. Wadlinger, "A Computer Program to Fit a Hyperellipse to a Set of Phase-Space Points in as Many as Six Dimensions," Los Alamos Scientific Laboratory report LA-8271-MS (March 1980).

85. J. D. Lawson, The Physics of Charged-Particle Beams (Clarendon Press, Oxford, 1977), Chapt. 6 and references contained therein.

86. J. W. Staples and R. A. Jameson, "Possible Lower Limit to Linac Emittance," Proc. 1979 Particle Accelerator Conf., San Francisco, California, March 12-14, 1979, IEEE Trans. Nucl. Sci. 26, p. 3698 (1979).

☆U.S GOVERNMENT PRINTING OFFICE:1982-0-576-020/5